Journal of Alloys and Compounds 838 (2020) 155274

Contents lists available at ScienceDirect

Journal of Alloys and Compounds

journal homepage: http://www.elsevier.com/locate/jalcom

Review

Progress in research on hybrid metal matrix composites

M.Y. Zhou [a, b, c], L.B. Ren [d], L.L. Fan [a, b], Y.W.X. Zhang [a, b], T.H. Lu [a, b], G.F. Quan [a, b, **], M. Gupta [c, *]

[a] Key Laboratory of Advanced Technologies of Materials, Ministry of Education, Sichuan, Chengdu, 610031, PR China
[b] School of Materials Science and Engineering, Southwest Jiaotong University, Sichuan, Chengdu, 610031, PR China
[c] Department of Mechanical Engineering, National University of Singapore, 9 Engineering Drive 1, Singapore, Singapore
[d] Center for Advancing Materials Performance from the Nanoscale, State Key Laboratory for Mechanical Behavior of Materials, Xi'an Jiaotong University, Xi'an, 710049, PR China

ARTICLE INFO

Article history:
Received 16 March 2020
Received in revised form
16 April 2020
Accepted 18 April 2020
Available online 11 May 2020

Keywords:
Hybrid metal matrix composites
Processing techniques
Mechanical properties
Strengthening mechanisms
Tribological properties
Physical properties

ABSTRACT

Hybrid metal matrix composites (MMCs) exhibit superior overall mechanical and functional response when compared to their conventional counterparts and as a result have greater potential to be widely used for structural engineering and functional device applications. This review focuses on the recent developments in the fabrication techniques and properties characterization of Al, Mg, Ti, Cu, Fe/steel and Ni matrix composites containing hybrid reinforcements. The hybrid reinforcements are classified according to different types, shapes and sizes. Novel processing techniques proposed for achieving homogeneous distribution of hybrid reinforcements and forming special structures are critically reviewed. The mechanical properties of various matrix systems are summarized and analyzed, while the strengthening mechanisms triggered by hybrid reinforcements are discussed. Meanwhile, a prediction model for yield strength of hybrid MMCs is also proposed. The effects of hybrid reinforcements and fabrication conditions on functional properties, including tribological, thermal, and electrical properties, of the hybrid composites are also described systematically. Finally, future work for promoting further development of this field is also addressed.

© 2020 Elsevier B.V. All rights reserved.

Contents

* Corresponding author.
** Corresponding author. Key Laboratory of Advanced Technologies of Materials, Ministry of Education, Sichuan, Chengdu, 610031, PR China.
E-mail addresses: quangf@home.swjtu.edu.cn (G.F. Quan), mpegm@nus.edu.sg (M. Gupta).

https://doi.org/10.1016/j.jallcom.2020.155274
0925-8388/© 2020 Elsevier B.V. All rights reserved.

1. Introduction

Metal matrix composites (MMCs) exhibit higher specific strength and specific elastic modulus than their monolithic counterparts [1]. In addition, with careful composition control, they can also exhibit high thermal conductivity, high electric conductivity, good dimensional stability, high damping capacity, and excellent wear resistance [2]. To note that extensive research conducted on MMCs in past four decades has enabled to overcome some challenging technical issues such as cost-effective processing, material design, characterization and matrix-reinforcement interfacial control [3,4]. Therefore, MMCs are being more frequently used in military, ground transportation, aerospace, electronics and even some recreational and infrastructure industries. The wide use of MMCs also triggered more research for further advancement in their compositional design and applications.

Conventional MMCs reinforced with fibers or micron particulates can achieve ultra-high strength and enhanced elastic modulus with high content of reinforcements, while the ductility and toughness drop dramatically with the increase in the volume amount of reinforcements due to the traditional trade-off between strength and ductility [5]. Recently, researchers have demonstrated that adding nano-reinforcements could improve the strength and modulus of metal matrix alloys without deteriorating the ductility and toughness [6]. In addition, the nano-reinforcements have much higher strengthening efficiency than their micron counterparts [7,8]. However, uniform dispersion of high content of nano-reinforcements in MMCs is too difficult because of the action of strong van der Waals' forces and intrinsic incompatibility between the nano-reinforcements and most metal matrix alloys. Thus, the limited content of nano-reinforcements always results in limited increase in strength in most metal matrix nano-composites (MMNCs) restricting the application spectrum of MMCs in engineering and biomedical sectors.

In order to solve this bottleneck for MMCs, a variety of research efforts have been attempted. One of the important strategies is developing MMCs with bioinspired structure [9]. The key idea of this approach is constructing laminated structure by imitating the structure of bone and nacre. The laminated structure can provide various toughening and strengthening mechanisms, leading to the materials that are both strong and damage-tolerant [10–12]. For example, carbon nanotubes (CNTs) reinforced MMCs with sandwiched structure were fabricated by coating CNTs onto metal foils or sheets uniformly, and then stacking these metal layers with CNTs via hot rolling [13,14]. Finally, both improvements in strength and toughness were obtained. Similar strengthening and toughening effects were also achieved in a recent work in which reduced graphene oxide (RGO) containing Al matrix composites with a bioinspired nano-laminated structure were fabricated by using a flake powder metallurgy route assisted with electrostatic adsorption [15,16].

Hybrid reinforcing is another novel and significant strategy to design and fabricate advanced MMCs. The core idea of this route is adding a variety of hybrid reinforcements into metal matrix, and relying on the hybrid reinforcements to exert their respective advantages to achieve synergistic effects, leading to excellent overall performance [17,18]. Compared with constructing bioinspired structure, hybrid reinforcement approach is more convenient and promising to produce bulk MMCs, because it is based on the selection of suitable type, content and ratio of the hybrid reinforcements to achieve high performance. Thus, the currently used methods for fabricating MMCs are also basically applicable to synthesize hybrid MMCs. In addition, combination of excellent mechanical properties, good wear resistance, and other good physical properties (such as thermal and electric conductivity) can also be obtained by judicious selection of hybrid reinforcements. Therefore, the development of hybrid composites has the potential to pave the way to effectively expand the application scope of MMCs.

Accordingly, the aim of this paper is to provide an overview of recent progress in this field covering hybrid reinforcements, processing methods, properties (mechanical and physical), and strengthening mechanisms. In addition, the outlook of potential applications is also provided.

2. Hybrid reinforcements

The commonly used reinforcements in MMCs can be categorized into two groups:

a. Continuous reinforcements
b. Discontinuous reinforcements

Table 1 shows the mechanical and physical properties of the common reinforcements. Carbon fibers (C_f), SiC fibers (SiC_f) and

Table 1
Common reinforcements used in MMCs.

Reinforcement type	Reinforcements			T_m (°C)	ρ (g·cm^{-3})	E (GPa)	CTE ($10^{-6} \times K^{-1}$)	UTS (GPa)
Continuous	Carbon fiber			\	1.7~2.0	231~827	-1.5~-0.6	1.6~7.0
	SiC fiber			\	2.3~3.4	175~420	3.1	1.0~3.5
	Al_2O_3 fiber			\	2.5~4.2	152~410	6.8~8.8	1.4~3.4
	B fiber			\	2.4~2.6	365~440	4.5	2.3~8.0
	Steel wire			\	7.8	203	\	4.2
	W wire			\	19.4	413	\	4.1
Discontinuous	Particles	Ceramic	SiC	2700	3.2	430	4	\
			Al_2O_3	2050	3.6	300	7.2	\
			B_4C	2447	2.5	445	4.8	\
			TiB_2	2980	4.5	500	4.6~8.1	\
			AlN	2200	3.3	310	4.5	\
			ZrB_2	3245	6.1	489	5.9	\
			Si_3N_4	2100	3.2	330	2.8~3.2	\
			ZrO_2	2680	5.9	\	\	\
			TiC	3160	4.9	440	6.5~7.2	\
			ZrC	3540	6.7	\	6.7	\
			SiO_2	1650	2.2	\	\	\
			Y_2O_3	2410	5	\	\	\
			MgO	2852	3.6	\	13.8	\
			La_2O_3	2217	6.5	\	5.8~12.1	\
			TiO_2	1850	3.8~4.2	\	\	\
		Metal	Ti	1660	4.5	110	10.8	\
			Cu	1083	8.9	119	16.5	\
			Ni	1453	8.9	207	13	\
			Zr	1852	6.5	\	3.6	\
		Carbon	Graphite	3652	2.3	\	1	\
			Diamond	3550	3.5	1220	1.1	\
	Linear	Short fiber	C_f	\	1.7~2.0	231~827	-1.5~-0.6	1.6~7.0
			SiC	\	2.3~3.4	175~420	3.1	1.0~3.5
			Al_2O_3	\	2.5~4.2	152~410	6.8~8.8	1.4~3.4
		Whisker	SiC	2316	3.2	482	\	12.9~13.7
			Al_2O_3	2082	3.9	550	\	13.8~27.6
			Si_3N_4	1900	3.2	382	\	3.9
			TiB	2200	4.5	425~480	8.6	\
			$Al_{18}B_4O_{33}$	1440	2.9	392	\	7.8
			$Mg_2B_2O_5$	1360	2.9	265	\	3.9
		Others	CNTs	3379	1.7~2.1	1000	1	30
	Sheet	Graphene	GNPs	3852	2	1000	1	130

Note: T_m is melting point, ρ is density, E is elastic modulus, CTE is coefficient of thermal expansion.

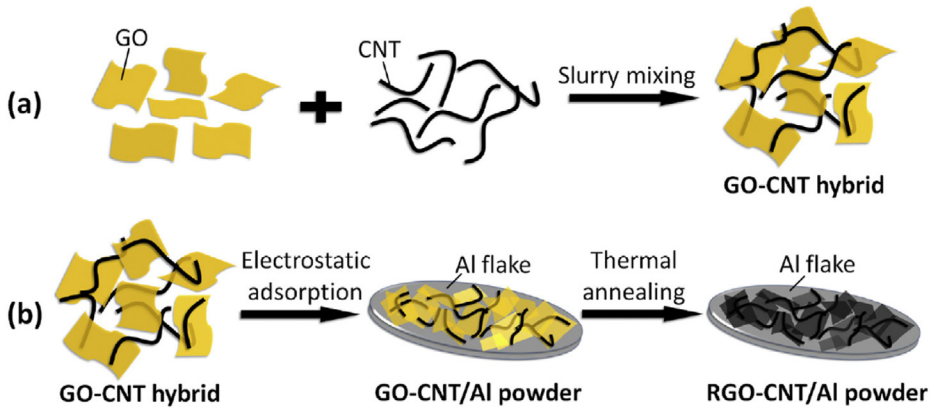

Fig. 1. Illustration of the fabrication procedure of RGO-CNT/Al composite powders. (a) The spontaneous formation of GO-CNT hybrid through π-π interactions. (b) Electrostatic adsorption of GO-CNT hybrid on Al flake and the reduction of GO to RGO through thermal annealing [17].

Al_2O_3 fibers (Al_2O_{3f}) are three most common and widely used continuous reinforcements in MMCs, and some metal wires are also employed as the continuous reinforcements. The continuously reinforced MMCs (CRMMCs) have high strength, however, their applications are greatly limited due to the mechanical anisotropy and expensive manufacturing costs. Compared with CRMMCs, discontinuously reinforced MMCs (DRMMCs) exhibit superior mechanical isotropy and lower cost of production and have undergone rapid development in recent years. According to different shapes, these discontinuous reinforcements can be divided into three types, namely, particle, linear and sheet forms. Ceramic particles, metal particles, graphite particles and diamond particles have been used as reinforcements for DRMMCs. Among these particles, some ceramic particles, such as SiC, Al_2O_3, and TiC are

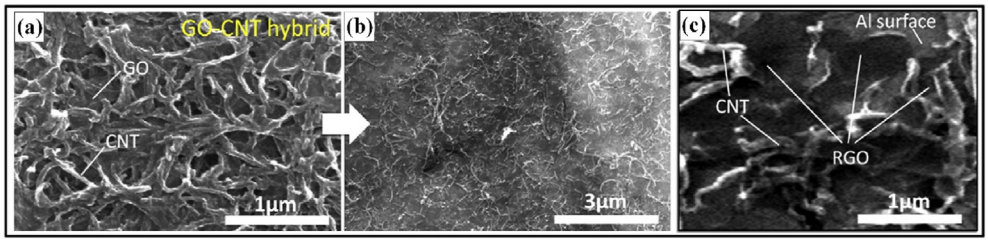

Fig. 2. (a) SEM image of the GO-CNT hybrid before being adsorbed on Al flakes, (b) SEM image of the composite powders reinforced by GO-CNT hybrid after adsorption and annealing process, and (c) the magnified rendition of the composite flake surface of (b) [17].

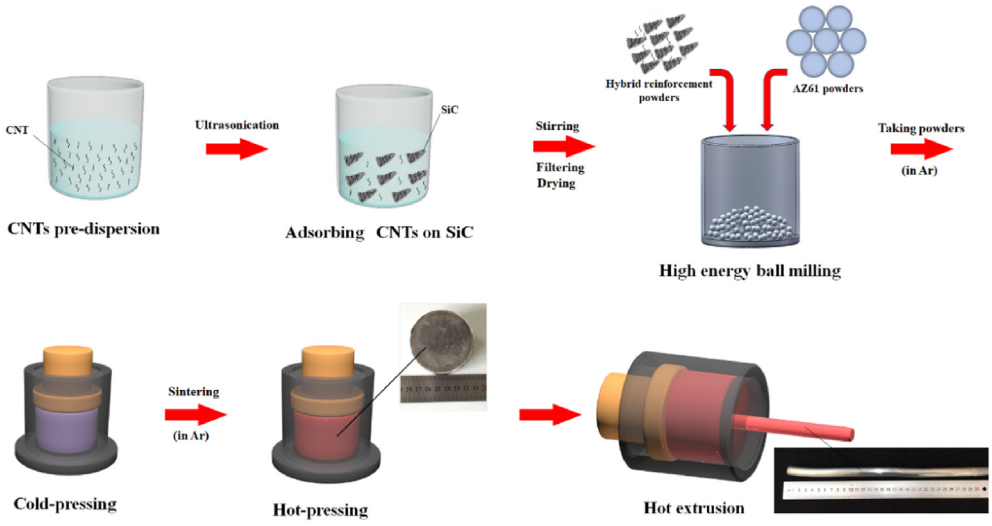

Fig. 3. Schematic illustration of the fabrication process of multi-scale hybrid micron SiC and CNTs reinforced AZ61 alloy composites [33].

most widely used. Linear discontinuous reinforcements include short fibers, whiskers and carbon nanotubes (CNTs). Discontinuous sheet type reinforcement is mainly about two-dimensional graphene nanoplates (GNPs). CNTs and GNPs are considered as the ideal reinforcement candidates due to their excellent mechanical and physical properties.

The hybrid reinforcements can also be categorized into two groups based on their components:

a. Hybrid continuous and discontinuous reinforcements (HCDRs)
b. Hybrid discontinuous reinforcements (HDRs)
   (i) Hybrid micron discontinuous reinforcements (HMDRs)
   (ii) Hybrid nano discontinuous reinforcements (HNDRs)
   (iii) Hybrid multi-scale discontinuous reinforcements (HMSDRs)

HDRs can be divided into three types according to the size of the hybrid reinforcements, which can be expressed as HMDRs, HNDRs and HMSDRs. For HMDRs, all components are micron length scale reinforcements, such as hybrid micron SiC and Al_2O_3 particles [19], hybrid micron TiB whiskers and TiC particles [20]. HNDRs contain two or more kinds of nano-reinforcements, like hybrid CNTs and GNPs [21], hybrid CNTs and nano SiC particles [22]. HMSDRs include multi-scale reinforcements, such as hybrid micron SiC particles and CNTs [23], hybrid micron and nano SiC particles [24].

Different combination of properties can be realized by choosing different combination of metallic matrices and hybrid reinforcements. For tougher, stronger and lighter materials to be used in aerospace and automotive industries, light metallic matrix, such as those based on Mg, Al and Ti can be suitable, and the HMSDRs may have the potential to balance strength and ductility of the composites, which have been demonstrated in the previous work [18]. For combination of high mechanical properties and high thermal and/or electric conductivity, hybrid CNTs and GNPs reinforced Cu matrix composites may be the ideal candidates [2,25]. For high-temperature applications, creep resistance is an essential parameter to determine the selection of suitable materials. Hybrid in-situ TiB whiskers and TiC particles reinforced Ti matrix composites may meet the stringent requirements at elevated temperatures [26]. In addition, carbon base materials, such as graphite particles, CNTs and GNPs, as hybrid reinforcements are beneficial in improving both strength and wear performance of the composites, due to their self-lubricating property [27]. Capabilities of different hybrid reinforcements to enhance different properties of the MMCs will be discussed in detail in forthcoming sections.

3. Processing techniques

To achieve good comprehensive mechanical properties of hybrid reinforced MMCs, the key points are the attainment of homogeneous dispersion of hybrid reinforcements, good interfacial bonding between matrix and reinforcements, and the structural integrity of hybrid reinforcements (especially for carbonaceous reinforcing materials, like CNTs [28] and GNPs [29]). Therefore, a variety of processing techniques have been developed in recent past that not only can disperse hybrid reinforcements but also can obtain good interfacial bonding and maintain the structural integrity of the hybrid reinforcements. According to the different methods of incorporating

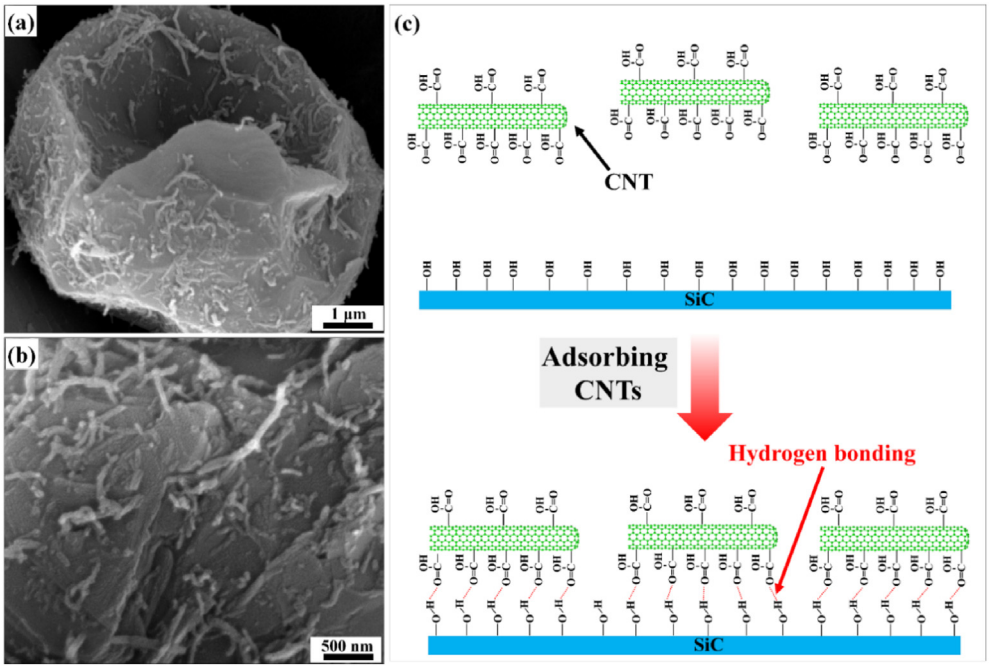

Fig. 4. (a) and (b) SEM images of the CNTs adsorbed on SiC surface, (c) schematic of adsorption of CNTs onto the surface of SiC [33].

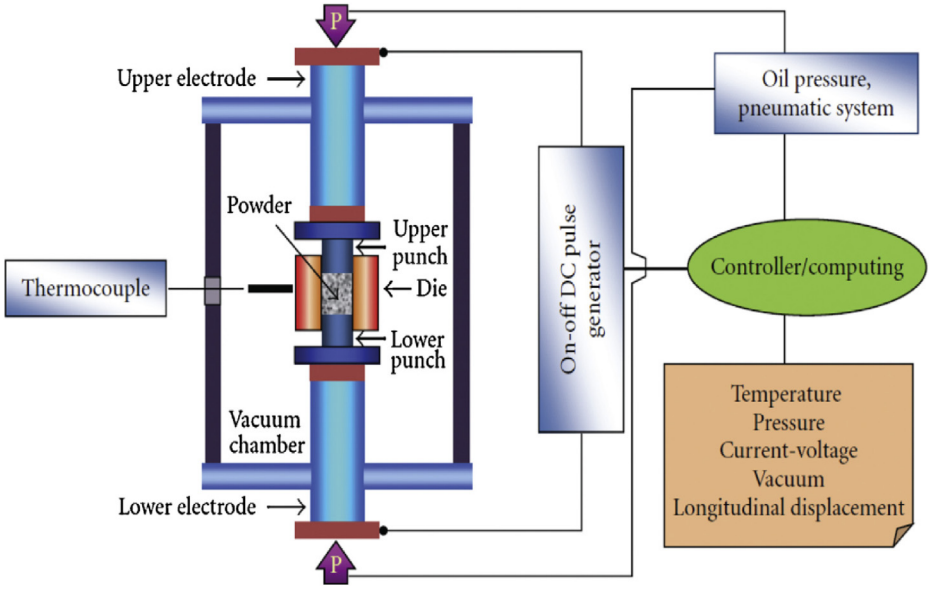

Fig. 5. Schematic of spark plasma sintering facility [37].

the hybrid reinforcements into the matrix, the processing techniques can be categorized into two types: (i) ex-situ processing routes, and (ii) in-situ processing routes. The essential difference between these two routes is whether or not the reinforcements are generated by in-situ reaction during the processing. Thus, most ex-situ processing techniques are also suitable for in-situ processing route. Moreover, additive manufacturing (AM), a novel processing method, is becoming more and more important to fabricate MMCs recently and is discussed in the last part of the forthcoming section.

3.1. Ex-situ processing techniques

3.1.1. Powder metallurgy processing

Powder metallurgy is one of the most popular and widely used processes for fabricating hybrid MMCs due to its flexibility, simplicity and scalability. In general, this technique involves several steps, namely: (i) dispersion of the hybrid reinforcements, (ii) compaction and (iii) sintering. In certain cases, secondary thermal mechanical treatments such as hot extrusion, hot rolling, hot

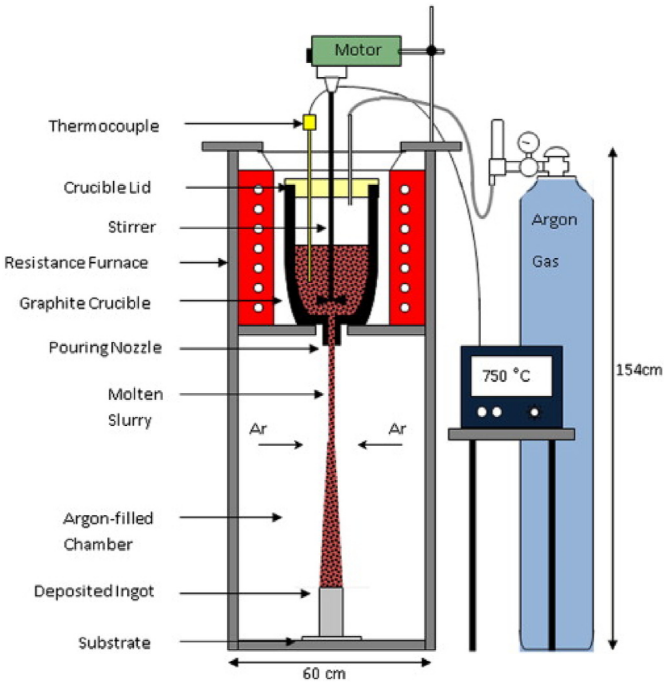

Fig. 6. Schematic diagram of disintegrated melt deposition setup [7].

forging and equal channel angular processing are also employed to further disperse the reinforcements and consolidate the compacts, leading to improved mechanical performance of the composites.

Dispersion is one of the most important steps in powder metallurgy route to fabricate MMCs with high performance. Ball milling is the most common method to disperse the reinforcements in the metallic matrix due to its efficiency and convenience [30]. The energy collision between grinding media during ball milling not only can disperse most of the common reinforcements, but also can refine matrix grain, which is beneficial to the mechanical properties of the composites. However, for some special carbonaceous nanofillers such as CNTs and GNPs, the severe impact of balls during milling can damage their structure during the long-time ball milling process which will affect the mechanical properties [31]. To solve this problem, Li et al. [17] proposed a novel flake powder metallurgy via slurry blending (shown in Fig. 1) to fabricate hybrid CNTs and GNPs reinforced Al matrix composites. First, the Al flakes were obtained by ball milling. Then, the spontaneous formation of graphene oxide (GO)-CNT hybrid was achieved through π-π interactions. Following that, electrostatic adsorption of GO-CNT hybrid on Al flakes and the reduction of GO to RGO through thermal annealing was realized. Finally, the RGO-CNT/Al composite powders were compacted, hot pressed and hot extruded to highly densified bulk RGO-CNT/Al composite. It is worthy to note that GO-CNT hybrid is negatively charged in aqueous media due to the existence of carboxyl (-COOH) and other ionogenic groups, while the fresh Al flake becomes ionized and positively charged in water. Therefore, GO-CNT hybrid can be uniformly and quickly adsorbed onto the Al flakes by electrostatic attractions. Uniform distribution (Fig. 2) and perfect structural integrity of GO-CNT hybrid were obtained, resulting in the synergistic strengthening effect. Hybrid RGO-CNT reinforced Cu matrix composite fabricated by similar method has also been reported [32].

For magnesium alloy matrix composites, the flake powder metallurgy method may be inappropriate due to the strong chemical activity of Mg as it could be severely oxidized during the slurry blending and electrostatic adsorption process [14]. Thus, Zhou et al. [33] developed a novel powder metallurgy route which is efficient and suitable for Mg matrix to prepare multi-scale hybrid micron SiC and CNTs reinforced high performance Mg matrix composites, and the schematic of the process is shown in Fig. 3. This route involves a multi-step dispersion process. First, the CNTs were uniformly adsorbed onto the surface of the SiC (Fig. 4) through hydrogen bonding between the carboxyl (-COOH) groups and hydroxyl (-OH) groups, which were decorated on the surfaces of the CNTs and SiC, respectively. Then, shift-speed ball milling was employed to achieve a uniform dispersion of the hybrid reinforcements in the end composites.

In this process, the micron SiC particles can act as carrier to transfer the CNTs from the surface of the SiC into the matrix. Because micron size SiC particles can be easily dispersed in metallic matrix uniformly via ball milling, the ball milling time needed to disperse CNTs uniformly in the matrix can be much shorter than common ball milling methods. Therefore, this route can significantly improve the dispersion efficiency of the CNTs in the matrix. In addition, the shorter ball milling time can also contribute in maintaining the structural integrity of CNTs. By ensuring structural integrity of reinforcement and uniformly dispersion of multi-scale hybrid reinforcements in the Mg matrix, good combination of ultra-high strength and good ductility was successfully achieved.

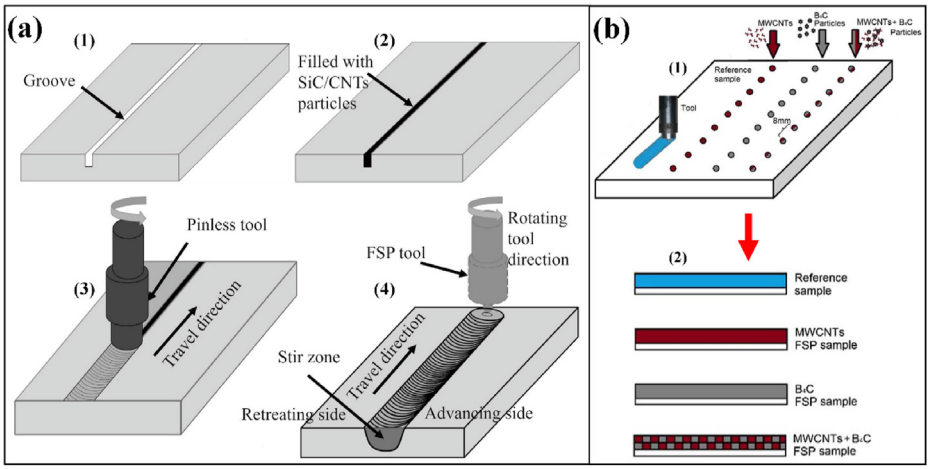

Fig. 7. Schematic diagram of FSP using different reinforcements incorporating methods: (a) grooves [23] and (b) cavities [50].

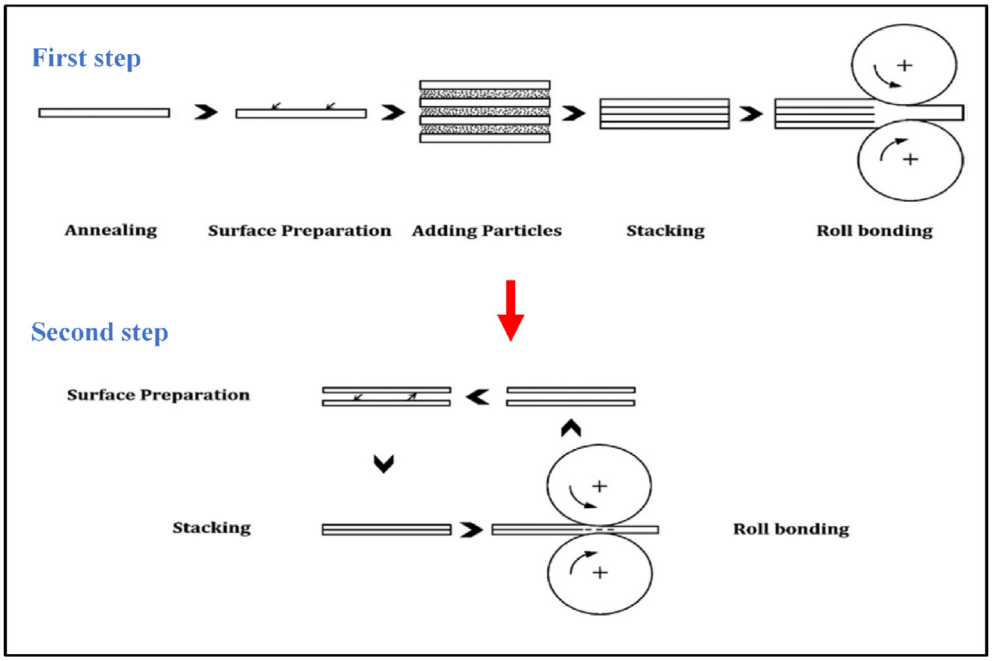

Fig. 8. Schematic procedure to produce hybrid MMCs via ARB process [57].

Table 2
Reaction systems of in-situ developed ceramic phases.

Reaction systems	Reaction equations	References
Al–Ti–C system	$Ti + C \rightarrow TiC$	[58]
	$4Al + 3C \rightarrow Al_4C_3$	
	$Ti + 3Al \rightarrow Al_3Ti$	
	$3Al_3Ti + Al_4C_3 \rightarrow 3TiC + 13Al$	
	$Al_3Ti + C \rightarrow TiC + 3Al$	
Al–Ti–B system	$Al + 2B \rightarrow AlB_2$	[58]
	$Ti + 3Al \rightarrow Al_3Ti$	
	$Al_3Ti + 2B \rightarrow TiB_2 + 3Al$	
	$Ti + 2B \rightarrow TiB_2$	
	$Ti + 3Al \rightarrow Al_3Ti$	[59]
	$2H_3BO_3 + 3Al \rightarrow Al_2O_3 + AlB_2 + 3H_2O$	
	$Al_3Ti + AlB_2 \rightarrow TiB_2 + 4Al$	
	$Al + 2B \rightarrow AlB_2$	[60]
	$6TiO_2 + 2Al \rightarrow 3Ti_2O_3 + \gamma - Al_2O_3$	
	$Ti_2O_3 + 2AlB_2 \rightarrow 2TiB_2 + \alpha - Al_2O_3$	
	$3AlB_2 + 3TiO_2 + Al \rightarrow 3TiB_2 + 2\alpha - Al_2O_3$	
	$3TiO_2 + 13Al \rightarrow 3Al_3Ti + 2\alpha - Al_2O_3$	
	$AlB_2 + Al_3Ti \rightarrow TiB_2 + 4Al$	
Ti–C system	$Ti + C \rightarrow TiC$	[58]
Ti–B_4C system	$5Ti + B_4C \rightarrow 4TiB + TiC$	[58]
	$3Ti + B_4C \rightarrow 2TiB_2 + TiC$	
Ti–TiB_2 system	$TiB_2 + Ti \rightarrow 2TiB$	[58]
Ti–SiC system	$3Ti + 2SiC \rightarrow Ti_3SiC_2 + Si$	[61]
	$Ti + SiC \rightarrow Si + TiC$	
	$3Si + 5Ti \rightarrow Ti_5Si_3$	
Molten salt system	$2TiO_2 + 2Na_3AlF_6 \rightarrow 2Na_2TiF_6 + Na_2O + Al_2O_3$	[62]
	$2Na_2TiF_6 + 6Al \rightarrow 4NaF + 4F_2 + 2TiAl_3$	
	$Al_2O_3 + 2Na_3AlF_6 \rightarrow 4Na_2O + 4Al + 6F_2$	
	$2Na_2TiF_6 + 4Al + KBF_4 \rightarrow TiAl_3 + TiB + 4NaF + AlF_3 + KF + 4F_2$	
	$2Na_2TiF_6 + 3Al + 2KBF_4 \rightarrow TiAl_3 + TiB_2 + 4NaF + 2KF + 7F_2$	
	$Na_2TiF_6 + KBF_4 \rightarrow TiB + 2NaF + KF + 4F_2$	

Sintering is another important process in powder metallurgy route, which can significantly affect the mechanical properties of the composites by influencing the relative density, interface between metal powders and matrix grain size. For conventional sintering, high temperature and long sintering time should be used to obtain denser products with good interfacial bonding [14]. In recent past, spark plasma sintering (SPS), also known as field assisted sintering, has attracted more and more attention in the field of MMCs, especially MMNCs, due to its advantages of low processing temperature and short sintering time for obtaining fully dense MMCs [34]. Fig. 5 shows the schematic of the SPS process. In this technique, the direct current (DC) pulse discharge could generate spark plasma, Joule heating, and an effective electrical field diffusion effect. In addition, the application of pressure can help plastic flow of the materials during sintering, which can further promote the consolidation of the materials. Therefore, the nanostructure features of hybrid reinforced MMCs obtained from ball milling can be preserved by preventing or at least minimizing grain growth through careful control of the SPS parameters, which is promising to achieve superior mechanical properties. Hybrid reinforced Al and Cu nanocomposites prepared by SPS have been reported recently [35,36].

Gupta's research group developed another innovative sintering technique mainly for manufacturing Mg and Al based composites, called microwave assisted hybrid sintering technique [7]. This method involves a pre-calibrated temperature exposure near the melting point of the metallic matrix in a microwave oven using SiC as the microwave susceptor material. This can provide a more uniform temperature gradient within the billet and compensate the shortcomings of heating via conventional heating or microwaves only. In addition, this technique can reduce more than 80% in the sintering time and energy consumption when compared to conventional sintering while realizing higher mechanical properties of the composites. This hybrid sintering method is economically viable for industries and is friendly to environment [38].

3.1.2. Liquid metallurgy processing

Casting is the most conventional processing technique to synthesize MMCs, which is simple and economical to obtain large-size composite products by using common casting equipment. Thus, this route has greater potential in commercial applications than powder metallurgy route. However, it is challenging to achieve

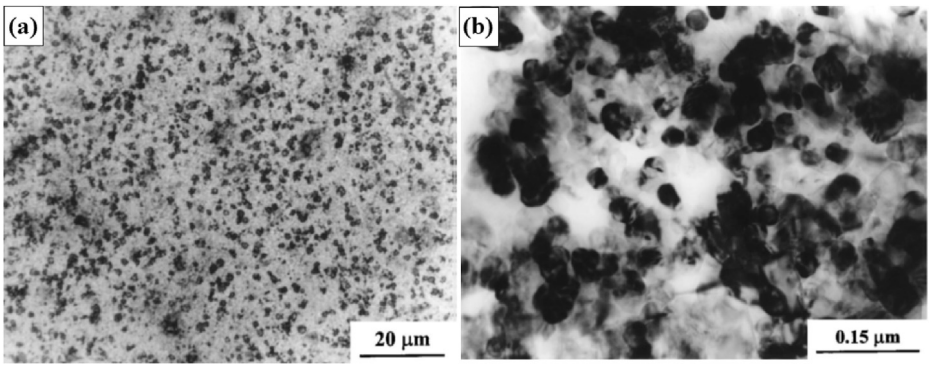

Fig. 9. (a) Optical micrograph showing uniform distribution of fine Al_2O_3 and TiB_2 particulates in aluminum matrix, (b) TEM micrograph showing fine Al_2O_3 and TiB_2 particulates and clean interfaces [58].

uniform dispersion of high volume fraction of reinforcements in metallic matrix due to the intrinsic incompatibility and large density difference between most reinforcements and metallic matrices. This also limits its use for mass production of MMCs. For preparing hybrid reinforced MMCs, stir casting, squeeze casting and infiltration are three most commonly used casting techniques. In stir casting process, the metal or alloy matrix is melted in a protective atmosphere, and then the hybrid reinforcements are incorporated into the molten metallic matrix by using mechanical stirring followed by casting. For hybrid reinforcements containing nano reinforcements, mechanical stirring cannot effectively achieve homogeneous dispersion, thus ultrasonic assisted process is often used to create and maintain a better distribution of the hybrid reinforcements in the matrix. In addition, secondary thermal mechanical processing, like hot extrusion or hot rolling, is often employed to improve the mechanical properties by eliminating defects and refining matrix grains. Many hybrid MMCs with high performance, such as Al [39], Mg [40], and Cu [41] matrix composites, have been successfully fabricated using this route. For example, Shen et al. [18] prepared hybrid micron and nano SiC (micron/nano = 9:1) reinforced AZ31 matrix composites using ultrasonic assisted stir casting and hot extrusion methodology and reported the combination of high strength (YS: 323 MPa, UTS: 402 MPa, respectively) and good ductility (elongation: 8.3%).

Squeeze casting is a new casting technique, which has been developed to compensate for the shortcomings of the conventional casting techniques [42]. The main idea of this technique is rendering solidification of molten metal under pressure by using a hydraulic press, and the pressure should be held on the metal until complete solidification. This not only can increase the rate of heat flow, but also can effectively eliminate casting defects, such as porosity. Thus, this method has greater potential to manufacturing less defective MMC cast components, and it is one of the most popular fabrication techniques for MMC products, especially for Al and Mg matrix composites [43]. Zhang et al. [44] fabricated hybrid SiC whiskers and SiC nano-particles containing Al composites by using squeeze casting technique and ultrahigh strength (YS: 553 MPa, UTS: 607 MPa) and elastic modulus (129 GPa) were

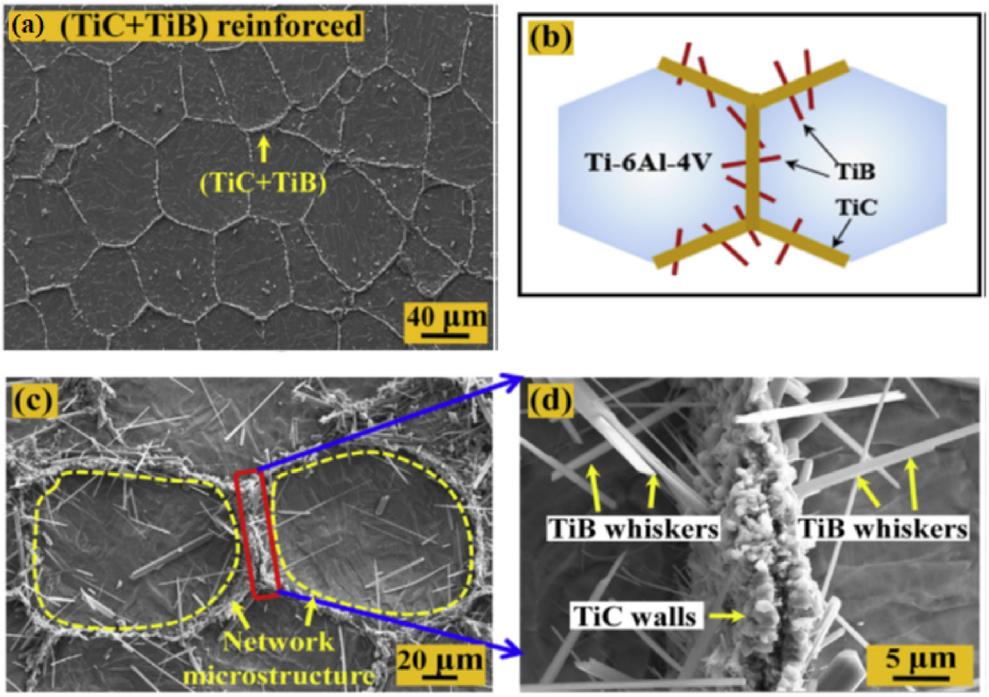

Fig. 10. (a) SEM image of Ti−6Al−4V/(TiC + TiB), (b) schematic of microstructural design, (c) microstructure after deep etching, (d) magnified network microstructure [20].

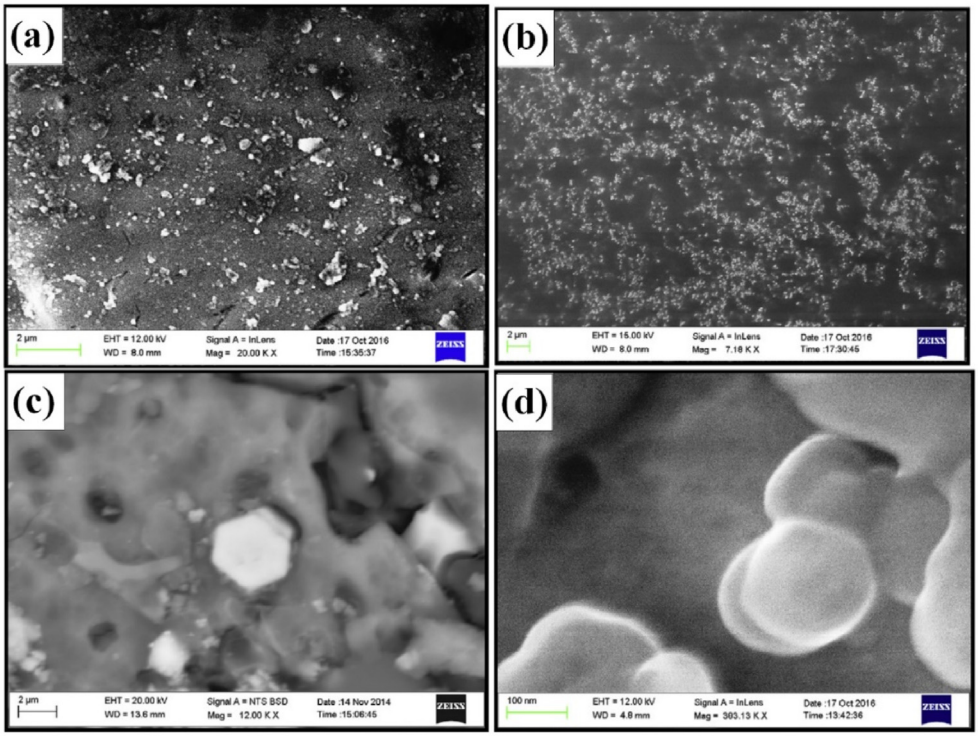

Fig. 11. SEM images of AA6061/(TiB_2+Al_2O_3) in-situ composites containing TiB_2+Al_2O_3: (a) 5 wt% (TiB_2+Al_2O_3), (b) 10 wt% (TiB_2+Al_2O_3), and the interfaces between matrix and TiB_2 (c) and Al_2O_3 (d) particulates, respectively [59].

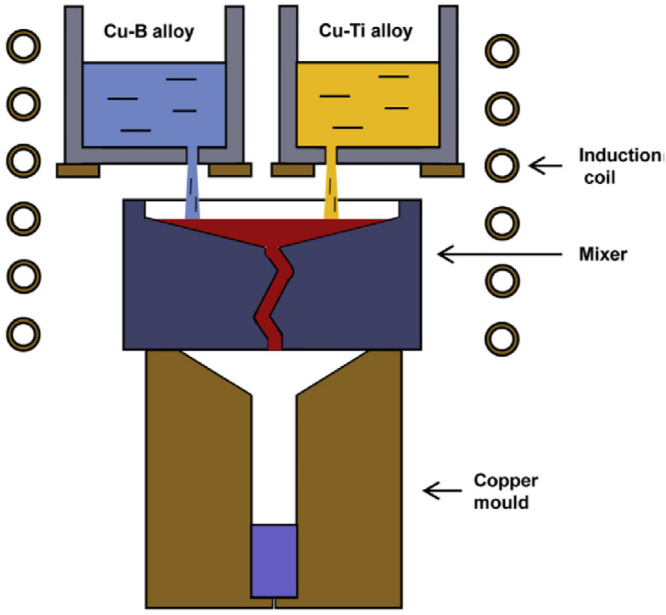

Fig. 12. Schematic diagram of fabrication of (TiB_w-TiB_{2p})/Cu composites [67].

obtained without further secondary thermal mechanical processing.

Infiltration process is a widely used technique for MMCs with high loading of reinforcements [45]. This method involves two main steps: (i) preparation of a porous preform of hybrid reinforcements (typically by using powder metallurgy route) and (ii) infiltration of molten metal or alloy into the porous preform to make the final composites structure. According to whether pressure is employed during infiltration process, this technique can be divided into pressure infiltration and pressure-less infiltration. For hybrid reinforced MMCs, this method is mainly used to synthesize Al and Mg matrix composites, and previous studies have demonstrated that this route is suitable for both continuous and discontinuous reinforcements [46–48]. Compared to stir casting and squeeze casting, this method has a higher chance to achieve uniform distribution of reinforcements. However, MMCs prepared by this method always exhibit low ductility due to the high volume of the reinforcements and coarse matrix grain size. Another drawback is that it is hard to conduct secondary thermo-mechanical treatment to further improve the mechanical performance.

Disintegrated melt deposition (DMD) is a novel cost-effective technique innovated by Gupta et al. in mid 1990s [7]. The schematic diagram of this technique is shown in Fig. 6. This method combines the advantages of spray processing and conventional stir casting, which can produce bulk MMCs by using higher superheat temperatures and lower impinging gas jet velocities. The merits of DMD method include uniform distribution of reinforcements, fine matrix grain size and low porosity because of the high solidification rate of the atomized metal melt leading to superior mechanical properties [7]. This method is also designed to provide almost 100% yield of the pored metals/alloys/composites. Sankaranarayanan et al. [49] have successfully synthesized hybrid micron Ti particles and nano-alumina particles reinforced Mg matrix composites by using ball milling assisted DMD technique, and reported that the enhanced strength was accompanied by the retention of ductility.

3.1.3. Other processing methods

In addition to the above powder metallurgy and liquid metallurgy processing routes, there are also some special methods adopted to fabricate hybrid reinforced MMCs, such as friction stir processing (FSP) and accumulative roll bonding (ARB) processing.

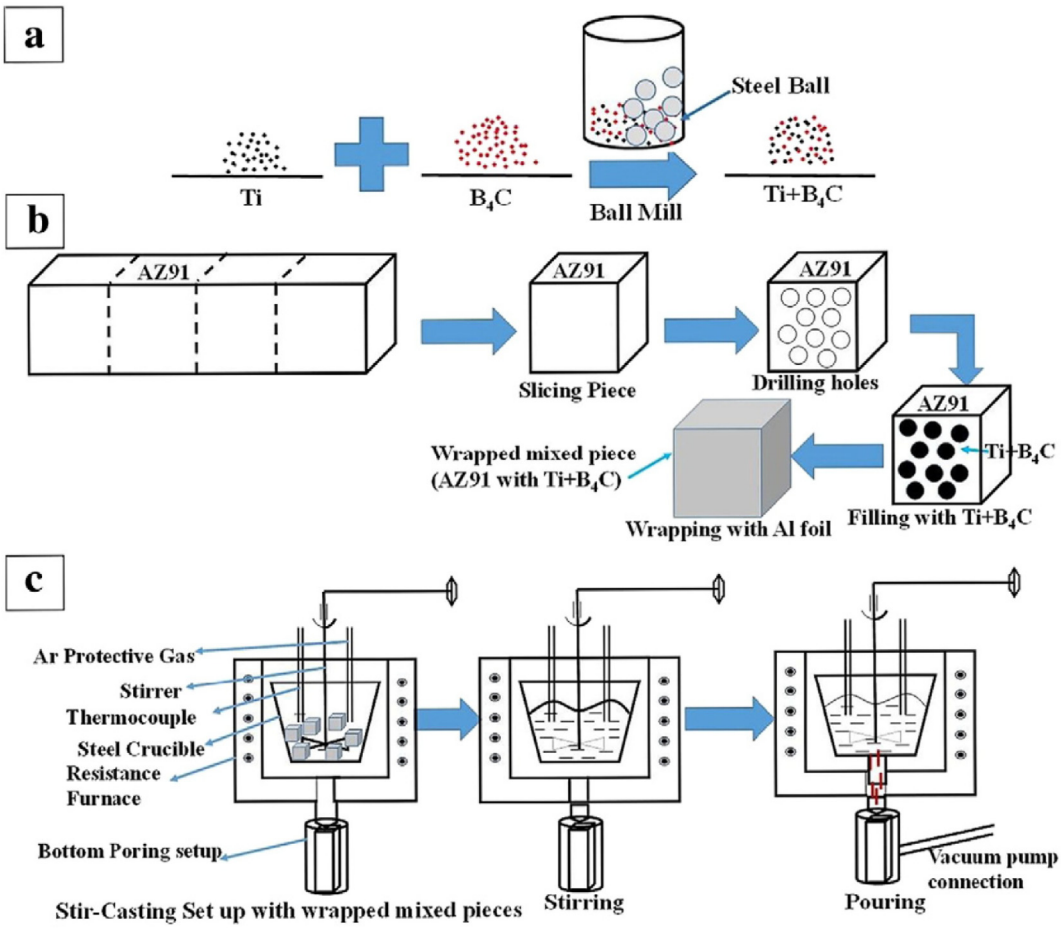

Fig. 13. Schematic illustration of fabrication process of in-situ hybrid TiC and TiB_2 reinforced Mg matrix composite [68].

The former process, derived from the modification of friction stir welding, is a novel severe plastic deformation (SPD) technique. The main idea of this method is to disperse reinforcements uniformly in metallic matrix and refine grain size via the rotation of tool pin. To produce hybrid MMCs, there are two ways to place the hybrid reinforcements. A long groove is cut on the surface of the metallic matrix in the path of tool followed by filling with reinforcements and treating with FSP (as shown in Fig. 7(a) [23]). Alternatively, hybrid reinforcements are introduced into the cavities drilled in a metallic plate followed by FSP (as shown in Fig. 7(b)) [50]. Eskandari et al. [51] successfully fabricated hybrid TiB_2 particles and Al_2O_3 particles reinforced Al matrix composites using FSP and found that the wear resistance of the processed hybrid nanocomposites over the un-reinforced matrix alloy was improved up to more than eight times due to the homogeneous distribution of the hybrid reinforcements. A similar result was also reported in a study on hybrid $ZrSiO_4$ and Al_2O_3 reinforced Mg matrix composites prepared by using FSP [52]. Moreover, FSP is also an effective technique for secondary mechanical treatment for the MMCs in order to obtain uniform distribution of reinforcements, especially nano-reinforcements, in the metallic matrix [53].

ARB processing is another novel SPD method, also known as sandwich processing, which can be used to produce MMCs with ultra-fine grains [54]. From Fig. 8, this method involves several steps: (i) annealing the metal strips or sheets, (ii) surface preparation through degreasing by acetone and scratching with a steel brush, (iii) adding reinforcements, (iv) stacking, and (v) roll bonding. In the third step, the reinforcements, especially nano-reinforcements, are usually dispersed in the dispersion solution, and subsequently sprayed onto the surfaces of the metal strips or sheets followed by drying in the air [55]. Electrophoretic deposition can also be used to disperse the reinforcements onto the metal strips, which has been demonstrated in the study on CNTs reinforced Mg [14] and Cu [56] matrix composites prepared by electrophoretic deposition and hot rolling. Baazamat et al. [57] produced hybrid WO_3 and SiC nanoparticles reinforced Al matrix nanocomposites through ARB process, and the results revealed that after 9 cycles, the hybrid nanocomposites exhibited an excellent distribution of the nanoparticles with good interfacial bonding between the reinforcements and the matrix. This technique may become popular for fabricating advanced MMCs with high performance due to its ease of processing [28].

3.2. In-situ processing techniques

In-situ methods involves synthesis of MMCs in which the reinforcements are generated in a metallic matrix by using chemical reactions between elements or between elements and compounds during the fabrication process of the composites [58]. Moreover, compared to the MMCs fabricated by using ex-situ processing techniques, the in-situ MMCs have three main merits [58]: (i) the reinforcements formed by in-situ reactions are thermodynamically stable in the metallic matrix, which can be employed in elevated-temperature services; (ii) the clean interface between in-situ reinforcements and metallic matrix always leads to a good interfacial bonding; (iii) the in-situ formed reinforcements are always fine in

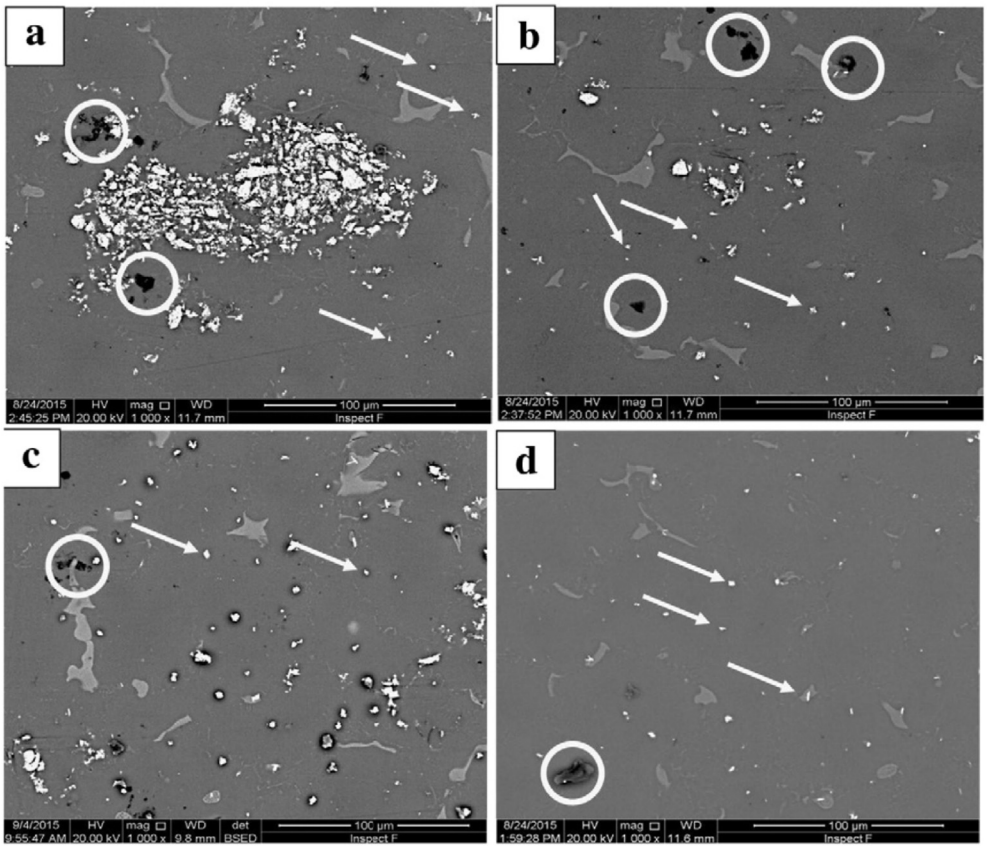

Fig. 14. SEM microstructure of in-situ hybrid TiC and TiB_2 reinforced Mg matrix composites fabricated at 900 °C with different holding time (a) 30 min, (b) 1 h, (c) 1.30 h and (d) 2 h [68].

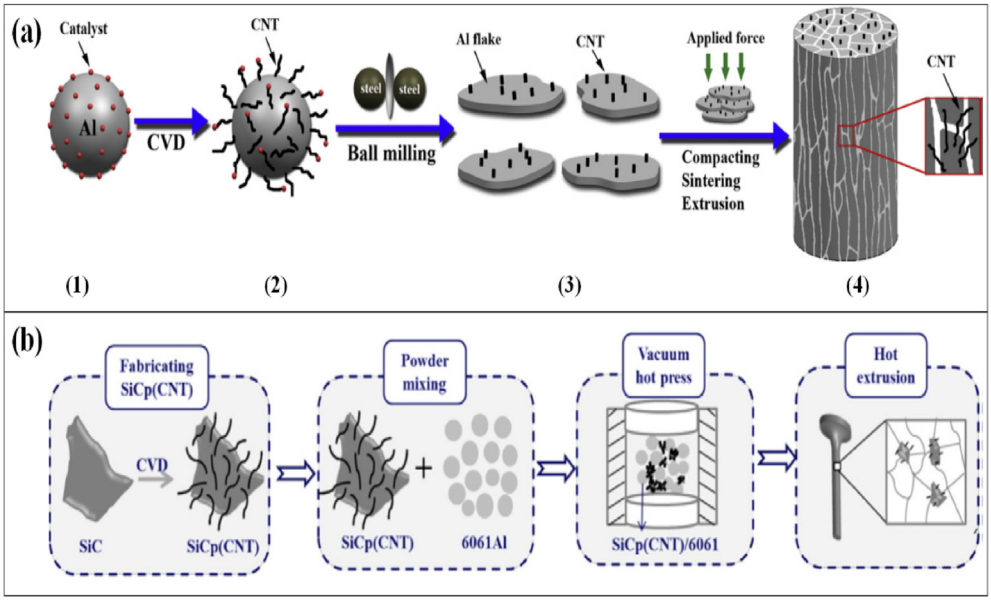

Fig. 15. Schematic illustration of the fabrication procedure of in-situ carbon nanomaterials reinforced MMCs: (a) metal powder carrier [77], (b) ceramic particle carrier [79].

size and distribute more homogenously in metallic matrix when compared to ex-situ reinforcements. Therefore, the in-situ MMCs exhibit superior room and elevated temperature mechanical performance due to the above mentioned advantages and hence have the great potential for widespread applications. Thus, more and more attention has been paid to develop new techniques and

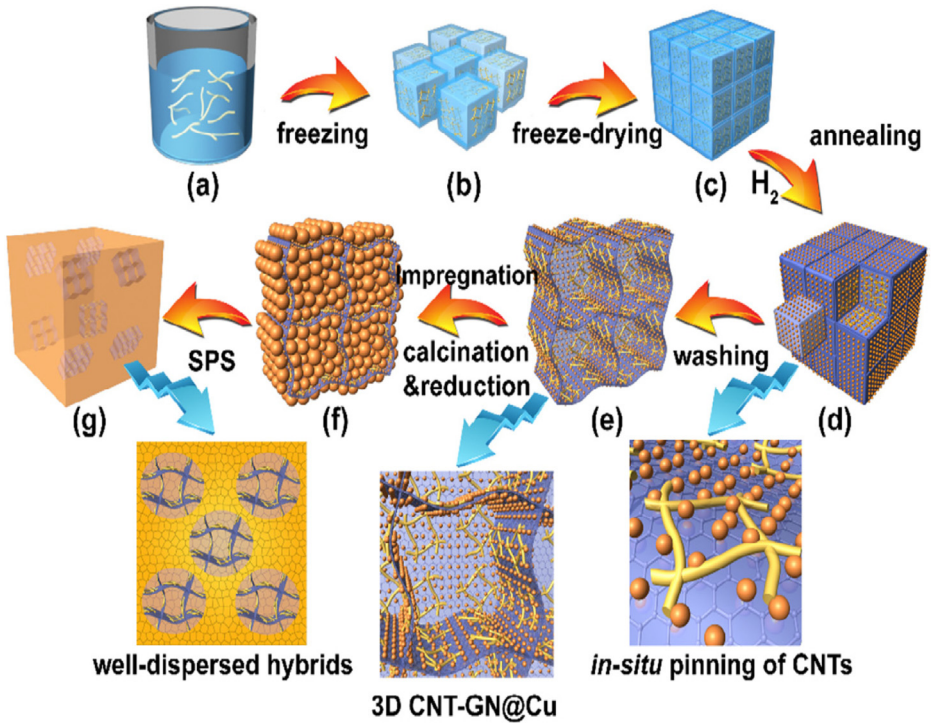

Fig. 16. Schematic illustration of the fabrication process of 3D CNT-GN/Cu bulk materials. (a) Mixed water suspension, (b) rapidly cooled solids and (c) freeze-dried assembled powders of CNTs–$C_6H_{12}O_6$–$Cu(NO_3)_2$–NaCl; (d) 3D CNT-GN@Cu NPs coated NaCl powders; (e) 3D CNT-GN@Cu NPs powders; (f) 3D CNT-GN@Cu encapsulated by impregnated reduced Cu particles; (g) 3D CNT-GN/Cu bulk composites [80].

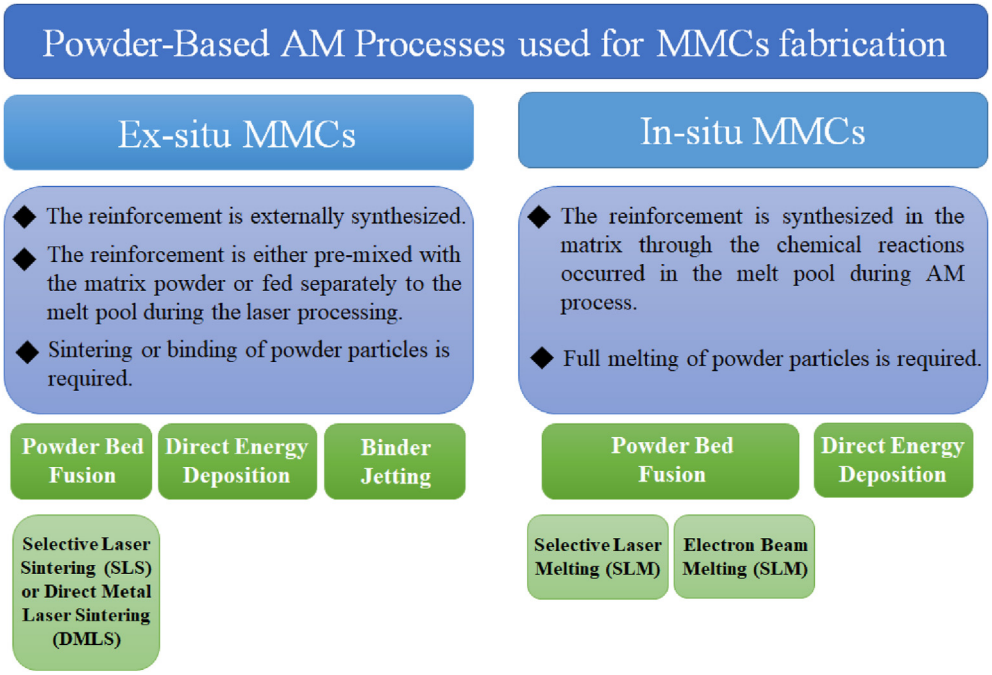

Fig. 17. Powder-based AM processes used for fabricating two different categories of MMCs [83].

optimizing processing parameters for in-situ methods during the past decades. According to the different types of in-situ reinforcements, we catagorized two groups of in-situ techniques: (i) in-situ ceramic phases, and (ii) in-situ carbonaceous materials.

3.2.1. *In-situ ceramic phases*

During the past three decades, a number of reactive systems have been developed to produce in-situ ceramic phases reinforced MMCs [58]. Among them Al, Ti, C and B are four most frequently

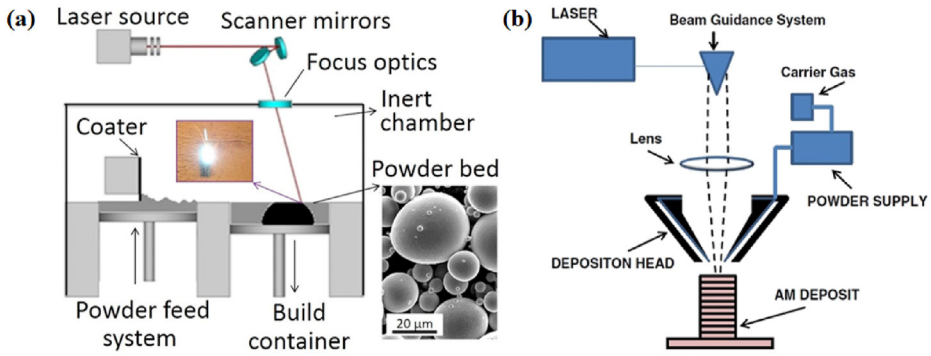

Fig. 18. Schematics of (a) the SLM/SLS process [85] and (b) laser deposition [86].

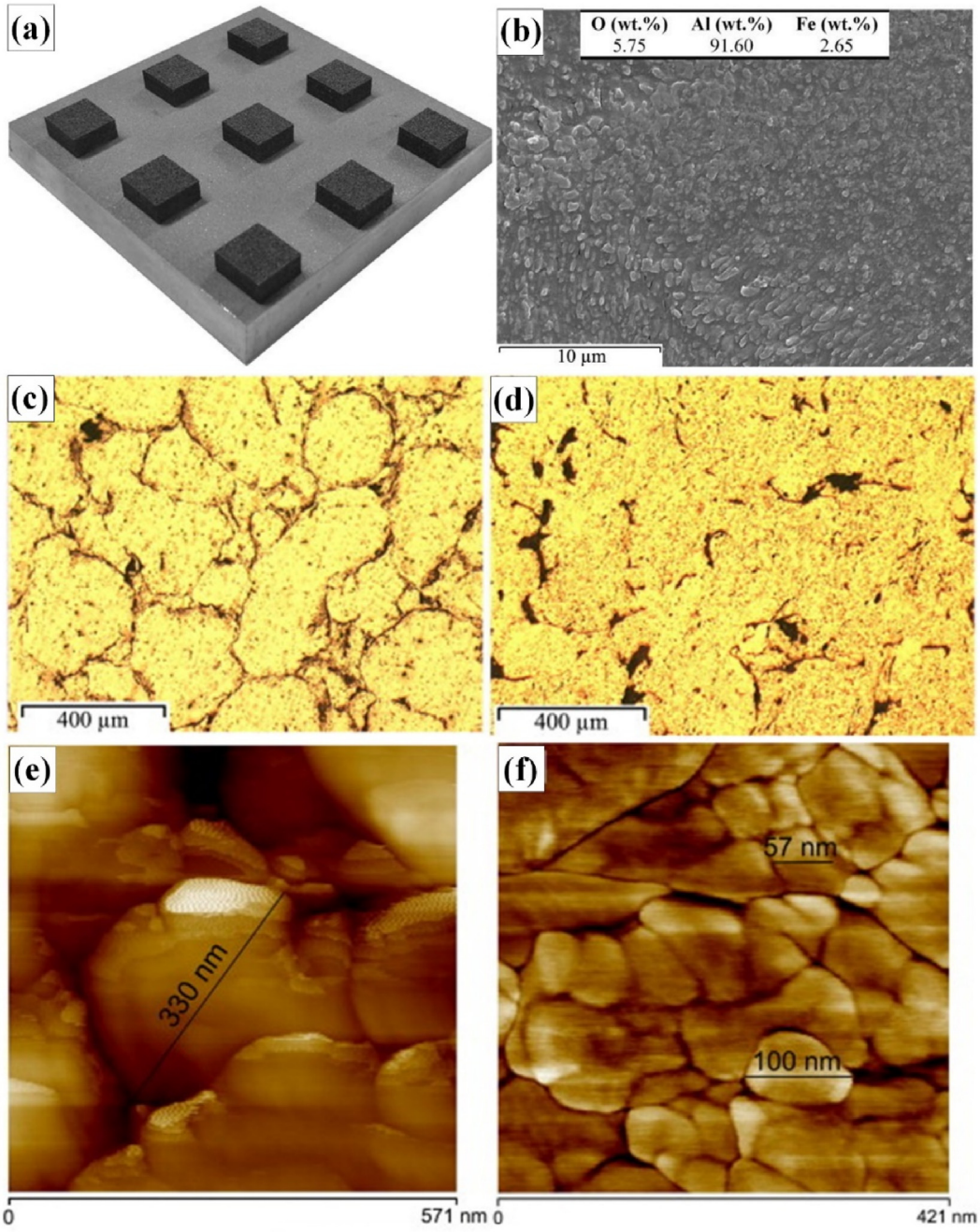

Fig. 19. (a) and (b) are the typical multilayer cubic parts and SEM morphology showing fine particles of Al/5 wt% Fe_2O_3 produced by SLM, respectively [87], (c) and (d) are polished surface of Al/5 wt% Fe_2O_3 and Al/15 wt% Fe_2O_3 produced by SLM, respectively [88], (e) and (f) are AFM images presenting ultrafine/nanoscale particles in the cross section of the SLM parts made from Al/15 wt%Fe_2O_3 and (c) AlSi10Mg/15 wt%Fe_2O_3, respectively [89].

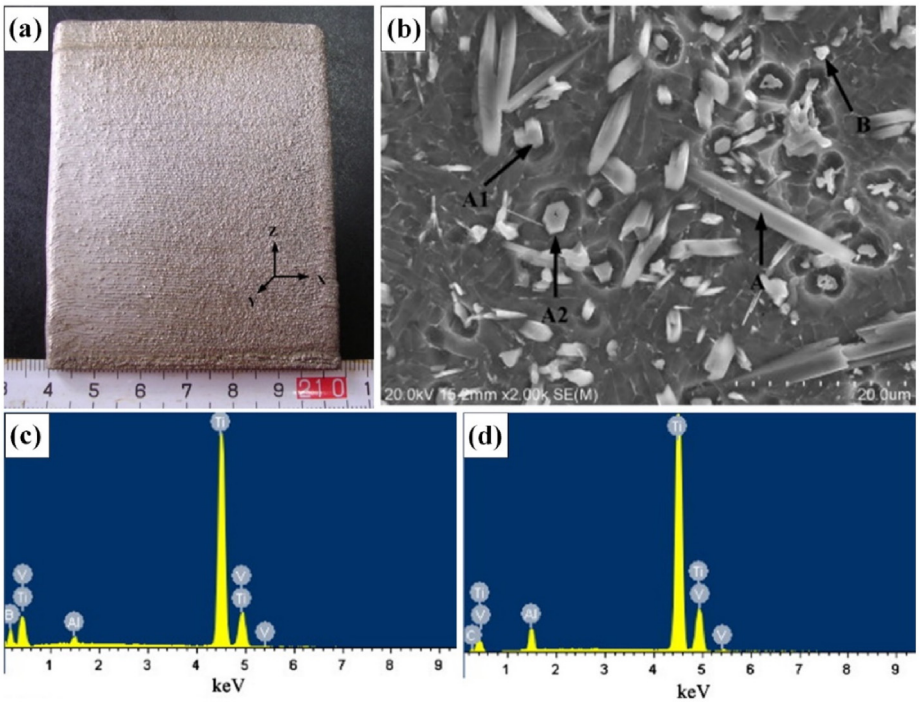

Fig. 20. (a) Appearance of laser direct deposited Ti matrix composite thin wall, (b) SEM morphology, (c) and (d) EDS for phases shown by point A and point B, respectively [91].

used elements to form in-situ ceramic phases. The reaction equations of six typical reactive systems, i.e. Al—Ti—C, Al—Ti—B, Ti—C, Ti—B_4C, Ti—TiB_2, and molten salt system, are summarized in Table 2.

In general, all the ex-situ method can be utilized to prepare in-situ ceramic particles reinforced MMCs as long as the certain ex-situ method can provide suitable conditions for the in-situ reactions. Powder metallurgy and stir casting are two most commonly used routes to produce hybrid MMCs containing in-situ ceramic particles. In powder metallurgy route, ball milling is always employed to disperse the reactants or compounds uniformly onto the surfaces of metallic matrix powders. In this step, the appropriate parameters of ball milling should be chosen to avoid severe plastic deformation and oxidation [20]. The milled mixtures are subsequently compacted or hot-pressed and sintered at optimized parameters obtained via thermodynamic and kinetic calculations as well as experimental verifications. Compared to stir casting counterpart, the in-situ reinforcements formed in powder metallurgy route usually are distributed more homogeneously in the metallic matrix due to the effective dispersion conditions during ball milling. Ma et al. [63] fabricated in-situ hybrid Al_2O_3 and TiB_2 particulates reinforced Al matrix composites with superior mechanical properties by using powder metallurgy technique. High performance of the composite was attributed to the uniform distribution of the fine and equiaxed in-situ Al_2O_3 and TiB_2 particulates in Al matrix (Fig. 9 (a)) and the clean interfaces between the in-situ reinforcements and Al matrix (Fig. 9 (b)). Wei et al. [20] reported that the in-situ powder metallurgy method can also be conducted to prepare hybrid in-situ Ti alloy matrix composites with enhanced high-temperature oxidation resistance due to formation of hybrid (TiC particles + TiB whiskers) networks (as shown in Fig. 10).

In-situ stir casting route refers to a technique in which reactant powders or compacts of reactant powders, are directly added into metallic melt and the in-situ ceramic reinforcements are formed through the direct reaction between the reactants or between reactants and some components of the metallic melt [58,64]. Selvam et al. [59] prepared hybrid in-situ TiB_2 and Al_2O_3 particles reinforced 6061 alloy matrix composites by directly adding Ti and boric oxide (H_3BO_3) powders into the molten Al alloy. A homogenous distribution of both particles with good interfacial bonding was successfully achieved (as shown in Fig. 11). Nakata et al. [65] prepared different kinds of in-situ carbide particulates, such as TiC, ZrC and TaC, reinforced Al matrix composites based on the reaction between Al alloy melt containing thermodynamically stable carbide formation element, such as Ti, Zr and Ta, and relative unstable carbides such as Al_4C_3 and SiC as the carbon source. Some mixed salts containing reactive elements, such as K_2TiF_6+KBF_4, Na_3AlF_6+KBF_4, and K_2TiF_6+ KBF_4+ Na_3AlF_6 [58], can also be directly added into the molten metallic matrix to form in-situ reinforced MMCs. Zhang et al. [66] fabricated hybrid in-situ Al_3Zr and ZrB_2 particles containing Al matrix composites by magneto-chemistry in-situ reaction by direct addition of the mixed K_2ZrF_6+KBF_4 salts. The results revealed that the composites exhibited significantly enhanced dry sliding wear properties.

Some innovative ways were also employed to promote the uniform dispersion of the in-situ formed ceramic reinforcements. Liang et al. [67] designed a two-step method to fabricate hybrid in-situ TiB whiskers and TiB_2 particles reinforced Cu matrix composites. First, Cu—B and Cu—Ti master alloys with same weight were separately melted, and then the two molten master alloys were simultaneously poured into a mixer at the same speed to generate TiB whiskers and TiB_2 particles via in-situ reactions between Ti and B. The schematic diagram of this method is shown in Fig. 12. Homogenous distribution of the hybrid reinforcements in Cu matrix was obtained by this in-situ mixing cast technology. Sahoo et al. [68] proposed a new method to produce hybrid in-situ TiC and TiB_2 particulates reinforced Mg matrix composites. Fig. 13 shows the fabrication process of this method. By filling the ball milled Ti + B_4C powders into the drilled holes in the AZ91 alloy ingots, the hybrid in-situ TiC and TiB_2 particulates distributed more uniformly in the end composites. In addition, the authors found that the longer

Table 3
Typical hybrid reinforced Al matrix composites and their resulting properties in literature.

Matrix	Hybrid reinforcements (vol%)	Reinforcement type	Processing technique	YS (MPa)	UTS (MPa)	Ductility (%)	E (GPa)	Hardness (HV)	References
Al	20 $TiNi_{fiber-\mu m}$ + 20 $SiC_{p-\mu m}$	HCDMRs	Pressure infiltration	108	211	7.2	73	\	[96]
6061	(13 $Al_2O_{3\ short\ fiber}$ + 7 $Al_2O_{3p})_{\mu m}$	HMDRs	Squeeze casting	313	397	2.1	92.8	\	[97]
	(10 $Al_2O_{3\ short\ fiber}$ + 10 $Al_2O_{3p})_{\mu m}$	HMDRs	Squeeze casting	322	409	2.2	94.8	\	
	(7 $Al_2O_{3\ short\ fiber}$ + 13 $Al_2O_{3p})_{\mu m}$	HMDRs	Squeeze casting	333	408	1.8	95	\	
7075	(50 SiC_p + 5 $Cr_p)_{\mu m}$	HMDRs	Squeeze casting	451	549	0.8	\	\	[98]
6082	(2 Coconut ash + 8 $ZrO_{2p})_{\mu m}$ (wt%)	HMDRs	Stir casting	138	205	8.5	\	58 (HB)	[99]
1100	(Al_2O_{3p} + 10 $ZrC_p)_{\mu m}$	HMDRs	ARB (in-situ)	\	405	11.9	\	94	[69]
7075	(40 SiC_p + 5 $Ti_p)_{\mu m}$	HMDRs	Squeeze casting	527	626	1.2	\	\	[100]
A359	5 (SiC + $Si_3N_4)_{p-\mu m}$ (2:1) (wt%)	HMDRs	Squeeze casting	295 (C)	420 (C)	27.5 (C)	\	62	[101]
	10 (SiC + $Si_3N_4)_{p-\mu m}$ (2:1) (wt%)	HMDRs	Squeeze casting	318 (C)	441(C)	21 (C)	\	69	
	15 (SiC + $Si_3N_4)_{p-\mu m}$ (2:1) (wt%)	HMDRs	Squeeze casting	336 (C)	453 (C)	19.2 (C)	\	81	
7075	(5 HEA powder + 40 $SiC)_{p-\mu m}$	HMDRs	Squeeze casting	662	712	0.8	171	225 (HB)	[102]
Al	0.5 (CNTs + RGO)	HNDRs	PM (Flake)	244	300	12.1	76.5	\	[17]
	1.5 (CNTs + RGO)	HNDRs	PM (Flake)	358	415	8.2	83	\	
	3.0 (CNTs + RGO)	HNDRs	PM (Flake)	405	430	3.2	84.1	\	
A356	(Al_2O_{3p} + $Al_3Zr_p)_{nm}$	HNDRs	Magnetochemistry (in-situ)	340	394	4.7	\	\	[103]
Al	0.5 (GN + Cu_{p-nm}) (wt%)	HNDRs	PM + HE	121	190	20.3	\	102.1	[104]
	0.75 (GN + Cu_{p-nm}) (wt%)	HNDRs	PM + HE	140	224	17.5	\	123.4	
	1.0 (GN + Cu_{p-nm}) (wt%)	HNDRs	PM + HE	126	201	12.8	\	109.3	
Al	1 $Diamond_{\ p-nm}$+ 1 CNTs	HNDRs	PM	600(F)	759(F)	\	\	127	[105]
A356	(1.0 Al_2O_3 + 1.0 $SiC)_{p-nm}$ (wt%)	HNDRs	UA stir casting	221	322	7.5	\	\	[39]
Al	1.5 TiC_{p-nm} + 0.7 CNTs	HNDRs	Ball milling + HR	264	346	4.5	\	\	[106]
Al	0.8 CNTs+1.2 $SiC_{p-sub-\mu m}$ (wt%)	HMSDRs	PM + HR	226	323	11.4	\	\	[107]
2024	20 $SiC_{whisker-sub-\mu m}$ + 2 SiC_{p-nm}	HMSDRs	Squeeze casting	326	452	\	131	\	[44]
	20 $SiC_{whisker-sub-\mu m}$ + 2 SiC_{p-nm}	HMSDRs	Squeeze casting	361	450	\	128	\	
	20 $SiC_{whisker-sub-\mu m}$ + 2 SiC_{p-nm}	HMSDRs	Squeeze casting	553	607	\	129	\	
Al	2 CNTs + 0.5 $Ti_{p-\mu m}$ (wt%)	HMSDRs	PM	141	175	12.3	\	\	[108]
	2 CNTs + 2.0 $Ti_{p-\mu m}$ (wt%)	HMSDRs	PM	170	222	15.5	\	\	
Al−17Si	49.5 $B_4C_{p-\mu m}$ + 0.5 GNPs	HMSDRs	Semi-PM + infiltration	547(C)	709(C)	4.4C	\	182	[109]
2024	10 ($Al_3Zr_{p-\mu m}$ + Al_2O_{3p-nm})	HMSDRs	PM (in-situ)	175	261	2.3	\	\	[110]
2124	7.5 $SiC_{whisker-Sub-\mu m}$ + 7.5 $SiC_{p-\mu m}$	HMSDRs	PM	548	585	3.5	\	\	[111]
	5 $SiC_{whisker-Sub-\mu m}$ + 10 $SiC_{p-\mu m}$	HMSDRs	PM	503	552	3.4	\	\	
	3.75 $SiC_{whisker-Sub-\mu m}$ + 11.25 $SiC_{p-\mu m}$	HMSDRs	PM	477	526	3	\	\	
6061	7 ($SiC_{p-\mu m}$ + $CNTs_{-in-situ}$)	HMSDRs	PM + HE (in-situ CNTs)	365	428	8.5	98	\	[79]
	13 ($SiC_{p-\mu m}$ + $CNTs_{-in-situ}$)	HMSDRs	PM + HE (in-situ CNTs)	355	412	7	98	\	
Al	1 CNTs+1 $SiC_{p-sub-\mu m}$	HMSDRs	PM (SPS) + HR	214	292	15.8	\	\	[112]
	1 CNTs+3 $SiC_{p-sub-\mu m}$	HMSDRs	PM (SPS) + HR	236	319	9	\	\	
	1 CNTs+5 $SiC_{p-sub-\mu m}$	HMSDRs	PM (SPS) + HR	243	339	8.1	\	\	
Al	16.2 Al_3Ti_{p-nm} + 7.8 $Al_2O_{3p-sub-\mu m}$	HMSDRs	ARB	230	312	70	\	90	[113]
	16.2 Al_3Ti_{p-nm} + 7.8 $Al_2O_{3p-sub-\mu m}$	HMSDRs	ARB + SPS	580	635	22	\	211	
Al	$Al_3Ti_{p-\mu m-(in-situ)}$ + Al_2O_{3p-nm}	HMSDRs	PM (in-situ)	352	423	5.2	\	\	[114]
5083	Al_2O_{3p-nm} + $Gr_{p-\mu m}$	HMSDRs	FSP	240	372	16.5	\	\	[115]

Note: HEA: high-entropy alloy; UA: ultrasonic-assisted; (C): compressive strength; (F): flexure strength; HR: hot rolling; HE: hot extrusion.

holding time at 900 °C before casting can also lead to a more homogenous distribution of the hybrid reinforcements (Fig. 14).

In addition to above methods, a unique technology combining anodizing and accumulative rolling bonding is used to fabricate in-situ Al_2O_3 reinforced Al matrix composites. This method always involves the following steps: (i) the Al strips were anodized to form in-situ Al_2O_3 on the surfaces of the strips after annealing treatment followed by degreasing; (ii) dispersion of the ex-situ reinforcements on the surfaces of the anodized Al strips uniformly; (iii) the surface preparation for non-anodized Al strips; (iv) stacking of the anodized Al strips with ex-situ reinforcements and non-anodized Al strips; (v) accumulative rolling bonding. Hybrid $Al_2O_{3\ in-situ}$ + $ZrC_{\ ex-situ}$ [69], $Al_2O_{3\ in-situ}$ + $CNTs_{\ ex-situ}$ [70], $Al_2O_{3\ in-situ}$ + $TiC_{\ ex-situ}$ [71], and $Al_2O_{3\ in-situ}$ + $SiC_{\ ex-situ}$ [72] reinforced Al matrix composites were successfully fabricated using this method.

3.2.2. In-situ carbonaceous materials

In-situ synthesis of carbonaceous nanomaterials, such as CNTs and GNPs, in MMCs is an innovative and effective strategy to fabricate advanced MMCs with high performance. This method ensures homogenous dispersion and perfect structural integrity of the carbon nanomaterials after the fabrication process [2]. Powder metallurgy route is usually employed to fabricate these MMCs with in-situ carbon based nano-reinforcements. According to the different types of the carriers for the in-situ carbonaceous materials, this technique can be categorized into two groups: (i) the direct synthesis of carbon nanomaterials on metal matrix powders [73] and (ii) synthesis of carbon nanomaterials on the ceramic carriers, such as SiC and Al_2O_3 particles, and then their transfer into the matrix [74]. The former also has two different methods. For transition metal matrix, such as Cu, Fe, Co and Ni, the in-situ carbonaceous nanomaterials can be directly synthesized on these metal powders without using additional catalyst [2]. However, for other metallic matrices without catalytic function, such as Al [75] and Mg [76], the additional catalyst should be used to assist the growth of the carbon nanomaterials on the surface of metal powders. The schematic illustration of such a typical fabrication process is shown in Fig. 15 (a). This route always involves several steps, first, the additional catalyst particles are decorated on the metal powders through impregnation in the transition metal salt solution followed by drying and calcination in the protective atmosphere. The second step involves in-situ synthesis of the carbon nanomaterials, like CNTs, on metal powders by CVD. Finally, the composites powders containing in-situ carbon materials are compacted, sintered and hot extruded to the end MMC materials. Sometimes, ball milling is also employed to further disperse these in-situ nano-reinforcements and to promote a better interfacial bonding between metal powders [77].

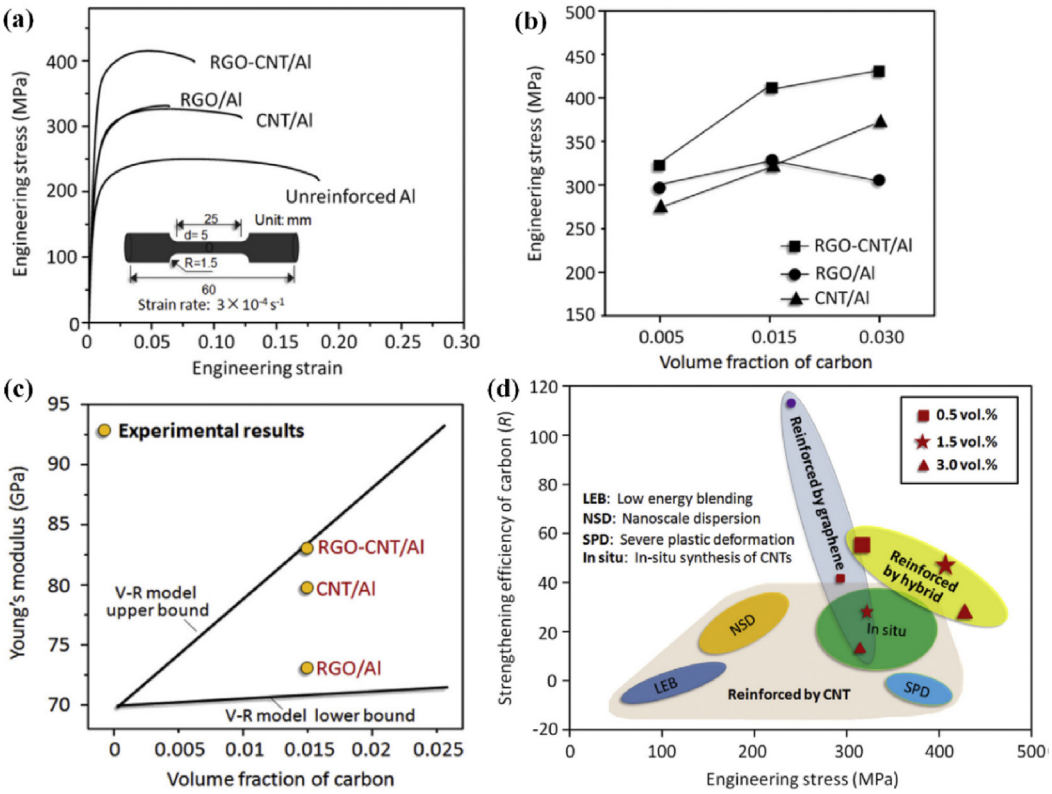

Fig. 21. (a) Stress-strain curves of Al and composites reinforced by 1.5 vol% of the hybrid, individual RGO, and individual CNT, (b) Comparison of the tensile strength of various composites reinforced by different volume fraction of carbon nanomaterials, (c) Comparison of the Young's modulus between experimental results and the values predicted by Voight-Reuss (V-R) model, (d) Comparison of the tensile strength and strengthening efficiency of carbon in RGO-CNT/Al composite with the reported CNT- and graphene-reinforced Al matrix composite systems [17].

Utilizing micron ceramic particles as the carrier of in-situ carbon nanomaterials is a promising way to fabricate advanced multi-scale hybrid reinforcements containing MMCs with excellent properties. The schematic is shown in Fig. 15 (b), and the process is similar to that of metal powder carrier. The main difference is that the catalyst particles are attached on the surface of the ceramic particle reinforcements rather than on metal matrix powders. Hybrid in-situ CNTs and SiC particles reinforced Al matrix composites [78] and hybrid in-situ CNTs and Al_2O_3 particles reinforced Mg matrix composites [74] have been successfully prepared by this method, and high mechanical performance of both these types of MMCs were reported.

A novel in-situ method was also proposed to fabricate well-dispersed 3D graphene (GN)/carbon nanotubes hybrid copper nanocomposites [80]. Fig. 16 shows the schematic diagram of this innovative method. In fact, this method involves in-situ synthesis of 3D graphene network and molecular level mixing. First, the CNTs functionalized with −COOH were dispersed in the solution of $C_6H_6O_6$-$Cu(NO_3)_2$-NaCl under ultrasonication followed by rapid freezing using liquid nitrogen to avoid agglomeration of CNTs. Then, the assembled powders of CNTs-$C_6H_6O_6$-$Cu(NO_3)_2$-NaCl were obtained by using the freeze-drying technology. Next, the assembled powders were calcinated and cooled rapidly to room temperature under H_2 atmosphere. The calcinated powder were subsequently washed with deionized water to obtain 3D CNT-GN@Cu powders. The 3D CNT-GN@Cu powders were further coated with copper through an impregnation-calcination-reduction process to achieve a uniform dispersion of 3D CNT-GN in Cu powders. Finally, the 3D CNT-GN/Cu bulk composite was produced by SPS method. A superior combination of strength and ductility was successfully achieved due to the well-dispersed 3D network structure of hybrid CNTs and GN by using this in-situ and molecular level mixing strategy.

3.3. Additive manufacturing

Additive manufacturing (AM), also known as 3D printing, has drawn worldwide attention in recent decades due to its advantages in the fabrication of complex shaped objects guided by a digital model [81]. For metallic materials, AM processes can be clarified into four types [82]: (I) powder bed fusion (PBF), (II) direct energy deposition (DED), (III) binder jetting, and (IV) sheet lamination. Although all of the AM processes could fabricate MMCs reinforced with either particulates or fibers, most of the studies focus on particulate reinforced MMCs prepared by powder-based processes [83]. The powder-based AM processes for MMCs can be divided into two major categories, i.e. ex-situ and in-situ reinforced MMCs (as shown in Fig. 17).

Among these powder-based methods, laser-based processes are particularly versatile to manufacture hybrid reinforced MMCs [83,84]. Fig. 18 shows the schematics of the selective laser melting/sintering and laser deposition processes. Hybrid MMCs fabricated by AM often contain in-situ reinforcement components. Dadbakhsh et al. [87] fabricated Al matrix composites containing hybrid in-situ Al_2O_3 and iron combinations (such as $Fe^{2+}Al_2O_4$) particles from a powder mixture of Al/5 wt % Fe_2O_3 by using selective laser melting. Fig. 19 (b) shows that the hybrid in-situ reinforcements distribute uniformly within the grains with a good particle/matrix interface.

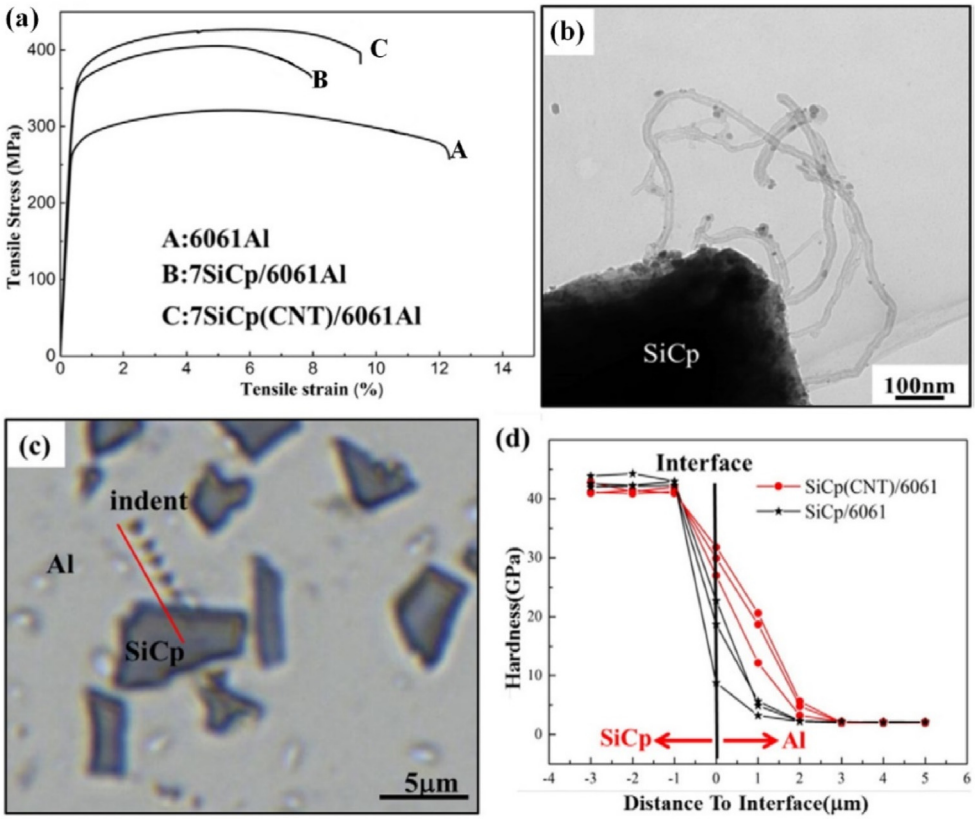

Fig. 22. (a) Stress-strain curves of 7 SiC_p(CNT)/6061Al, 7 SiC_p/6061Al composite and 6061Al matrix; (b) TEM image of 7 SiC_p(CNT) hybrid reinforcement; (c) OM image of a typical indentation array with 120 nm indentation depth and 1 μm indentation spacing; (d) variation of indentation hardness across the interface for 7 SiC_p/6061Al and 7 SiC_p(CNT)/6061Al composites treated under 3 different processing conditions [79].

The authors also investigated the effects of the Fe_2O_3 content [88] and alloying elements [89] on the microstructure and mechanical properties of the hybrid reinforced Al matrix composites. Fig. 19 (c) and (d) display the polished surface of Al/5 wt % Fe_2O_3 and Al/15 wt % Fe_2O_3 composites produced by SLM, respectively. It can be observed that grain boundaries disappear due to the intensified fusion of solid zones when the content of Fe_2O_3 increases up to 15 wt %. Fig. 19 (e) and (f) shows that the alloy composition of the main powder can significantly influence the SLM consolidation performance. By adding Si and Mg alloying elements, much finer in-situ particles typically around 50–100 nm in size were formed in the composites due to more intensive nucleation effects. The ultrafine in-situ hybrid reinforcements also led to significantly enhanced microhardness of the composites than that of Al alloys. Chang et al. [90] prepared in-situ Al_4SiC_4+SiC hybrid reinforced by adding SiC particles with different sizes to AlSi10Mg alloy via SLM method. They found that the microstructure of the composites could be influenced by the size of primary SiC particles due to the in-situ reaction between SiC and AlSi10Mg alloy matrix. Their results also revealed that the addition of fine SiC (5 μm) particles could remarkably improve the densification and microhardness of the hybrid reinforced Al matrix composites, which could be attributed to the homogeneous distribution of the residual SiC particles with a reduced size of 3 μm and plate-like and particle-structured in-situ Al_4SiC_4.

In addition to Al matrix composites, some hybrid Ti matrix and iron matrix composites were also successfully fabricated by using laser-based AM processes. Zhang et al. [91] prepared in-situ (TiB + TiC)/TC4 composites by adding mixed TC4 and B_4C powders via laser direct deposition process. They observed hybrid needle-like and prismatic TiB and granular TiC particles dispersed uniformly in the matrix, as shown in Fig. 20. Das et al. [92] employed laser direct deposition method to synthesize hybrid in-situ (TiB + TiN) reinforced Ti6Al4V alloy coatings by using premixed BN and Ti6Al4V powders. The microhardness and Young's modulus of the top surface of the coatings increased from 543 to 877 HV and from 170 to 204 GPa, respectively, as the BN content increased from 5 to 15 wt%, indicating great potential as wear-resistant contact surfaces. Song et al. [93] produced hybrid nano-micro SiC reinforced iron matrix composites by SLM process. They found that Fe/SiC composite displayed much higher strength than that of pure iron due to the combined effects of the presence of nanosized iron grains, amorphous iron, and the retained micro-scaled and nano-sized SiC particles.

Nano components of hybrid reinforcements are essential for obtaining excellent overall mechanical properties. However, based on the above discussion of processing techniques, the difficulty for fabricating hybrid MMCs containing nano particles is to distribute these nano reinforcements homogenously. As established over years, micron size reinforcements are much easier to be uniformly dispersed in metal matrix than their nano counterparts, thus, the micro reinforcements can be used as carriers to promote the dispersion of nano reinforcements, which has been demonstrated in above processing techniques (both ex-situ and in-situ methods). This strategy can be extended to more processing methods to effectively improve the strengthening efficiency of nano reinforcements. Therefore, multi-scale hybrid reinforced MMCs may achieve excellent overall properties by optimizing processing methods and contents, components and ratios of the hybrid reinforcements, and is likely to attract more and more attention in near future.

Table 4
Typical hybrid reinforced Mg matrix composites and their resulting properties in literature.

Matrix	Hybrid reinforcements (vol%)	Reinforcement type	Processing technique	YS (MPa)	UTS (MPa)	Ductility (%)	E (GPa)	Hardness (HV)	References
AZ91	45 $C_{f\text{-}\mu m}$ + $SiC_{nanowire}$	HCDMSRs	Vacuum infiltration	\	352	10.1	\	\	[118]
AZ91	$C_{f\text{-}\mu m}$ + CNTs	HCDMSRs	Squeeze casting	\	372	4.5	\	\	[119]
AM60	5 $Al_2O_{3\text{-short fiber-}\mu m}$+3 $Al_2O_{3p\text{-}\mu m}$	HMDRs	Squeeze casting	142	192	1.6	54	\	[120]
	5 $Al_2O_{3\text{-short fiber-}\mu m}$+3 $Al_2O_{3p\text{-}nm}$	HMSDRs		140	216	3.5	53	\	
AZ91	(TiC + TiB_2)$_{p\text{-}\mu m}$	HMDRs	Stir casting (in-situ)	95	202	5.4	\	\	[121]
	(TiC + TiB_2)$_{p\text{-}\mu m}$	HMDRs	Stir casting + FSP-1P (in-situ)	175	338	10.1	\	\	
	(TiC + TiB_2)$_{p\text{-}\mu m}$	HMDRs	Stir casting + FSP-2P (in-situ)	242	443	16.3	\	\	
AZ91	(TiC + TiB_2) $_{p\text{-}\mu m}$	HMDRs	Stir casting + T6 (in-situ)	228	328	6.6	\	129.6	[122]
AZ91	(TiC + TiB_2) $_{p\text{-}\mu m}$	HMDRs	Stir casting + HR (in-situ)	218	354	8	\	\	[123]
ZK60	24 ($SiC_{whisker\text{-}\mu m}$ + $B_4C_{p\text{-}\mu m}$)	HMDRs	Pressure infiltration	\	429	2.3	80.6	\	[124]
AZ91	(0.5 SiC+0.5 TiC)$_{p\text{-}nm}$ (wt%)	HNDRs	UA stir casting + HE	346	397	5.2	\	\	[125]
Mg	0.1 CNTs+0.5 GNPs (wt%)	HNDRs	Semi-PM	185	234	16.4	\	56	[21]
Mg	0.3 CNTs+0.7 $SiC_{p\text{-}nm}$ (wt%)	HNDRs	PM	153	195	3.3	\	46	[22]
	0.5 CNTs+0.5 $SiC_{p\text{-}nm}$ (wt%)	HNDRs	PM	152	188	2.3	\	45	
	0.7 CNTs+0.3 $SiC_{p\text{-}nm}$ (wt%)	HNDRs	PM	140	183	2.1	\	44	
AZ31	9 $SiC_{p\text{-}\mu m}$+1 $SiC_{p\text{-}nm}$	HMSDRs	UA stir casting + HE	323	402	8.3	\	\	[18]
AZ31	1.5 $Al_2O_{3p\text{-}nm}$+0.5 $Cu_{p\text{-}sub\text{-}\mu m}$	HMSDRs	PM	242	311	8.7	\	77.7	[126]
	1.5 $Al_2O_{3p\text{-}nm}$+1.0 $Cu_{p\text{-}sub\text{-}\mu m}$	HMSDRs	PM	252	328	9.3	\	83.3	
	1.5 $Al_2O_{3p\text{-}nm}$+1.5 $Cu_{p\text{-}sub\text{-}\mu m}$	HMSDRs	PM	289	354	5.5	\	90.9	
AZ61	5.0 $SiC_{p\text{-}\mu m}$ + 0.1 CNTs	HMSDRs	PM + HE	262	345	7.4	\	114	[33]
	5.0 $SiC_{p\text{-}\mu m}$ + 0.2 CNTs	HMSDRs	PM + HE	292	376	7.6	\	118	
	5.0 $SiC_{p\text{-}\mu m}$ + 0.5 CNTs	HMSDRs	PM + HE	345	412	8	\	126	
	5.0 $SiC_{p\text{-}\mu m}$ + 1.0 CNTs	HMSDRs	PM + HE	368	420	4.7	\	128	
Mg	5.6 $Ti_{p\text{-}\mu m}$+0.5 $SiC_{p\text{-}nm}$	HMSDRs	DMD + HE	167	228	9.6	\	74	[127]
	5.6 $Ti_{p\text{-}\mu m}$+1.0 $SiC_{p\text{-}nm}$	HMSDRs	DMD + HE	204	260	9.2	\	83	
	5.6 $Ti_{p\text{-}\mu m}$+2.0 $SiC_{p\text{-}nm}$	HMSDRs	DMD + HE	192	250	4.6	\	86	
Mg	1 ($Al_2O_{3p\text{-}\mu m}$ + $CNTs_{in\text{-}situ}$) (wt%)	HMSDRs	PM + HE (in-situ CNTs)	\	213	4.4	\	62	[128]
	2 ($Al_2O_{3p\text{-}\mu m}$ + $CNTs_{in\text{-}situ}$) (wt%)	HMSDRs	PM + HE (in-situ CNTs)	\	239	4.9	\	63	
	4 ($Al_2O_{3p\text{-}\mu m}$ + $CNTs_{in\text{-}situ}$) (wt%)	HMSDRs	PM + HE (in-situ CNTs)	\	243	5.2	\	65	
AZ31	1.5 $Al_2O_{3p\text{-}\mu m}$+0.2 $SiC_{p\text{-}nm}$ (wt%)	HMSDRs	Semi-PM	198	293	10.6	\	67	[129]
	1.5 $Al_2O_{3p\text{-}\mu m}$+0.5 $SiC_{p\text{-}nm}$ (wt%)	HMSDRs	Semi-PM	208	306	7.5	\	78	
	1.5 $Al_2O_{3p\text{-}\mu m}$+1.0 $SiC_{p\text{-}nm}$ (wt%)	HMSDRs	Semi-PM	230	322	4.3	\	92	
AZ31	4 $SiC_{p\text{-}\mu m}$+1 $SiC_{p\text{-}nm}$	HMSDRs	UA stir casting + HE	224	302	7.4	\	\	[24]
	9 $SiC_{p\text{-}\mu m}$+1 $SiC_{p\text{-}nm}$	HMSDRs	UA stir casting + HE	250	315	4.1	\	\	
	14$SiC_{p\text{-}\mu m}$+1 $SiC_{p\text{-}nm}$	HMSDRs	UA stir casting + HE	274	362	3.7	\	\	

4. Mechanical properties

The primary motive for adding hybrid reinforcements into a metallic matrix is to achieve significantly enhanced mechanical properties. Final performance of the hybrid MMCs depends on metallic matrix systems, hybrid reinforcement types and contents, and the fabrication technique due to its significant role in the dispersion and structural integrity of reinforcements and interfacial bonding between metallic matrix and reinforcements [28]. In this section, brief reports, specific to several MMC systems (Al, Mg, Ti, Cu, Fe/steel and Ni), on improved mechanical properties are presented, respectively. In addition, strengthening mechanisms triggered by hybrid reinforcements are also discussed in detail in the last part of this section.

4.1. MMC systems with hybrid reinforcements

4.1.1. Hybrid Al matrix composites

Al and its alloys have become the most popular and most commonly used base matrices in MMCs due to their great weight loss potential. Al matrix composites, combining the advantages of the matrix and reinforcements, exhibit higher mechanical properties, lower thermal expansion coefficient and higher corrosion resistance [94], which are critical for high-performance applications including aerospace, military, automotive, and electronic sectors [95]. For hybrid Al matrix composites, a large number of attempts have been made to further improve the mechanical and physical properties of the conventional Al matrix composites. Different fabrication techniques (ex-situ and in-situ) and different types of hybrid reinforcements (containing HCDRs, HMDRs, HNDRs, and HMSDRs) have been employed to prepare hybrid Al matrix composites. Table 3 compiles an overview of different Al matrices, hybrid reinforcement contents and types, fabrication methods, and mechanical properties at room temperature for hybrid Al matrix composites reported in the literature.

In this section, we mainly focus on the hybrid discontinuous reinforcements reinforced Al matrix composites due to their superior mechanical properties. For HMDRs, micron ceramic particles, graphite particles, short fibers, some metal particles, whiskers and even coconut ash have been used as a component of hybrid reinforcements to enhance the properties of Al-based composites. Many studies have shown that high volume of HMDRs are always used in these Al matrix composites (as shown in Table 3). Thus, high strength and high elastic modulus can be obtained, however, the ductility is poor [102]. In addition, researchers are also concerned about wear and physical properties of this kind of materials [98], which will be discussed in detail in subsequent sections.

HNDRs are composed of hybrid nano-particles containing nano ceramic particles and/or carbonaceous nanomaterials, such as CNTs and GNPs. Due to the strong van der Waals' force, the volume fraction of HNDRs added into metallic matrix is always less than 5 vol%. However, hybrid nano-reinforcements can achieve more uniform dispersion in metallic matrix than that of single nano-reinforcement due to the interactions between different kinds of nano particles, such as π-π interactions between CNTs and GNPs [116], leading to much higher mechanical properties in HNDRs Al matrix composites. Li et al. [17] fabricated hybrid CNTs and RGO reinforced Al matrix composites by using flake powder metallurgy route, a planar interconnected network of RGO-CNT hybrid as well as their well-aligned distribution was achieved due to π-π interactions between the hybrid

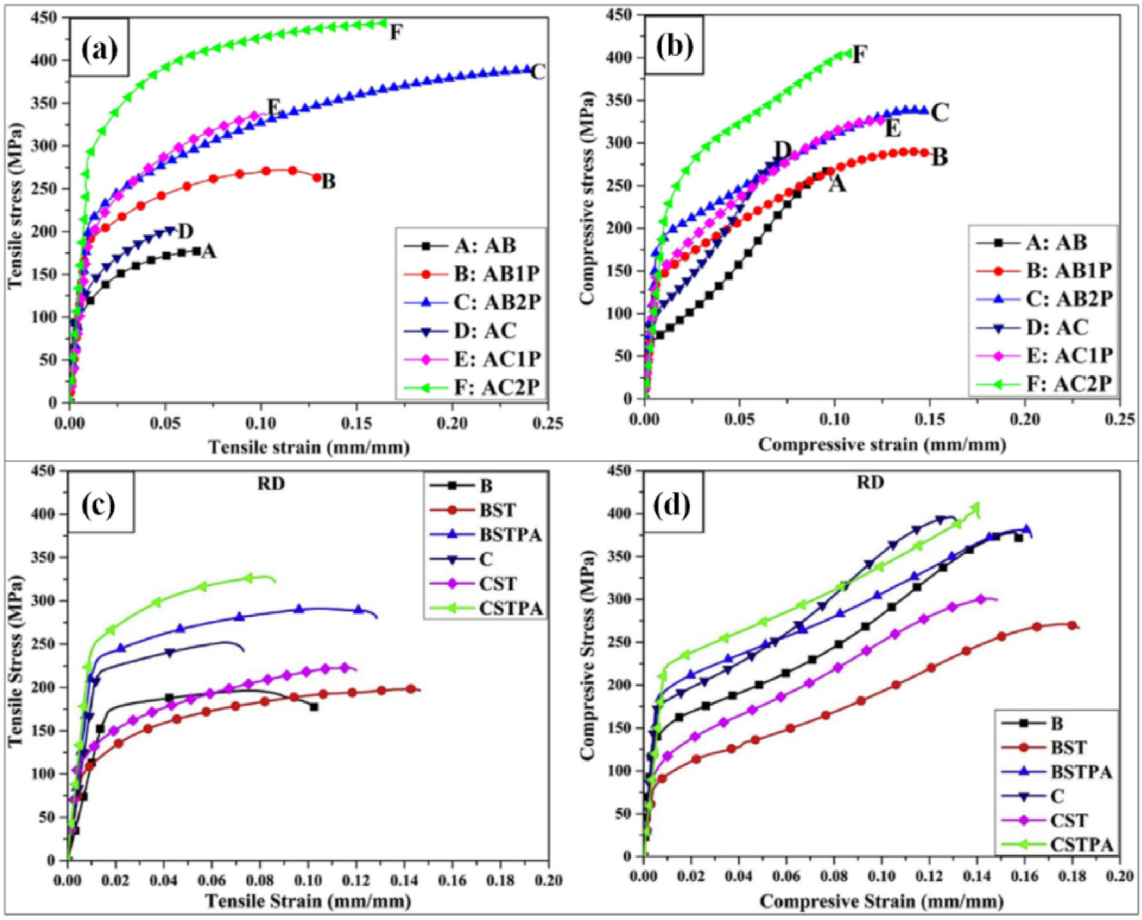

Fig. 23. Engineering stress-engineering strain curve: (a) as-cast and FSP-ed materials in tension test, (b) as-cast and FSP-ed materials in compression test, (c) as-rolled and heat-treated materials in tension test, and (d) as-rolled and heat-treated materials in compression test. (Note: AB: as-cast base; AC: as-cast composite; 1/2P: FSP pass; B: base, BST: base solution Treatment; BSTPA: base solution treatment peak aged; C: composite; CST: composite solution treatment; CSTPA: composite solution treatment peak aged) [121,123].

reinforcements. Fig. 21 shows the comparison of mechanical properties and strengthening efficiency of hybrid CNT-RGO reinforced and individual CNTs/RGO reinforced Al matrix composites. It is clear that the hybrid reinforced Al composites exhibit much higher strength and elastic modulus as well as strengthening efficiency than Al composites containing the same volume fraction of single CNTs/RGO, indicating that synergistic strengthening effect was successfully achieved. However, when the volume fraction of hybrid CNT-RGO reached 3.0 vol%, the ductility of the composite also drops sharply, in addition, the strengthening efficiency also decreases with the increase in the volume fraction of the hybrid reinforcements. Thus, choosing appropriate content of the hybrid nano-reinforcements is very important for obtaining MMNCs with high mechanical performance.

HMSDRs usually contain micron, nano, and/or sub-micron reinforcements involving ceramic particles, whiskers and carbon nanomaterials, such as CNTs and GNPs. This kind of hybrid reinforcements combine the advantages of micron reinforcements and nano reinforcements, which may be a promising strategy to obtain superior mechanical performance of the hybrid MMCs with combination of high strength and good ductility. Li et al. [79] fabricated a nano/micro-sized hybrid reinforcement reinforced 6061Al matrix composites by using a novel powder metallurgy approach, in which CNTs were homogeneously grown on the surface of micro-sized SiC_p, and then the hybrid reinforcements were dispersed uniformly in the matrix by using ball milling. A striking improvement in tensile properties was achieved due to the remarkable strengthening effect of the hybrid reinforcements, which can be attributed to the increase of the "punched zone" size with the presence of CNTs on the surface of SiC_p (see Fig. 22).

4.1.2. Hybrid Mg matrix composites

Mg and its alloys are lightest structural metals, which are much lighter than other commonly used metals such as Al (−33%), Ti (−61%), and steel (−77%), making them promising candidates for applications in automotive, aerospace as well as consumer electronic industries [7]. Additionally, Mg alloys possess various other advantages involving high damping capacity, good electromagnetic shielding and ease of machinability. However, they also have some limitations including low absolute strength and elastic modulus, high corrosion rate, and poor creep resistance. Adding reinforcements, especially hybrid reinforcements, into Mg matrix to create Mg-based composites with high performance is an effective measure to overcome these limitations [117]. Compared to hybrid reinforced Al matrix composites, the number of reports on hybrid reinforced Mg matrix composites are fewer, but due to the compelling need for lightweight, Mg-based composites will play an increasingly important role and will attract more and more attention in very near future. Table 4 lists the typical hybrid Mg matrix composites and their properties reported in literature.

Similar to hybrid Al matrix composites, the successfully fabricated Mg matrix composites containing different types of hybrid reinforcements (containing HCDRs, HMDRs, HNDRs, and HMSDRs) have been reported, and the matrices used are mainly pure Mg and Mg—Al—Zn alloys (as shown in Table 4). Sahoo et al. [121] fabricated

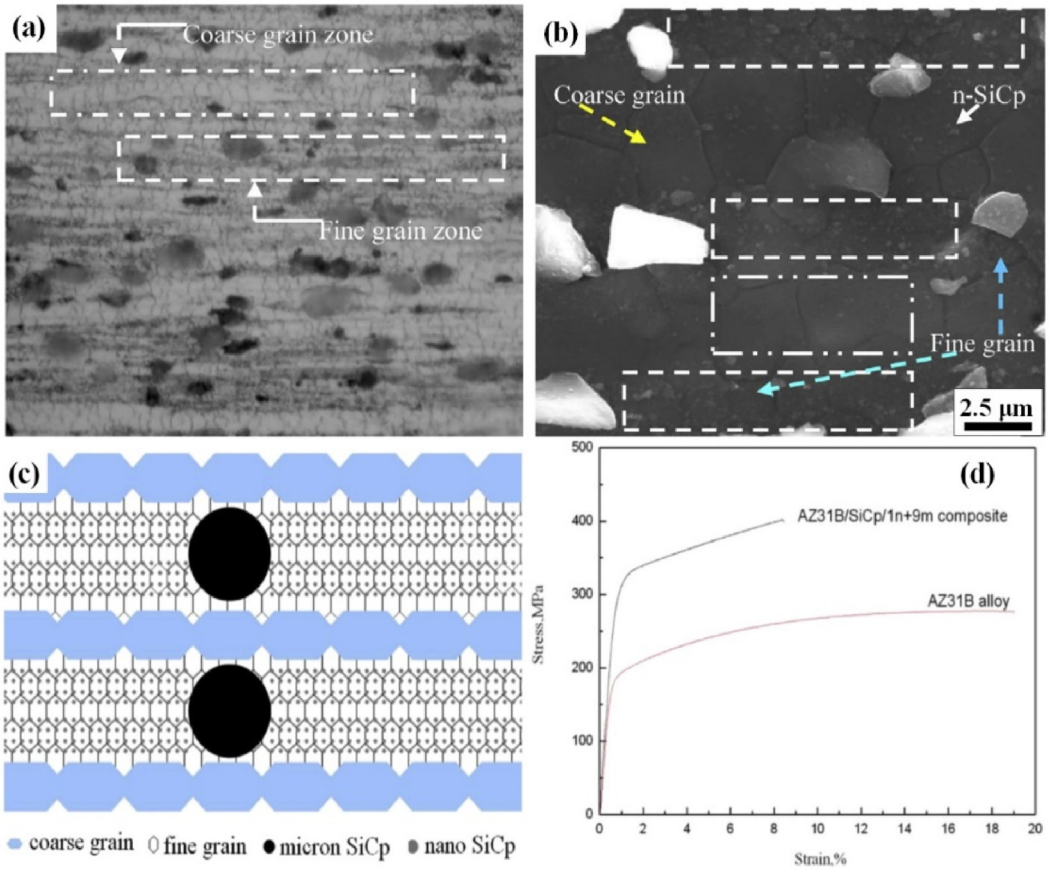

Fig. 24. (a) (b) OM and SEM image of as-extruded AZ31B/SiC_p/1n+9 m composite, respectively, (c) schematic illustration of the SiCp (nano and micron) distribution and microstructural evolution in the AZ31B/SiC_p/1n+9 m composite after hot extrusion, and (d) tensile strain-stress curves of AZ31B and its composite [18].

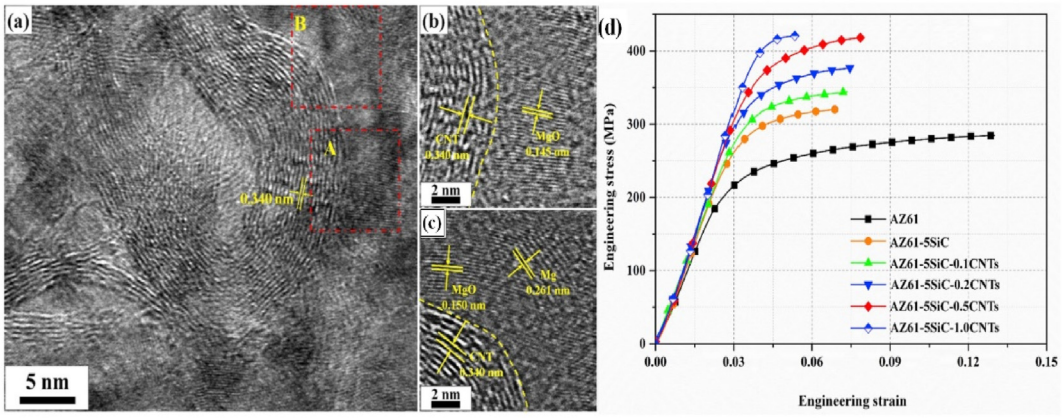

Fig. 25. (a) HRTEM image showing interfacial microstructure in AZ61-5SiC-0.5 CNTs composite, (b) (c) partial enlargement at selection region (A and B, respectively), and (d) engineering tensile stress-strain curves of AZ61 and its composites [33].

hybrid in-situ micron TiC—TiB_2 particles reinforced AZ91 alloy matrix composites by using stir casting method. The composites were also subjected to thermal-mechanical treatment, such as FSP and hot rolling, and/or heat treatment to further improve their mechanical properties. The simultaneously enhanced strength and ductility of the composites were reported after hot rolling and heat treatment, which is shown in Fig. 23. In addition, the tension-compression yield asymmetry of the secondary treated composites was significantly reduced due to suppression of the twin nucleation and growth caused by the presence of in-situ hybrid reinforcements and precipitates [123].

Several attempts on multi-scale hybrid reinforced Mg matrix composites have been conducted recently, and good combination of high strength and good ductility in several works have been obtained. Shen et al. [18] developed a new method to construct the bimodal size grained microstructure of the AZ31 alloy matrix

Table 5
Typical hybrid Ti matrix composites and their properties reported in literature.

Matrix	Hybrid reinforcements (vol%)	Reinforce-ment type	Processing technique	YS (MPa)	UTS (MPa)	Ductility (%)	E (GPa)	Hardness (HV)	Ref.
Ti−6Al−4V	0.5 (TiC_{p} + Ti_3SiC_{2bar} + $Ti_5Si_{3needle}$)-μm	HMDR	PM (in-situ)	850	944	13.8	117.2	\	[133]
	1.0 (TiC_{p} + Ti_3SiC_{2bar} + $Ti_5Si_{3needle}$)-μm	HMDR	PM (in-situ)	867	969	11.7	119.5	\	
	2.0 (TiC_{p} + Ti_3SiC_{2bar} + $Ti_5Si_{3needle}$)-μm	HMDR	PM (in-situ)	891	1003	8.5	118.8	\	
	5.0 (TiC_{p} + Ti_3SiC_{2bar} + $Ti_5Si_{3needle}$)-μm	HMDR	PM (in-situ)	928	1064	5	122.8	\	
	8.0 (TiC_{p} + Ti_3SiC_{2bar} + $Ti_5Si_{3needle}$)-μm	HMDR	PM (in-situ)	1002	1064	2.9	129.2	\	
Ti	1.0 (Ti_5Si_{3rod} + Ti_2C_p)-μm	HMDR	PM (in-situ)	668	852	28.9	\	\	[134]
	3.0 (Ti_5Si_{3rod} + Ti_2C_p)-μm	HMDR	PM (in-situ)	789	868	6.58	\	\	
	5.0 (Ti_5Si_{3rod} + Ti_2C_p)-μm	HMDR	PM (in-situ)	846	858	1.53	\	\	
Ti−5Al−5Mo−5V−1Fe−1Cr	0.4 $TiB_{Whisker\text{-}\mu m}$ + 0.1 $TiC_{p\text{-}\mu m}$	HMDR	AM + HR (in-situ)	1070	\	18	\	\	[135]
TC4	1 (Ti_5Si_3 + $TiC_{0.67}$)$_{p\text{-}\mu m}$ (wt%)	HMDR	PM (in-situ)	1302(C)	1482(C)	19.2	\	421	[136]
	2 (Ti_5Si_3 + $TiC_{0.67}$)$_{p\text{-}\mu m}$ (wt%)	HMDR	PM (in-situ)	1313(C)	1605(C)	21.2	\	452	
	5 (Ti_5Si_3 + $TiC_{0.67}$)$_{p\text{-}\mu m}$ (wt%)	HMDR	PM (in-situ)	1482(C)	1711(C)	19.5	\	511	
	8 (Ti_5Si_3 + $TiC_{0.67}$)$_{p\text{-}\mu m}$ (wt%)	HMDR	PM (in-situ)	1620(C)	1778(C)	13.4	\	502	
	10 (Ti_5Si_3 + $TiC_{0.67}$)$_{p\text{-}\mu m}$ (wt%)	HMDR	PM (in-situ)	1706(C)	1826(C)	13	\	505	
TC4	2.53 $TiB_{Whisker\text{-}\mu m}$ + 0.63 $TiC_{p\text{-}\mu m}$	HMDR	PM (in-situ)	1078	\	17	\	\	[137]
	5.06 $TiB_{Whisker\text{-}\mu m}$ + 1.26 $TiC_{p\text{-}\mu m}$	HMDR	PM (in-situ)	1135	\	6.5	\	\	
	7.59 $TiB_{Whisker\text{-}\mu m}$ + 1.89 $TiC_{p\text{-}\mu m}$	HMDR	PM (in-situ)	1129	\	3	\	\	
Ti	8.29 $TiB_{Whisker\text{-}\mu m}$ + 1.71 $TiC_{p\text{-}\mu m}$	HMDR	AM + HF (in-situ)	1115	1229	3.3	132.6	\	[138]
	8.29 $TiB_{Whisker\text{-}\mu m}$ + 1.71 $TiC_{p\text{-}\mu m}$ + 0.59 $La_2O_{3p\text{-}sub\text{-}\mu m(nm)}$	HMSDR		1171	1299	4.2	129.5	\	
Ti−B20	(0.9 $TiB_{Whisker}$ +1.3 TiC_p)$_{\mu m}$	HMDR	AM + HF (in-situ)	1439	1554	5.8	\	\	[139]
	(0.9 $TiB_{Whisker}$ +1.3 TiC_p)$_{\mu m}$	HMDR	AM + HF + HT (in-situ)	1366	1425	13	\	\	
Ti−6Al−4V	1.5 $TiB_{Whisker\text{-}\mu m}$ + 1.5 $TiC_{p\text{-}\mu m}$	HMDR	PM (in-situ)	1066	1129	2.4	120.2	\	[140]
	2.5 $TiB_{Whisker\text{-}\mu m}$ + 2.5 $TiC_{p\text{-}\mu m}$	HMDR	PM (in-situ)	1100	1121	1.3	123.6	\	
Ti−6Al−4V	2.6 $TiB_{Whisker\text{-}\mu m}$ + 2.4 $TiC_{p\text{-}\mu m}$	HMDR	AM + HF + HE (in-situ)	1055	1129	12.6	\	\	[141]
Ti−6Al−4V	3.4 $TiB_{Whisker\text{-}\mu m}$ + 4 $Ti_5Si_{3p\text{-}\mu m}$	HMDR	PM (in-situ)	1050	1180	5	\	\	[142]
Ti−6Al-2.5Sn−4Zr-0.7Mo-0.3Si	2.5 ($TiB_{Whisker}$ + TiC_p)$_{\mu m}$	HMDR	AM + HF (in-situ)	1088	1169	5	\	\	[143]
	5 ($TiB_{Whisker}$ + TiC_p)$_{\mu m}$	HMDR	AM + HF (in-situ)	1103	1192	3.1	\	\	
	7.5 ($TiB_{Whisker}$ + TiC_p)$_{\mu m}$	HMDR	AM + HF (in-situ)	1146	1217	1.8	\	\	
Ti−6Al-2.5Sn−4Zr-0.7Mo-0.3Si	1.35 $TiB_{Whisker\text{-}\mu m}$ + 1.12 $TiC_{p\text{-}\mu m}$	HMDR	AM (in situ)	976	1040	2	128.3	\	[144]
	2.57 $TiB_{Whisker\text{-}\mu m}$ + 2.28 $TiC_{p\text{-}\mu m}$	HMDR	AM (in situ)	1009	1098	1.3	135.7	\	
	3.52 $TiB_{Whisker\text{-}\mu m}$ + 3.83 $TiC_{p\text{-}\mu m}$	HMDR	AM (in situ)	1077	1144	0.9	139.8	\	
Ti−Al−Sn−Zr−Nb−Mo−Si	1.82 $TiB_{whisker\text{-}\mu m}$ + $La_2O_{3p\text{-}sub\text{-}\mu m}$	HMSDR	AM + HR (in-situ)	1045.9	\	4.47	120.8	\	[145]
Ti−6Al−4V	0.79 $TiB_{Whisker\text{-}\mu m}$+0.09 $TiC_{p\text{-}\mu m}$ + 0.12 $La_2O_{3p\text{-}sub\text{-}\mu m(nm)}$	HMSDR	AM + HF (in-situ)	889	1041	3.6	\	\	[146]
	0.79 $TiB_{Whisker\text{-}\mu m}$+0.09 $TiC_{p\text{-}\mu m}$ + 0.12 $La_2O_{3p\text{-}sub\text{-}\mu m(nm)}$	HMSDR	AM + HF + HE (in-situ)	798	897	14.2	\	\	
	1.19 $TiB_{Whisker\text{-}\mu m}$+0.19 $TiC_{p\text{-}\mu m}$ + 0.12 $La_2O_{3p\text{-}sub\text{-}\mu m(nm)}$	HMSDR	AM + HF (in-situ)	875	942	2.7	\	\	
	1.19 $TiB_{Whisker\text{-}\mu m}$+0.19 $TiC_{p\text{-}\mu m}$ + 0.12 $La_2O_{3p\text{-}sub\text{-}\mu m(nm)}$	HMSDR	AM + HF + HE (in-situ)	801	925	13.2	\	\	
	1.60 $TiB_{Whisker\text{-}\mu m}$+0.28 $TiC_{p\text{-}\mu m}$ + 0.12 $La_2O_{3p\text{-}sub\text{-}\mu m(nm)}$	HMSDR	AM + HF (in-situ)	814	988	4.6	\	\	
	1.60 $TiB_{Whisker\text{-}\mu m}$+0.28 $TiC_{p\text{-}\mu m}$ + 0.12 $La_2O_{3p\text{-}sub\text{-}\mu m(nm)}$	HMSDR	AM + HF + HE (in-situ)	742	877	14.3	\	\	
Ti	10.8 $TiB_{Whisker\text{-}nm}$ + 2.76 $TiC_{p\text{-}\mu m}$	HMSDR	PM-SPS (in-situ)	916	1138	2.6	\	\	[147]
Ti	1.61 $TiC_{p\text{-}\mu m}$ + 6.89 $TiB_{whisker\text{-}sub\text{-}\mu m}$	HMSDR	PM-SPS + HE (in-situ)	\	1200	8.5	\	\	[148]
	2.70 $TiC_{p\text{-}\mu m}$ + 5.8 $TiB_{Whisker\text{-}sub\text{-}\mu m}$	HMSDR	PM-SPS + HE (in-situ)	\	1125	10	\	\	
	4.1 $TiC_{p\text{-}\mu m}$ + 4.4 $TiB_{Whisker\text{-}sub\text{-}\mu m}$	HMSDR	PM-SPS + HE (in-situ)	\	1032	9	\	\	
	5.53 $TiC_{p\text{-}\mu m}$+2.97 $TiB_{Whisker\text{-}sub\text{-}\mu m}$	HMSDR	PM-SPS + HE (in-situ)	\	950	11.5	\	\	
Ti	0.91 $TiC_{p\text{-}\mu m}$ + 3.87 $TiB_{Whisker\text{-}sub\text{-}\mu m}$	HMSDR	PM-SPS + HE (in-situ)	656	876	14.2	\	\	[149]
	1.58 $TiC_{p\text{-}\mu m}$ + 6.4 $TiB_{Whisker\text{-}sub\text{-}\mu m}$	HMSDR	PM-SPS + HE (in-situ)	766	995	7.8	\	\	
	2.76 $TiC_{p\text{-}\mu m}$ + 10.83 $TiB_{Whisker\text{-}sub\text{-}\mu m}$	HMSDR	PM-SPS + HE (in-situ)	916	1138	2.6	\	\	
Ti−6Al−4V	2.4 $TiC_{p\text{-}\mu m}$ + 2.6 $TiB_{Whisker\text{-}sub\text{-}\mu m}$	HMSDR	AM + HF + HE (in-situ)	968	1082	14.9	\	\	[150]

Note: AM: arc-melting; HF: hot forging; HT: heat treatment.

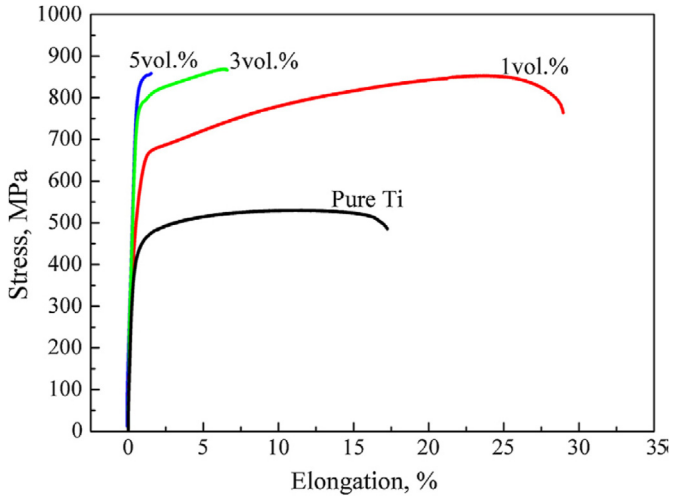

Fig. 26. Tensile stress–strain curves of the monolithic pure Ti and in situ (Ti_5Si_3 +Ti_2C)/Ti composites with a novel network microstructure fabricated by reaction hot pressing [134].

composites by adding bimodal sized SiC particles. The typical microstructure and tensile strain-stress curves are shown in Fig. 24. The fine grains were formed due to the particle stimulated nucleation (PSN) and grain boundary pinning effect. The coarse grains were obtained due to the formation of SiC free zones. The high strength can be attributed to the grain refinement, load transfer, thermal mismatch, and Orowan strengthening. The good ductility can be ascribed to the presence of coarse grains, which can enhance the strain hardening effect and act as crack arrester. Thus, a good combination of high strength and good ductility was successfully achieved.

Zhou et al. [33] proposed a multi-step dispersion method, which has been mentioned in Section 3.1, to fabricate hybrid multi-scaled micron SiC particles and CNTs reinforced AZ61 alloy matrix composites. Fig. 25 exhibits the interfacial microstructure and mechanical properties. High strength was achieved mainly due to grain refinement, load transfer and thermal mismatch strengthening mechanisms caused by the hybrid reinforcements. In addition, the higher amount of fine β-$Mg_{17}Al_{12}$ phase in composites also aided to improve strength. Moreover, the nano MgO on the surface of the hybrid reinforcements, formed by in-situ reactions between the groups containing oxygen and Mg element in the matrix were proposed to act as rivets to improve the interfacial bonding between the reinforcements and the matrix, leading to more efficient load transfer strengthening, and thus effectively enhancing the strength of the hybrid composites. The retention of good ductility of the composites with low CNTs contents (≤0.5 vol %) was attributed to weakened basal texture and grain refinement.

4.1.3. Hybrid titanium matrix composites

Titanium (Ti) and its alloys are promising structural materials in aerospace, automotive and defense sectors due to their light weight, high specific strength and excellent chemical resistance [130]. However, compared to steel and Ni-based alloys, the Young's modulus, heat resistance and wear resistance of Ti and its alloys are

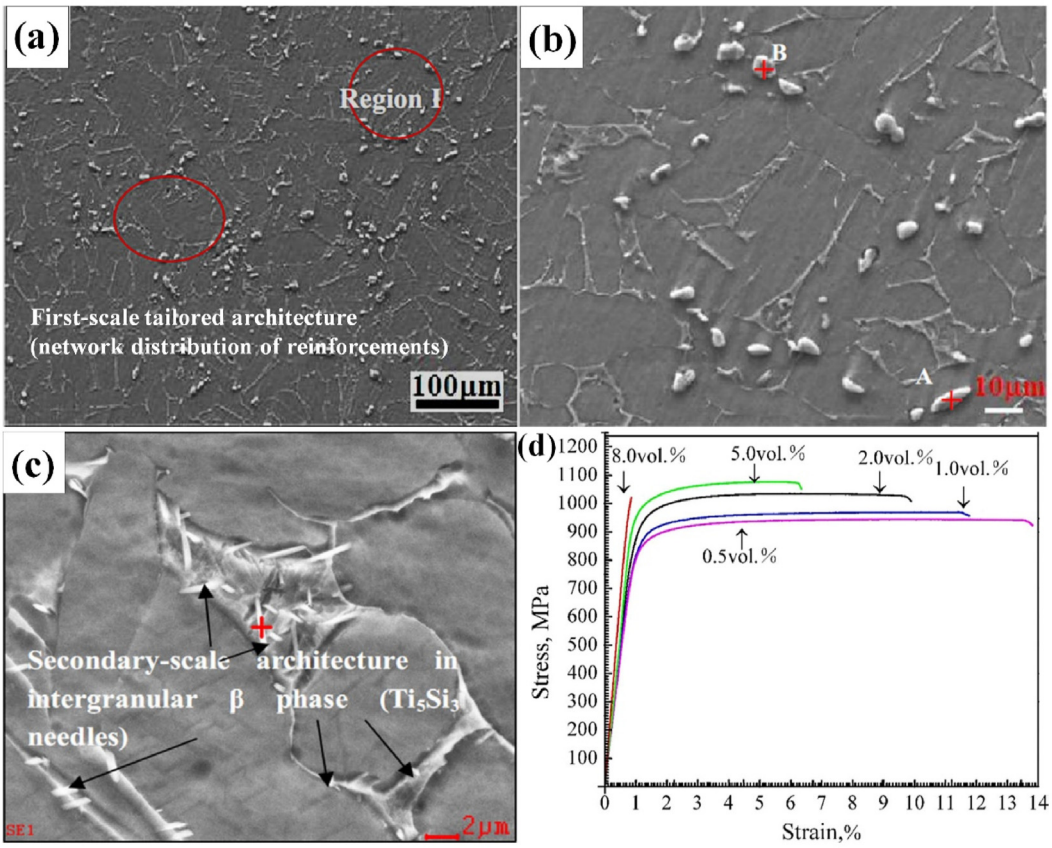

Fig. 27. (a) SEM micrographs (low magnification) of the composites, (b) SEM micrograph of the magnified Region I, (c) secondary-scale architecture in intergranular β phase (Ti_5Si_3 needles), and (d) the tensile stress-strain curves of 0.5, 1.0, 2.0, 5.0, 8.0 vol %, (TiC + Ti_3SiC_2+Ti_5Si_3)/Ti_6Al_4V composites [61].

Table 6
Hybrid reinforced Cu matrix composites and their properties reported in literature.

Matrix	Hybrid reinforcements (vol%)	Reinforcement type	Processing technique	YS (MPa)	UTS (MPa)	Ductility (%)	E (GPa)	Hardness (HV)	References
Cu	5 $(AlN + BN)_{p\text{-}\mu m}$	HMDR	FSP	97	160	14.1	\	75	[152]
	10 $(AlN + BN)_{p\text{-}\mu m}$	HMDR	FSP	99	175	12.7	\	76	
	15 $(AlN + BN)_{p\text{-}\mu m}$	HMDR	FSP	109	188	8.54	\	77	
Cu	(0.7 TiB_{2p} + 0.6 $TiB_{Whisker})_{sub\text{-}\mu m}$ (wt%)	HMDR	Casting + HR (in-situ)	437	471	7.2	\	\	[67]
	(1.0 TiB_{2p} + 0.9 $TiB_{Whisker})_{sub\text{-}\mu m}$ (wt%)	HMDR	Casting + HR (in-situ)	442	492	6	\	\	
	(1.4 TiB_{2p} + 1.2 $TiB_{Whisker})_{sub\text{-}\mu m}$ (wt%)	HMDR	Casting + HR (in-situ)	520	543	4.5	\	\	
Cu	0.5 Short $C_{f\text{-}\mu m}$ + 0.1 GO (wt%)	HMSDR	PM	60	184	22.8	\	60.3	[153]
	0.5 Short $C_{f\text{-}\mu m}$ + 0.4 GO (wt%)	HMSDR	PM	72	122	4.1	\	71.6	
Cu	1.5 (CNTs + RGO)	HNDR	PM (SPS)	308	412	4.5	\	\	[32]
Cu	0.35 $(CNTs + GNs_{\text{-in-situ}})$	HNDR	PM (SPS) (in-situ)	260	277	19	\	\	[80]
	1.15 $(CNTs + GNs_{\text{-in-situ}})$	HNDR	PM (SPS) (in-situ)	343	360	13	\	\	
Cu	1 $(RGO + Mo_2C_{p\text{-}nm})$	HNDR	PM (SPS)	238	292	17	\	\	[154]
Cu	0.6 $(RGO + Ag_{p\text{-}nm})$ (wt%)	HNDR	PM	332	478	23.8	\	\	[155]
Cu	2.5 RGO + 0.5 $SiO_{2p\text{-}nm}$ (wt%)	HNDR	PM (SPS)	\	365	31	\	54.1	[36]
	2.5 RGO + 1.5 $SiO_{2p\text{-}nm}$ (wt%)	HNDR	PM (SPS)	\	388	21.5	\	61.7	
	2.5 RGO + 2.5 $SiO_{2p\text{-}nm}$ (wt%)	HNDR	PM (SPS)	\	286	16.5	\	66.1	
Cu	0.5 $(GNs + Ni_{p\text{-}nm\text{-}in\text{-}situ})$	HNDR	PM (in-situ)	195	271	18.2	126	\	[156]
	1.0 $(GNs + Ni_{p\text{-}nm\text{-}in\text{-}situ})$	HNDR	PM (in-situ)	268	320	12.5	132	\	
Cu	2 $SiC_{p\text{-}nm}$ + 2 CNTs	HNDR	PM	258	\	\	125.5	92.3	[157]
	2 $SiC_{p\text{-}nm}$ + 4 CNTs	HNDR	PM	285	\	\	139.3	105.9	
	2 $SiC_{p\text{-}nm}$ + 6 CNTs	HNDR	PM	280	\	\	140.2	108.5	

relatively inferior, which hinder their wide applications to some extent. This can be circumvented by addition of ceramic particles or whiskers [131]. Thus, Ti matrix composites (TMCs) have seen significant development in the past three decades [132]. Typical hybrid Ti matrix composites and their resulting properties reported in literature are summarized in Table 5.

Compared to hybrid Al and Mg matrix composites, the hybrid reinforcement types are fewer in hybrid TMCs. Most of them are reinforced by hybrid micron ceramic particles and micron or submicron whiskers, especially TiC particles and TiB whiskers, and sometimes nano La_2O_3 particles are also employed as part of the hybrid reinforcements (as shown in Table 5). In addition, almost all the hybrid TMCs are prepared by in-situ method, whether by using powder metallurgy or arc melting. The strategy to obtain enhanced mechanical performance is through designing novel structure for hybrid TMCs, such as one-level network structure formed by hybrid TiC particles and TiB whiskers, which is shown in Fig. 10. Huang et al. [134] used this strategy to fabricate hybrid Ti_5Si_3 rods and Ti_2C particles reinforced pure Ti matrix composites, in which a network microstructure was successfully formed by in-situ reaction during hot pressing. Significantly enhanced strength and remarkable ductility (28.9%) were simultaneously achieved by forming a low volume fraction of in-situ hybrid reinforcements, which was ascribed to the tailored network microstructure and the refined matrix grains (Fig. 26). However, the ductility of the TMCs also decreased as the volume fraction of the in-situ hybrid reinforcements increased, although the strength could be further improved, indicating that the content of the hybrid reinforcements is an important factor to balance strength and ductility.

Liu et al. [61] designed a tailored two-scale architecture by using hybrid in-situ TiC particle, Ti_3SiC_2 bar and ultrafine Ti_5Si_3 needle reinforcements in Ti6Al4V composites. Microstructure and tensile response of these composites is shown in Fig. 27. The first-scale tailored architecture is the network formed by in-situ Ti_3SiC_2 bars and near equiaxed TiC particles (Fig. 27 (a) and (b)), and the secondary-scale architecture is the ultrafine Ti_5Si_3 needles precipitated in intergranular β phase, which distributed in center matrix particles (Fig. 27 (c)). Due to the unique two-scale architecture, the strength of the hybrid Ti6Al4V composites were effectively enhanced while maintaining good ductility (8.5%) when the volume fraction of the hybrid reinforcements reached 5 vol % (Fig. 27 (d)). Jiao et al. [151] also fabricated hybrid in-situ 4 vol % Ti_5Si_3 particles +1 vol % TiB whiskers containing Ti6Al4V composites with two-level network structures, and high strength (1150 MPa) and acceptable ductility (6.4%) were reported.

4.1.4. Hybrid Cu matrix composites

Cu and its alloys are important structural and functional materials due to their excellent electrical and thermal conductivity and chemical stability [25]. However, their poor mechanical properties, such as low absolute strength limits their wide uses. Introducing reinforcements, especially hybrid reinforcements, into Cu matrix to create Cu matrix composites with superior strength is an effective strategy to expand the scope of their applications. Table 6 lists the typical hybrid Cu matrix composites and their resulting properties reported in literature.

Liang et al. [67] fabricated hybrid TiB whiskers and TiB_2 particles reinforced Cu matrix composites by using an in-situ casting method followed by hot rolling, and ultra-high strengths with both YS and UTS exceeding 500 MPa were successfully achieved. However, the electrical conductivity dropped remarkably as the volume fraction of the reinforcements increased. When the strength reached the maximum value, the electrical conductivity only remained 75.2%. Similar results were also obtained in other research works in which other ceramic particles were employed as the reinforcements to fabricate Cu matrix composites [25].

Many studies have demonstrated that using CNTs and/or graphene as the reinforcement can significantly improve the mechanical properties of Cu and its alloys, while maintaining good thermal and electrical conductivity [2], thus making it possible to obtain Cu matrix composites with good structural-functional integration. Zhang et al. [80] fabricated well-dispersed three-dimensional graphene/carbon nanotube hybrid Cu nanocomposites using an in-situ space-confined method (mentioned in Section 3.2.2). Fig. 28 indicates that the balanced strength and ductility was achieved, and higher strengthening efficiency than that of most reported Cu matrix composite systems reinforced by different types of reinforcements was also obtained. They attributed the superior mechanical properties to the significant grain refinement and excellent load transfer caused by the in-situ 3D networks of hybrid reinforcements. Chen et al. [32] prepared Cu matrix composites reinforced with functionalized carbon nanotube-graphene hybrids by using powder metallurgy route, and a striking synergistic strengthening effect was also obtained in their work.

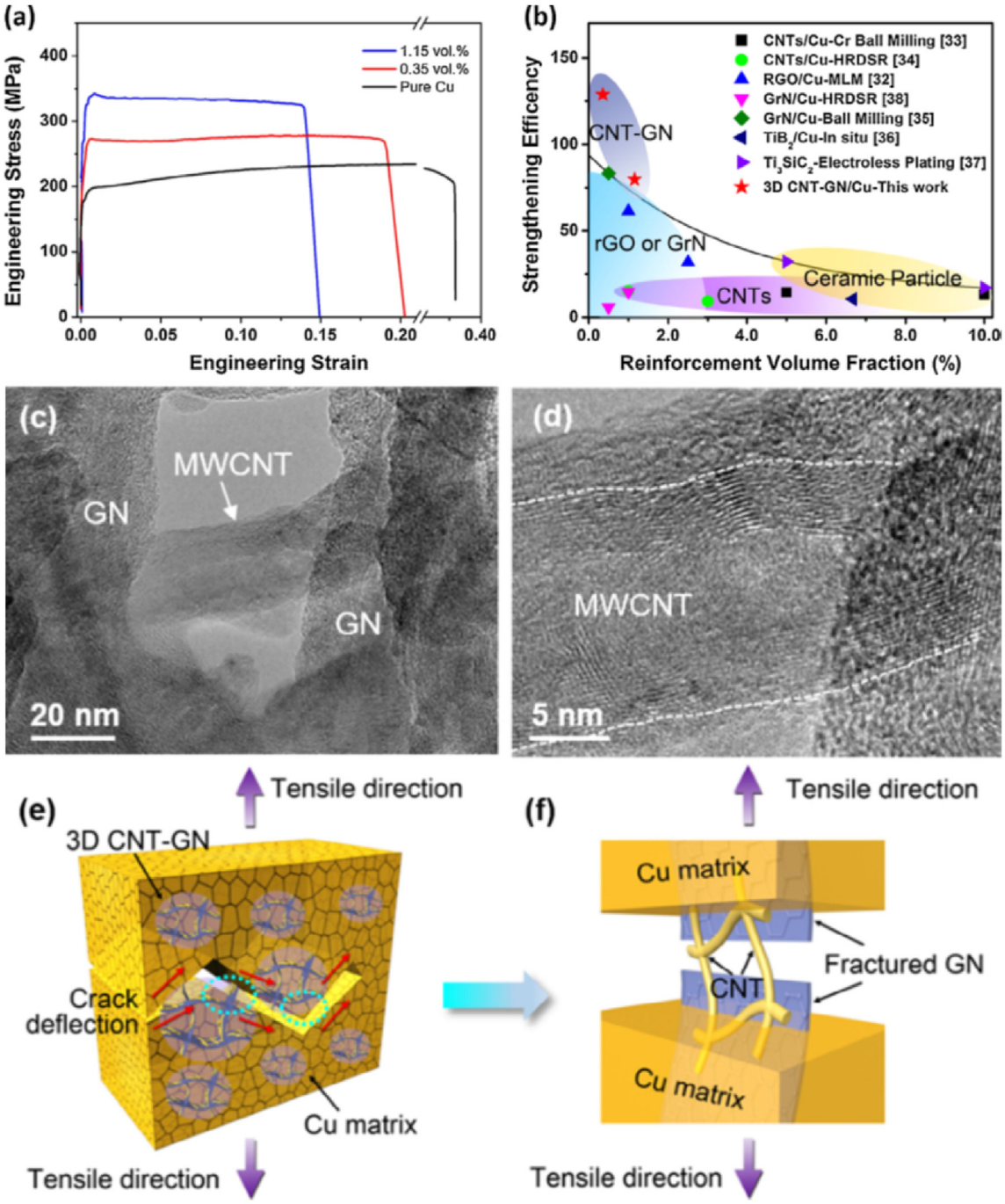

Fig. 28. (a) Stress-strain curves of Cu and composites reinforced by 0.35 vol% and 1.15 vol% of the 3D CNT-GN hybrid reinforcement; (b) Comparison of the strengthening efficiency of the hybrid reinforcements in 3D CNT-GN/Cu composite with the reported Cu matrix composite systems containing different types of reinforcements; (c, d) TEM images of the microstructure in the deformed zone near the fracture of 1.15 vol% 3D CNT-GN/Cu; (e, f) The schematic illustration showing crack deflection of 3D CNT-GN in the path of fracture and a close-up of the pull-out bridging of CNT during tensile deformation [80].

4.1.5. Other hybrid metal matrix composites

In addition to hybrid Al, Mg, Ti and Cu matrix composites which are extensively studied, there are also a few studies on other hybrid metal matrix composites, like hybrid Fe/steel and Ni matrix composites. Table 7 shows the typical hybrid Fe/steel and Ni matrix composites and their properties reported in literature.

Song et al. [93] fabricated hybrid nano-micro SiC particles reinforced iron matrix composites by using SLM method, and the microstructure and tensile stress-strain curves of the iron matrix and its hybrid composites are shown in Fig. 29. From Fig. 29 (b) and (c), both of the micro and nano SiC particles are seen to be distributed uniformly in the iron matrix during SLM process. In addition, nanosized iron grains and amorphous iron were also observed near the retained hybrid SiC particles. Due to the microstructural modification, the hybrid iron matrix composites displayed much higher strength than that of pure iron (Fig. 29 (d)). Akhtar [158] successfully prepared hybrid in-situ TiC/TiB_2 particles reinforced stainless steel matrix composites via utilizing PM

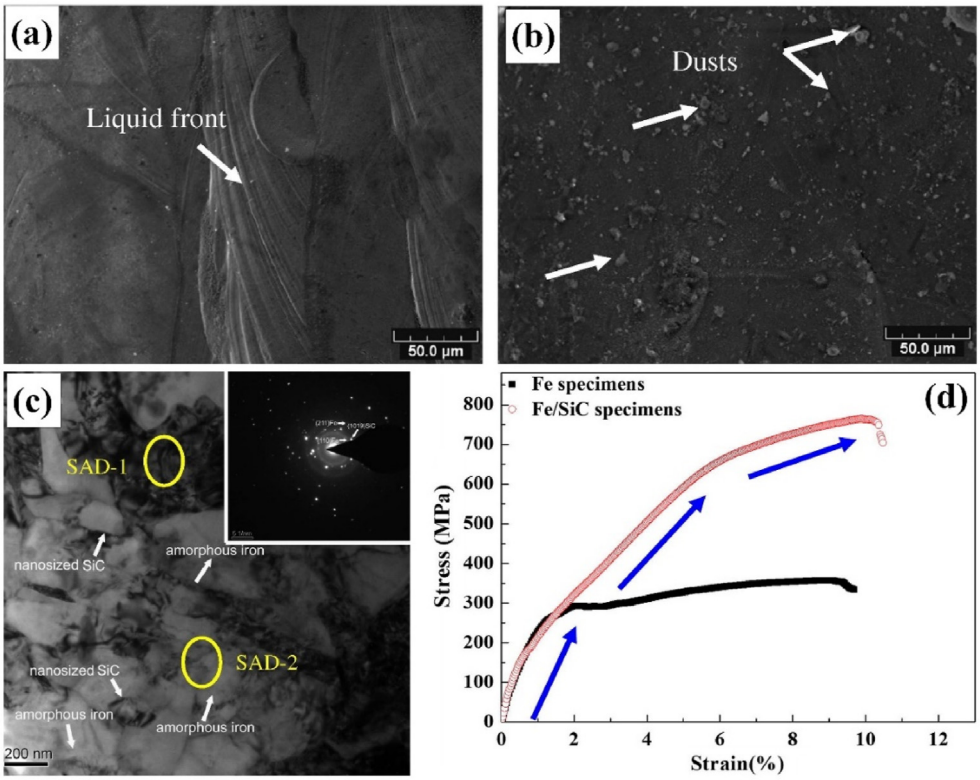

Fig. 29. SEM micrographs showing typical surface morphologies of SLM-fabricated (a) Fe and (b) Fe/SiC, (c) TEM image of cross-section of SLM-fabricated Fe/SiC composite and the corresponding SAD patterns, and (d) stress–strain curves of as-fabricated Fe/SiC composite and as-fabricated pure Fe specimen [93].

Table 7
Other hybrid metal matrix composites and their properties reported in literature.

Matrix	Hybrid reinforcements (wt%)	Reinforcement type	Processing technique	YS (MPa)	UTS (MPa)	Ductility (%)	E (GPa)	Hardness (HV)	References
Fe	2.2 ($SiC_{p\text{-}nm}$ + $SiC_{p\text{-}\mu m}$)	HMSDR	SLM	302	764	10.5	\	\	[93]
steel	30 (TiC + TiB_2)$_{p\text{-}\mu m}$	HMDR	PM (in-situ)	\	\	\	\	75 HRA	[158]
	55 (TiC + TiB_2)$_{p\text{-}\mu m}$	HMDR	PM (in-situ)	\	\	\	\	88 HRA	
	70 (TiC + TiB_2)$_{p\text{-}\mu m}$	HMDR	PM (in-situ)	\	\	\	\	92 HRA	
steel	(TiC + TiB_2)$_{p\text{-}\mu m}$	HMDR	SHS (in-situ)	\	\	\	\	57 HRC	[159]
Ni	0.25 (CNTs + OLC $_{in\text{-}situ}$)$_{nm}$	HNDR	PM (SPS) (in-situ)	182	458	21.1	\	211.6	[160]
	0.50 (CNTs + OLC $_{in\text{-}situ}$)$_{nm}$	HNDR	PM (SPS) (in-situ)	198	489	28.2	\	219.0	
	0.75 (CNTs + OLC $_{in\text{-}situ}$)$_{nm}$	HNDR	PM (SPS) (in-situ)	202	517	19.5	\	219.9	
	1.00 (CNTs + OLC $_{in\text{-}situ}$)$_{nm}$	HNDR	PM (SPS) (in-situ)	200	341	11.1	\	203.5	
Ni–Cr	11 Ni coated ZrO2 (μm + nm)	HMSDR	PM(SPS)	\	\	\	\	476.3	[161]
	11 $ZrO_{2p(\mu m+nm)}$	HMSDR	PM(SPS)	\	\	\	\	416.2	
	15 Ni coated $ZrO_{2p(\mu m+nm)}$	HMSDR	PM(SPS)	\	\	\	\	565.0	
	15 $ZrO_{2p(\mu m+nm)}$	HMSDR	PM(SPS)	\	\	\	\	446.7	
	19 Ni coated $ZrO_{2p(\mu m+nm)}$	HMSDR	PM(SPS)	\	\	\	\	435.2	
	19 $ZrO_{2p(\mu m+nm)}$	HMSDR	PM(SPS)	\	\	\	\	371.1	

Note: SHS: self-propagating high-temperature synthesis; OLC: onion-like carbon.

through the synthesis reaction from Ti, C and FeB. They found that the hardness of the composites could be significantly enhanced with the increase in the content of the hybrid reinforcements.

Wen et al. [160] produced hybrid CNTs and onion-like-carbon (OLC) reinforced Ni matrix nanocomposites by employing SPS technique. Part of CNTs was transformed into OLC during SPS process, which formed the hybrid CNTs and OLC reinforcements in the matrix (as shown in Fig. 30). Compared to pure Ni, 0.75 wt % (CNTs + OLC)/Ni composite exhibited much higher strength and ductility, indicating that significant strengthening and toughening effects could be obtained from the hybrid CNTs and OLC. Fattahi et al. [161] prepared Ni-coated and uncoated hybrid nano and micro ZrO_2 particles reinforced Ni–20Cr alloy matrix composites by using PM method. Their results revealed that the composites reinforced with Ni-coated hybrid ZrO_2 particles presented higher hardness than that of samples containing uncoated hybrid reinforcements, and the composite sample containing 15 wt% Ni-coated hybrid ZrO_2 particles exhibited the highest mechanical properties (+54%).

4.2. Strengthening mechanisms

Strength prediction is important for designing and synthesizing MMCs with high performance. In this section, we will discuss the

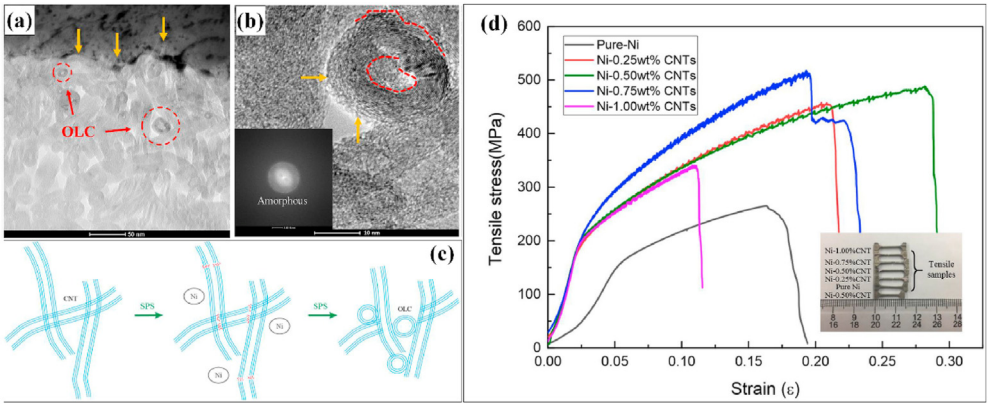

Fig. 30. (a) TEM image of OLC in Ni-1.00 wt% CNTs/OLC composites, (b) corresponding SAD patterns of OLC, (c) schematic illustration of the conversion from CNTs to OLCs during the SPS processing, (d) tensile stress-strain curves of pure Ni and CNTs/OLC-Ni composites [160].

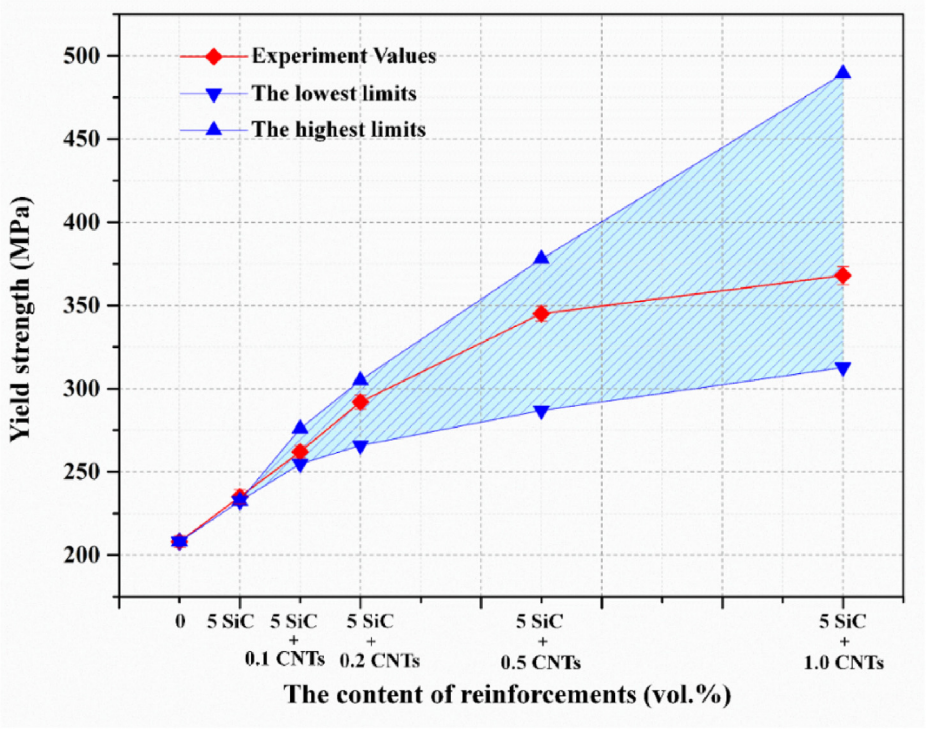

Fig. 31. The yield strength of AZ61 and the composites with different contents of hybrid reinforcements: comparison of experimental values with theoretical values (the lowest and highest limits of the shadow area correspond to the CNTs aspect ratio (S_{CNTs}) of 20 and 167, respectively) [33].

possible strengthening mechanisms in detail and build prediction models of yield strength for hybrid MMCs. The possible strengthening mechanisms of most individual reinforcements (whether nano or micron length scale) in MMCs have been proposed in previous studies and can be commonly categorized into four types: (i) Hall-Petch strengthening by grain refinement, (ii) coefficient of thermal expansion (CTE) mismatch strengthening, (iii) load transfer (LT) enhancement, and (iv) Orowan looping strengthening, which is mainly considered in MMCs containing nano-reinforcements. Therefore, the strengthening mechanisms mainly operating in hybrid reinforced MMCs can be expressed as coupling of the strengthening effects produced by different reinforcements, which can be written as follows (Eqn. (1) and (2))

$$\sigma_c = \sigma_m + \Delta\sigma_{c-Total} \tag{1}$$

$$\Delta\sigma_{c-Total} = \Delta\sigma_{R1} + \Delta\sigma_{R2} + \cdots + \Delta\sigma_{Rn} = \sum_{i=1}^{n} \Delta\sigma_{Ri} \tag{2}$$

where, σ_c and σ_m are yield strength of the composites and matrix, respectively. $\Delta\sigma_{c\text{-}Total}$ *and* $\Delta\sigma_{Ri}$ are the total increments in the yield strength of the composites due to hybrid reinforcements and a certain individual reinforcement, respectively. And n is the number of reinforcement types.

To predict the strength enhancement caused by a certain individual reinforcement, the following three approaches have

Table 8
Tribological properties of hybrid light metal matrix composites.

Matrix		Reinforcements	Processing Technique	Hardness	Wear Parameters	Wear Performance	COF	Ref.
Al	Al	10 $SiC_{p\text{-}nm}$ + 1 CNTs (wt%)	PM	1.61 GPa	10 N, 0.1 m/s	0.002 mm^3/Nm	0.63	[173]
		10 $SiC_{p\text{-}nm}$ + 5 $C_{p\text{-}nm}$ (wt%)	PM	0.76 Gpa	10 N, 0.1 m/s	0.005 mm^3/Nm	0.68	
	A355	5 $SiC_{p\text{-}nm}$	PM	155.9	20 N, 0.044 m/s	0.076 mm^3/Nm	0.78	[174]
		5 $SiC_{p\text{-}nm}$+1$Gr_{p\text{-}\mu m}$	PM	231.1	20 N, 0.044 m/s	0.034 mm^3/Nm	0.63	
		5 $SiC_{p\text{-}nm}$ +1GNSs	PM	242.1	20 N, 0.044 m/s	0.0015 mm^3/Nm	0.5	
	Al–Si	50 $B_4C_{p\text{-}\mu m}$	Pressure infiltration	104	10 N, 0.08 m/s	0.001325 mm^3/Nm	0.607	[175]
		49.75 $B_4C_{p\text{-}\mu m}$ + 0.25 GNPs	Pressure infiltration	170	10 N, 0.08 m/s	0.001222 mm^3/Nm	0.587	
		49.50 $B_4C_{p\text{-}\mu m}$ + 0.50 GNPs	Pressure infiltration	182	10 N, 0.08 m/s	0.00093 mm^3/Nm	0.521	
	LM25	(7.5 SiC + 2.5 TiO_2) $_{p\text{-}\mu m}$	Stir casting	\	30 N, 1.04 m/s	0.0291 mm^3/min	0.57	[176]
		(2.5 SiC + 7.5 TiO_2) $_{p\text{-}\mu m}$	Stir casting	\	30 N, 1.04 m/s	0.0258 mm^3/min	0.54	
	8026	$TiB_{2p\text{-}\mu m}$ + $Al_2O_{3p\text{-}nm}$	FSP-800 rpm- 2P	134.6	15 N, 0.5 m/s	0.0043 mg/m	\	[51]
			FSP-1600 rpm- 2P	130.2	15 N, 0.5 m/s	0.0034 mg/m	\	
			FSP-800 rpm- 4P	145.8	15 N, 0.5 m/s	0.0037 mg/m	\	
			FSP-1600 rpm- 4P	140.7	15 N, 0.5 m/s	0.0026 mg/m	\	
	A356	$SiC_{p\text{-}\mu m}$	FSP	90.2	10 N, 0.35 m/s	0.0114 mg/m	\	[177]
		$SiC_{p\text{-}\mu m}$ + $MoS_{2p\text{-}\mu m}$	FSP	81.5	10 N, 0.35 m/s	0.0082 mg/m	\	
		$SiC_{p\text{-}\mu m}$	FSP	90.2	25 N, 0.35 m/s	0.0133 mg/m	\	
		$SiC_{p\text{-}\mu m}$ + $MoS_{2p\text{-}\mu m}$	FSP	81.5	25 N, 0.35 m/s	0.0095 mg/m	\	
		$SiC_{p\text{-}\mu m}$	FSP	90.2	40 N, 0.35 m/s	0.0179 mg/m	\	
		$SiC_{p\text{-}\mu m}$ + $MoS_{2p\text{-}\mu m}$	FSP	81.5	40 N, 0.35 m/s	0.0099 mg/m	\	
	Al	5 $(Al_2O_3+AlB_2)_{p\text{-}nm}$ (wt%)	PM (In-situ)	108	10 N, 0.08 m/s	0.0464 mg/m	\	[178]
		10 $(Al_2O_3+AlB_2)_{p\text{-}nm}$ (wt%)	PM (In-situ)	134	10 N, 0.08 m/s	0.0343 mg/m	\	
		15 $(Al_2O_3+AlB_2)_{p\text{-}nm}$ (wt%)	PM (In-situ)	156	10 N, 0.08 m/s	0.0253 mg/m	\	
	Al	5 $SiC_{p\text{-}\mu m}$ (wt%)	PM	\	10 N, 1 m/s	0.0095 g/m	0.153	[179]
		5 $SiC_{p\text{-}\mu m}$ + 5 $Gr_{p\text{-}\mu m}$ (wt%)	PM	\	10 N, 1 m/s	0.0050 g/m	0.146	
		5 $SiC_{p\text{-}\mu m}$+10 $Gr_{p\text{-}\mu m}$ (wt%)	PM	\	10 N, 1 m/s	0.0069 g/m	0.148	
Mg	AE42	20 $Saffil_{\text{-short fiber-}\mu m}$	Squeeze casting	\	0.354 MPa, 0.837 m/s	0.41 × 10^{-3} mm^3/m	\	[180]
		15 $Saffil_{\text{-short fiber-}\mu m}$ + 5 $SiC_{p\text{-}\mu m}$	Squeeze casting	\	0.354 MPa, 0.837 m/s	0.31 × 10^{-3} mm^3/m	\	
		10 $Saffil_{\text{-short fiber-}\mu m}$ + 10 $SiC_{p\text{-}\mu m}$	Squeeze casting	\	0.354 MPa, 0.837 m/s	0.28 × 10^{-3} mm^3/m	\	
		10 $Saffil_{\text{-short fiber-}\mu m}$ + 15 $SiC_{p\text{-}\mu m}$	Squeeze casting	\	0.354 MPa, 0.837 m/s	0.25 × 10^{-3} mm^3/m	\	
		20 $Saffil_{\text{-short fiber-}\mu m}$	Squeeze casting	\	1.062 MPa, 0.837 m/s	2.31 × 10^{-3} mm^3/m	\	
		15 $Saffil_{\text{-short fiber-}\mu m}$ + 5 $SiC_{p\text{-}\mu m}$	Squeeze casting	\	1.062 MPa, 0.837 m/s	2.11 × 10^{-3} mm^3/m	\	
		10 $Saffil_{\text{-short fiber-}\mu m}$ + 10 $SiC_{p\text{-}\mu m}$	Squeeze casting	\	1.062 MPa, 0.837 m/s	1.84 × 10^{-3} mm^3/m	\	
		10 $Saffil_{\text{-short fiber-}\mu m}$ + 15 $SiC_{p\text{-}\mu m}$	Squeeze casting	\	1.062 MPa, 0.837 m/s	1.61 × 10^{-3} mm^3/m	\	
	AZ31	10 $SiC_{p\text{-}nm}$ + 0.2 RGO	PM	56	10 N, 0.5 m/s	4.35 × 10^{-5} mm^3/Nm	0.4	[181]
		10 $SiC_{p\text{-}nm}$ + 0.3 RGO	PM	61	10 N, 0.5 m/s	4.22 × 10^{-5} mm^3/Nm	0.32	
		10 $SiC_{p\text{-}nm}$ + 0.4 RGO	PM	67	10 N, 0.5 m/s	3.92 × 10^{-5} mm^3/Nm	0.29	
	AZ91	$(TiB_2 + TiC)_{p\text{-}\mu m}$	Stir casting (in-situ)	79	5 N	2.6509 × 10^{-10} m^3/m	\	[182]
		$(TiB_2 + TiC)_{p\text{-}\mu m}$	Stir casting (in-situ)	79	35 N	9.9477 × 10^{-10} m^3/m	\	
	Mg	5 (CNTs + $SiO_{2p\text{-}\mu m}$) (wt.%)	PM	\	0.5 N, 0.055 m/s	\	0.346	[183]
		10 (CNTs + $SiO_{2p\text{-}\mu m}$) (wt.%)	PM	\	0.5 N, 0.055 m/s	\	0.154	
	AZ91	1(SiC + $Gr)_{p\text{-}\mu m}$ (wt.%)	Stir casting	\	20 N, 1.047 m/s	0.0045 mm^3/m	\	[184]
		2(SiC + Gr) $_{p\text{-}\mu m}$ (wt.%)	Stir casting	\	20 N, 1.047 m/s	0.0041 mm^3/m	\	
		3(SiC + Gr) $_{p\text{-}\mu m}$ (wt.%)	Stir casting	\	20 N, 1.047 m/s	0.0037 mm^3/m	\	
Ti	Ti	(8 $TiB_{Whisker}$ +2 $TiC_p)_{\text{-}\mu m}$	PM (in-situ) + HE	580	40 N, 0.54 m/s	0.0125 g	\	[185]
		(5 $TiB_{Whisker}$ +5 $TiC_p)_{\text{-}\mu m}$	PM (in-situ) + HE	593	40 N, 0.54 m/s	0.0141 g	\	
		(2 $TiB_{Whisker}$ +8 $TiC_p)_{\text{-}\mu m}$	PM (in-situ) + HE	535	40 N, 0.54 m/s	0.0172 g	\	
		(8 $TiB_{Whisker}$ +2 $TiC_p)_{\text{-}\mu m}$	PM (in-situ) + HE	580	100 N, 0.54 m/s	0.0359 g	\	
		(5 $TiB_{Whisker}$ +5 $TiC_p)_{\text{-}\mu m}$	PM (in-situ) + HE	593	100 N, 0.54 m/s	0.0391 g	\	
		(2 $TiB_{Whisker}$ +8 $TiC_p)_{\text{-}\mu m}$	PM (in-situ) + HE	535	100 N, 0.54 m/s	0.0500 g	\	

been widely employed [162]: (i) arithmetic summation [163], (ii) quadratic summation [164], and (iii) compounding method [165], which can be expressed as follows (eqn. (3), (4) and (5), respectively):

$$\Delta\sigma_{Ri} = \Delta\sigma_{Ri(Hall-Petch)} + \Delta\sigma_{Ri(CTE)} + \Delta\sigma_{Ri(LT)} + \Delta\sigma_{Ri(Orowan)} \quad (3)$$

$$\Delta\sigma_{Ri} = \sqrt{(\Delta\sigma_{Ri(Hall-Petch)})^2 + (\Delta\sigma_{Ri(CTE)})^2 + (\Delta\sigma_{Ri(LT)})^2 + (\Delta\sigma_{Ri(Orowan)})^2} \quad (4)$$

$$\Delta\sigma_{Ri} = \sigma_m[(1+\frac{\Delta\sigma_{Ri(Hall-Petch)}}{\sigma_m})(1+\frac{\Delta\sigma_{Ri(CTE)}}{\sigma_m})(1+\frac{\Delta\sigma_{Ri(LT)}}{\sigma_m}) \times (1+\frac{\Delta\sigma_{Ri(Orowan)}}{\sigma_m}) - 1] \quad (5)$$

where, $\Delta\sigma_{Ri(Hall\text{-}Petch)}$, $\Delta\sigma_{Ri(CTE)}$, $\Delta\sigma_{Ri(LT)}$, and $\Delta\sigma_{Ri(Orowan)}$ are the increments in the yield strength due to Hall-Petch, thermal mismatch, load transfer, and Orowan looping strengthening, respectively, which are caused by a certain reinforcement.

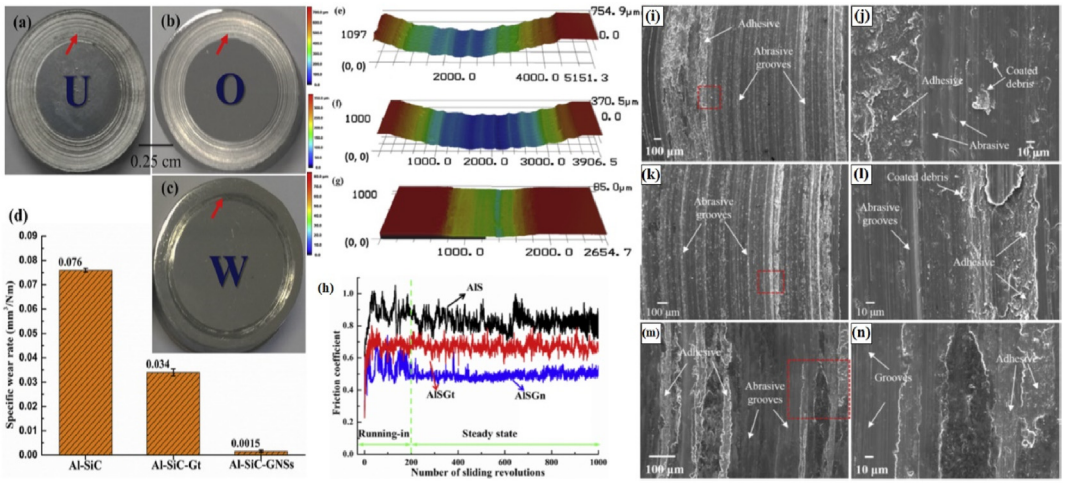

Fig. 32. Photos of the composite disks after the sliding wear tests: (a) Al−SiC, (b) Al−SiC-Gr and (c) Al−SiC-GNs. (d) Calculated specific wear rates of the three samples; Profiles of the wear scars obtained on the 3D laser microscope: (e) Al−SiC, (f) Al−SiC-Gr and (g) Al−SiC-GNs.; (h) Recorded COFs as a function of the sliding revolutions; SEM micrographs of the wear scar of the (i) Al−SiC, (k) Al−SiC-Gr and (m) Al−SiC-GNs., and corresponding enlarged views of the squared area of (j) Al−SiC, (l) Al−SiC-Gr and (n) Al−SiC-GNs, respectively [174].

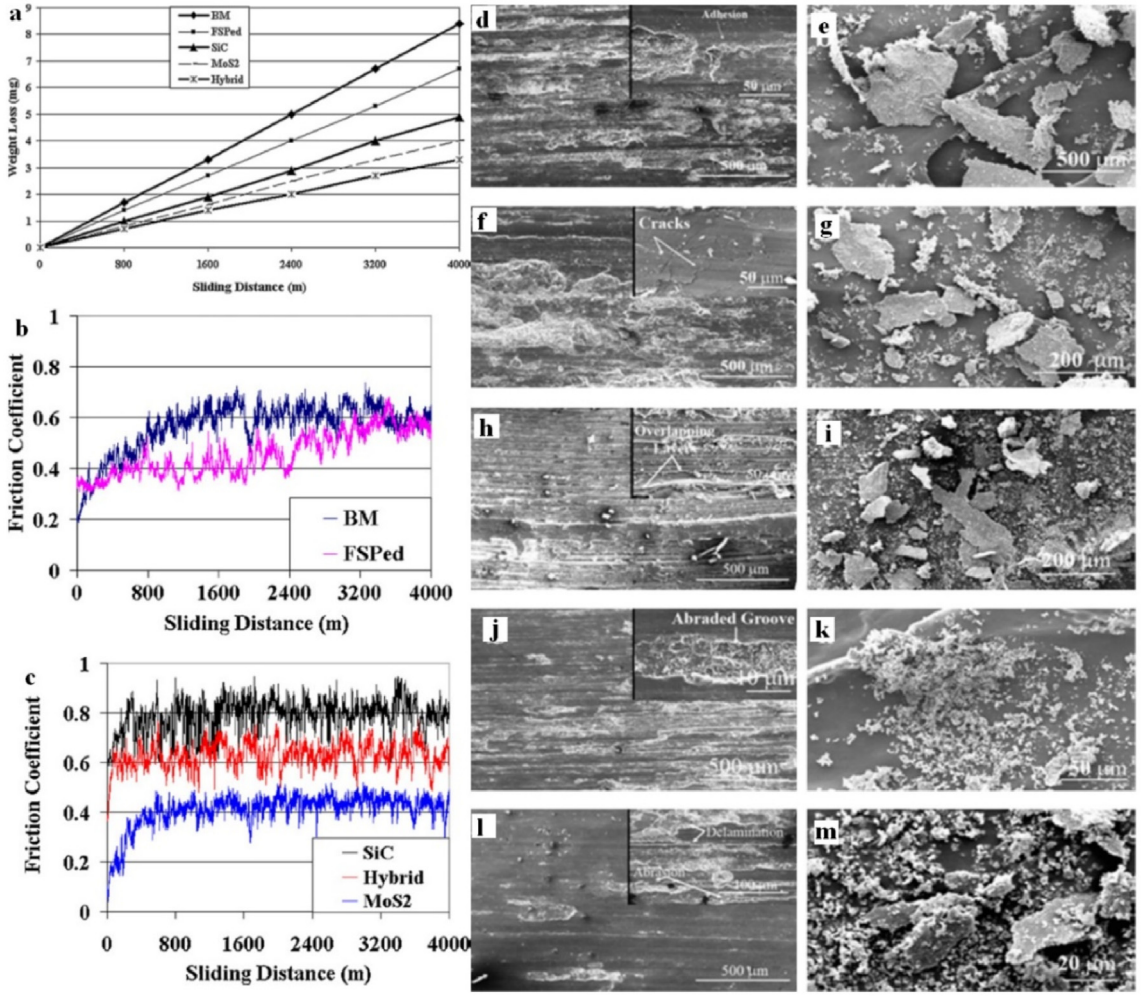

Fig. 33. (a) Variation of weight loss with sliding distance showing the highest wear resistance of hybrid composite amongst samples; Variations of friction coefficient of (b) BM and FSPed and (c) MoS_2, SiC and Hybrid composite samples with sliding distance; Scanning electron micrographs of the worn out track of (d) BM (f) FSPed, (h) MoS_2, (j) SiC and (l) hybrid composite and (e), (g), (i), (k) and (m) are worn debris of (d), (f), (h), (j) and (l), respectively [186].

Table 9
Tribological properties of hybrid Cu matrix composites.

Matrix	Reinforcements	Processing Technique	Hardness	Wear Parameters	Wear Performance	COF	Ref.
Cu	$TiC_{p\text{-}nm}$ + $Gr_{p\text{-}\mu m}$	PM (in-situ)	149.7	15 N, 25 m	0.0012 g	\	[188]
	$TiC_{p\text{-}nm}$ + CNTs	PM (in-situ)	152.3	15 N, 25 m	0.0010 g	\	
	$TiC_{p\text{-}nm}$ + GNPs	PM (in-situ)	171.4	15 N, 25 m	0.0006 g	\	
Cu	2 $SiC_{p\text{-}nm}$ + 2 CNTs	PM	92	15 N	\	0.38	[189]
	2 $SiC_{p\text{-}nm}$ + 4 CNTs	PM	105.7	15 N	\	0.22	
	2 $SiC_{p\text{-}nm}$ + 6 CNTs	PM	108.2	15 N	\	0.25	
Cu	4 $SiC_{p\text{-}\mu m}$ + 1 CNTs	PM	137.9	20 N, 0.31 m/s	1.247×10^{-3} mm^3/m	0.64	[190]
	4 $SiC_{p\text{-}\mu m}$ + 2 CNTs	PM	147.6	20 N, 0.31 m/s	0.932×10^{-3} mm^3/m	0.54	
	4 $SiC_{p\text{-}\mu m}$ + 4 CNTs	PM	171.5	20 N, 0.31 m/s	0.753×10^{-3} mm^3/m	0.51	
Cu	\	PM	30.5 B	10 N, 0.5 m/s	0.0244 mm^3/m	0.35	[191]
	2 (RGO + $MoS_{2p\text{-}nm}$)	PM (in-situ)	38.6 B	10 N, 0.5 m/s	4.135×10^{-4} mm^3/m	0.06	
Cu	(3 TiO_2 +1 $Gr)_{p\text{-}\mu m}$ (wt%)	Stir casting	63.8	20 N, 2 m/s	0.146×10^{-3} mm^3/m	0.41	[41]
	(6 TiO_2 +1 $Gr)_{p\text{-}\mu m}$ (wt%)	Stir casting	67.3	20 N, 2 m/s	0.076×10^{-3} mm^3/m	0.36	
	(9 TiO_2 +1 $Gr)_{p\text{-}\mu m}$ (wt%)	Stir casting	70.2	20 N, 2 m/s	0.010×10^{-3} mm^3/m	0.28	
Cu	(10 $SiC)_{p\text{-}\mu m}$	PM	/	20 N, 0.42 m/s	0.1074×10^{-3} mm^3/m	0.498	[192]
	(10 SiC + 3 Gr) $_{p\text{-}\mu m}$	PM	/	20 N, 0.42 m/s	0.0551×10^{-3} mm^3/m	0.358	
	(10 SiC + 7 Gr) $_{p\text{-}\mu m}$	PM	/	20 N, 0.42 m/s	0.0370×10^{-3} mm^3/m	0.343	
	(10 SiC + 10 Gr) $_{p\text{-}\mu m}$	PM	/	20 N, 0.42 m/s	0.0310×10^{-3} mm^3/m	0.311	
Cu	(10 TiC + 5 Gr) $_{p\text{-}\mu m}$	PM	88.5	12 N, 1.25 m/s	0.1881×10^{-3} mm^3/m	0.387	[193]
	(10 TiC + 10 Gr) $_{p\text{-}\mu m}$	PM	67.2	12 N, 1.25 m/s	0.1230×10^{-3} mm^3/m	0.314	
Cu	5 (AlN + BN) $_{p\text{-}\mu m}$	FSP	75.8	30 N, 1 m/s	0.777×10^{-3} mm^3/m	\	[152]
	10 (AlN + BN) $_{p\text{-}\mu m}$	FSP	76.9	30 N, 1 m/s	0.721×10^{-5} mm^3/Nm	\	
	15 (AlN + BN) $_{p\text{-}\mu m}$	FSP	77.2	30 N, 1 m/s	0.633×10^{-5} mm^3/Nm	\	

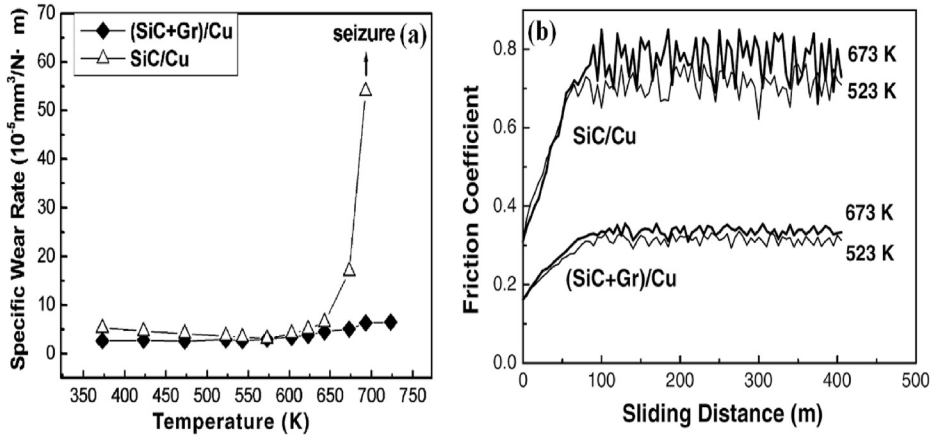

Fig. 34. (a) Specific wear rate plotted against temperature, and (b) variations of friction coefficient with sliding distance for the two composites [194].

4.2.1. Strengthening by grain refinement

The enhanced strength contribution by grain refinement can be calculated by Hall-Petch relationship as follows (Eqn. (6)) [166]:

$$\Delta\sigma_{Hall-Petch} = K(d_c^{-1/2} - d_m^{-1/2}) \quad (6)$$

where K is the Hall-Petch coefficient, which is different for different metallic matrices. For example, the values of K of Al and Mg are 0.04 and 0.13 MPa $m^{1/2}$, respectively. d_c and d_m are the average grain size of the hybrid reinforcements and the matrix, respectively. Actually, it is hard to distinguish the grain refinement attributed to a certain reinforcement in a hybrid reinforced MMC, thus, the strength contribution by grain refinement is usually obtained by calculating the total effects of the hybrid reinforcements [167].

4.2.2. Strengthening by thermal mismatch

The difference in the CTE between the matrix and the reinforcements can increase the dislocation density at the interface, leading to an enhancement of the yield strength. The strength contribution by this mechanism caused by a certain reinforcement can be written as (Eqn. (7)) [164]:

$$\Delta\sigma_{Ri(CTE)} = \sqrt{3}\beta G_m b\sqrt{\frac{12V_{Ri}\Delta\alpha\Delta T}{(1-V_{Ri})bd_{Ri}}} \quad (7)$$

where, β is a constant, G_m is the shear modulus of the matrix, b is the Burgers vector of the matrix, V_{Ri} is the volume fraction of the certain reinforcement, $\Delta\alpha$ is the difference in CTE between the matrix and the reinforcement, ΔT is the difference in temperature between the processing process and the room temperature, d_{Ri} is the diameter of the reinforcement. For rod-shaped reinforcements, the rule expressed in Eqn. (7) can also be used, but the shape factor should be considered, and an equivalent diameter $d_{Ri\text{-}eq}$ should be employed to substitute the particle diameter d_{Ri}, which can be expressed as (Eqn. (8)) [168]:

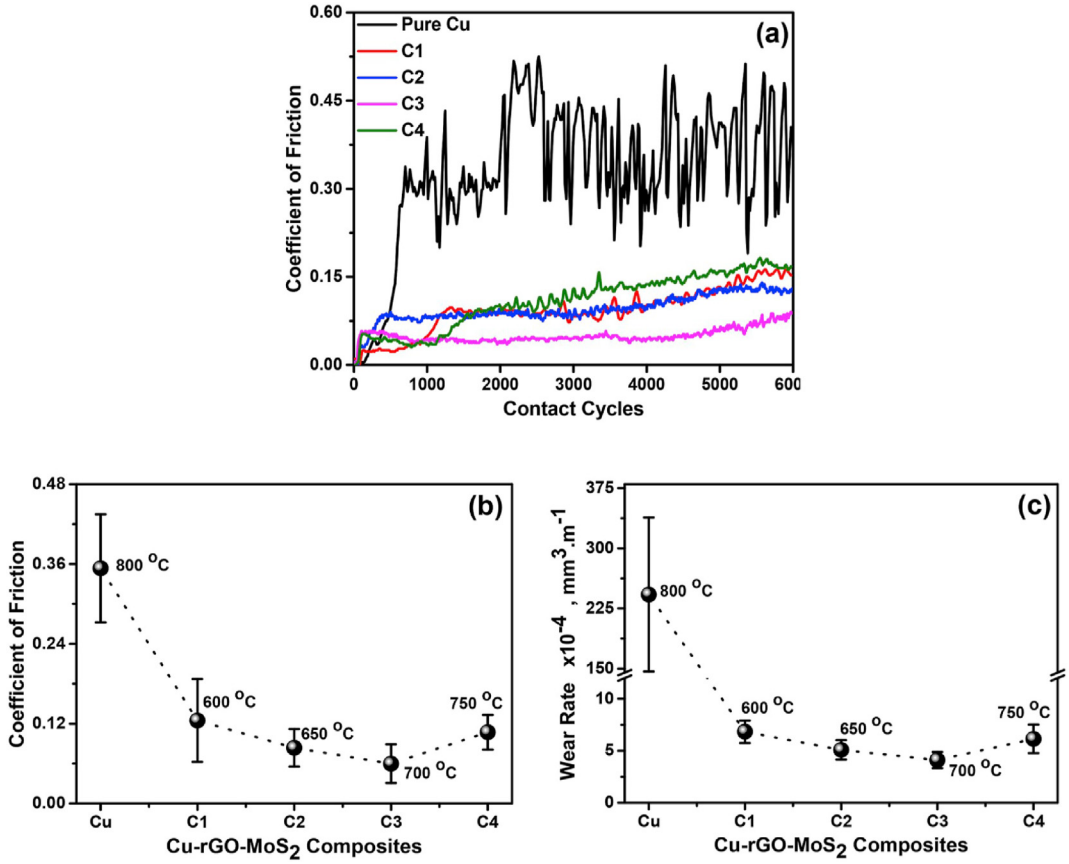

Fig. 35. (a) Variation of coefficient of friction with the number of sliding cycles, the (b) average coefficient of friction and (c) wear rate of copper and Cu-rGO-MoS_2composites. Load: 4 N; Sliding speed: 0.5 m s^{-1}; Counter body: steel ball [191].

$$d_{Ri-eq} = \sqrt[3]{\frac{3d_{Ri}^2 l_{Ri}}{2}} = d_{Ri}\sqrt[3]{\frac{3S_{Ri}}{2}} \tag{8}$$

where S_{Ri} is the aspect ratio of the rod-shaped reinforcements.

4.2.3. Strengthening by load transfer

The enhanced yield strength due to load transfer can be estimated by using the modified shear lag model proposed by Nardone and Prewo, which can be expressed as (Eqn. (9)) [169]:

$$\Delta\sigma_{Ri(LT)} = \sigma_m[\frac{V_{Ri}(S_{Ri}+2)}{2} + V_m] = 0.5S_{Ri}V_{Ri}\sigma_m \tag{9}$$

where, σ_m, V_{Ri} and S_{Ri} are the same defined above, and V_m is the volume fraction of matrix.

4.2.4. Strengthening by Orowan looping

For particles finer than 1 μm, this mechanism can play a significant role in improving the yield strength of the composites, but for particles larger than 1 μm, enhancement caused by Orowan strengthening can be ignored. The enhanced yield strength can be calculated using the following equation (Eqn. (10)) [165]:

$$\Delta\sigma_{Ri(Orowan)} = \frac{0.13G_m b}{\lambda}\ln\frac{d_{Ri}}{2b} \tag{10}$$

where, G_m, b and d_{Ri} are the same as defined above, and λ is the mean interparticle distance, which can be expressed as (Eqn. (11)):

$$\lambda = d_{Ri}[(\frac{1}{2V_{Ri}})^{1/3} - 1] \tag{11}$$

where, V_{Ri} and d_{Ri} are the same as defined above, but for rod-shaped reinforcements, d_{Ri} in Eqns. (10) and (11) should be replaced by $d_{Ri\text{-}eq.}$

Based on the predition model mentioned above, Zhou et al. [33] calculated the theoretical yield strength of hybrid micron SiC particles and CNTs reinforced AZ61 alloy matrix composites, and the comparison of the experimental values with the theoretical values of the yield strength is shown in Fig. 31. The experimental values were in good agreement with the preditions, indicating that the prediction model proposed in this work is effective to estimate the yield strength of hybrid MMCs.

5. Tribological properties

Tribological properties are important for the application of materials, because wear occurs during relative motion of two surfaces under many service conditions. According to different wear conditions, the wear mechanisms can be divided into several types, including adhesive wear, abrasive wear, delamination wear, erosive wear, fretting wear, fatigue wear, and corrosive/oxidative wear [27]. At high loads and high sliding speeds, the dominant mechanism is delamination, while it will change to abrasion when the wear condition changes to low loads and low sliding speeds.

In general, the wear resistance of MMCs is usually much higher than that of their monolithic counterparts. The wear volume or wear loss of MMCs depends greatly on their intrinsic material

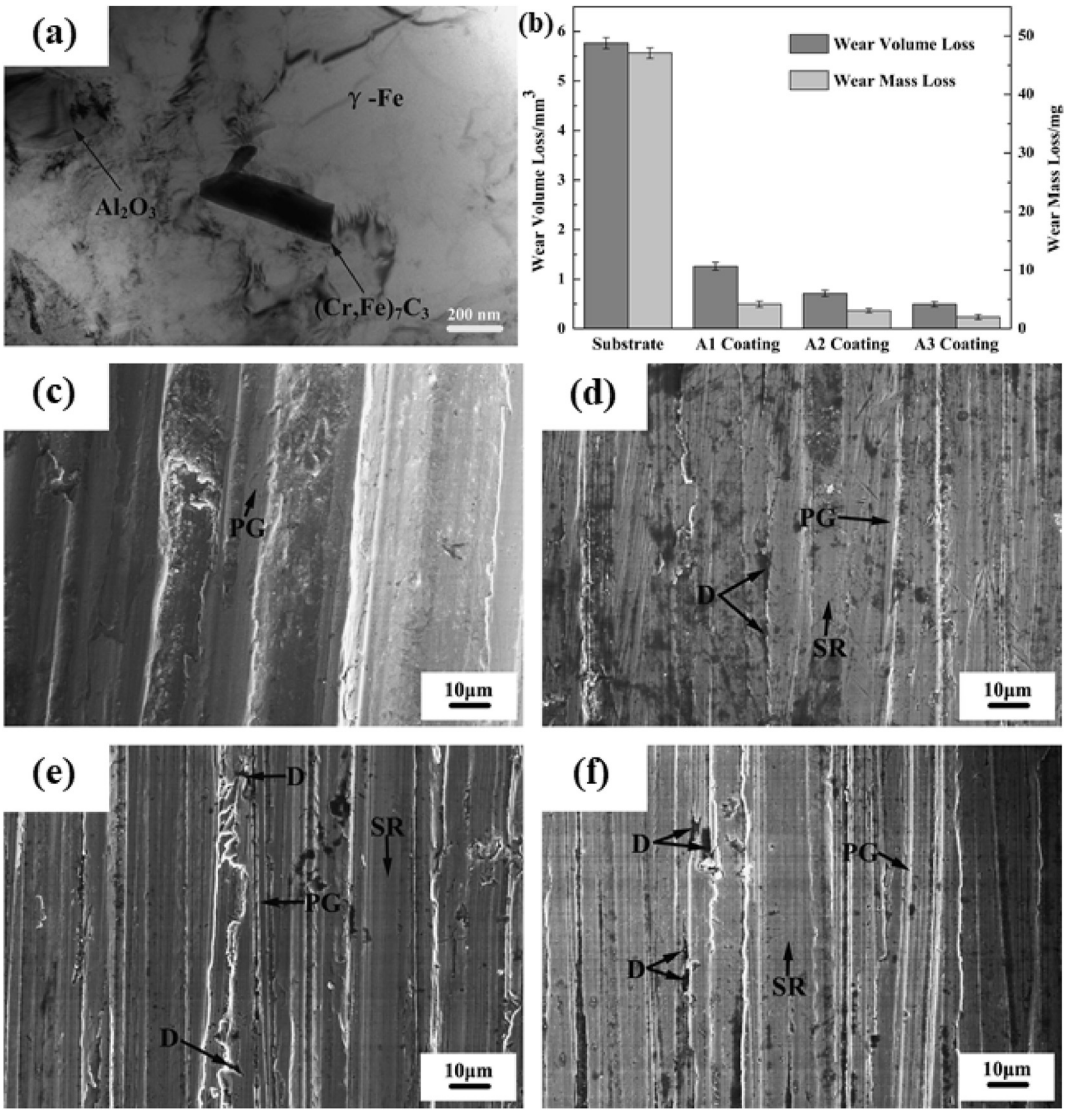

Fig. 36. (a) TEM image of γ-Fe with Al_2O_3 and $(Cr, Fe)_7C_3$ particle, (b) wear losses of the substrate and the composite coatings with different additions of thermite reactants: A1 coating-0%; A2 coating-5%; and A3 coating-10%, and the worn surface morphologies of the substrate and the composite coatings with different additions of thermite reactants: (c) the substrate; (d) 0%; (e) 5%; and (f) 10% [198].

Table 10
Tribological properties of hybrid iron/steel matrix composites.

Matrix	Reinforcements	Processing Technique	Hardness	Wear Parameters	Wear Performance	COF	Ref.
iron	1 $BN_{p\text{-}\mu m}$+4$Gr_{p\text{-}\mu m}$	PM	\	ILM (7 N/10 min)	4 N m	\	[199]
	1 $BN_{p\text{-}\mu m}$+6.5$Gr_{p\text{-}\mu m}$	PM	\	ILM (7 N/10 min)	1825 N m	\	
	1 $BN_{p\text{-}\mu m}$+9$Gr_{p\text{-}\mu m}$	PM	\	ILM (7 N/10 min)	7323 N m	\	
	2.5 $BN_{p\text{-}\mu m}$+7.5$Gr_{p\text{-}\mu m}$	PM	\	ILM (7 N/10 min)	6375 N m	\	
iron	(10 SiC_L+18Gr)$_{p\text{-}\mu m}$	PM	\	1323 N, 25 m/s	23.13 g	0.310666	[200]
	(10 SiC_S+18Gr)$_{p\text{-}\mu m}$	PM	\	1323 N, 25 m/s	46.06 g	0.340605	
	(15 SiC_L+18Gr)$_{p\text{-}\mu m}$	PM	\	1323 N, 25 m/s	7.04 g	0.300269	
	(15 SiC_S+18Gr)$_{p\text{-}\mu m}$	PM	\	1323 N, 25 m/s	32.02 g	0.330416	
	(20 SiC_L+18Gr)$_{p\text{-}\mu m}$	PM	\	1323 N, 25 m/s	3.93 g	0.260354	
	(20 SiC_S+18Gr)$_{p\text{-}\mu m}$	PM	\	1323 N, 25 m/s	16.99 g	0.320643	
steel	(TiC + TiB_2)$_{p\text{-}\mu m}$	SHS (in-situ)	57 HRC	25 N	1.595×10^{-10} m^3/m	\	[159]

Note: ILM: incremental loading mode.

properties, including the types of the metallic matrix and reinforcements, distribution state and size of the reinforcements, interfacial bonding between matrix and reinforcements, and extrinsic wear test conditions, such as applied loads and sliding speeds [2]. Furthermore, according to the different mechanisms for enhancing wear resistance, the reinforcements can be categorized into two types: (i) ceramic particles, such as SiC, B_4C and TiC and (ii) carbon-based materials and other lubricating materials, like graphite particles, CNTs, GNPs and MoS_2. The former enhances wear resistance by significantly improving the hardness of the

Table 11
Thermal properties of hybrid MMCs.

Matrix		Reinforcements	Processing techniques	Thermal conductivity $W \cdot m^{-1} \cdot K^{-1}$	CTE 10^{-6} K^{-1}	Ref.
Cu	Cu	\	PM (SPS) (in-situ)	352.03	17.00	[154]
		1 RGO	PM (SPS) (in-situ)	361.05	16.59	
		1(RGO + $Mo_2C_{p\text{-}nm\text{-}in\text{-}situ}$)	PM (SPS) (in-situ)	327.97	15.19	
	Cu	\	PM (HP-60 MPa)	282	\	[203]
		0.15 (RGO + $Ag_{p\text{-}nm}$) (wt %)	PM (HP-30 MPa)	291	\	
		0.15 (RGO + $Ag_{p\text{-}nm}$) (wt %)	PM (HP-40 MPa)	329	\	
		0.15 (RGO + $Ag_{p\text{-}nm}$) (wt %)	PM (HP-50 MPa)	344	\	
		0.15 (RGO + $Ag_{p\text{-}nm}$) (wt %)	PM (HP-60 MPa)	296	\	
Al	Al	1.0 CNTs + 1.0 $SiC_{p\text{-}sub\text{-}\mu m}$	PM + HR	\	22.56	[107]
		1.0 CNTs + 1.0 $SiC_{p\text{-}sub\text{-}\mu m}$	PM + HR + HT-530 °C	\	22.49	
		1.0 CNTs + 1.0 $SiC_{p\text{-}sub\text{-}\mu m}$	PM + HR + HT-550 °C	\	22.41	
		1.0 CNTs + 1.0 $SiC_{p\text{-}sub\text{-}\mu m}$	PM + HR + HT-570 °C	\	22.25	
		1.0 CNTs + 1.0 $SiC_{p\text{-}sub\text{-}\mu m}$	PM + HR + HT-590 °C	\	22.18	
		1.0 CNTs + 1.0 $SiC_{p\text{-}sub\text{-}\mu m}$	PM + HR + HT-610 °C	\	22.03	
		1.0 CNTs + 1.0 $SiC_{p\text{-}sub\text{-}\mu m}$	PM + HR + HT-630 °C	\	18.86	
	7075	50 $SiC_{p\text{-}\mu m}$	Squeeze casting	128	\	[98]
		55 $SiC_{p\text{-}\mu m}$	Squeeze casting	130	\	
		(50 SiC + 5 Cr)$_{p\text{-}\mu m}$	Squeeze casting	145	\	
	Al	S1: 30 $Y_2W_3O_{12p\text{-}\mu m}$	PM	\	14.53	[204]
		S2: (30 $Y_2W_3O_{12}$ + 5 AlN)$_{p\text{-}\mu m}$	PM	\	14.17	
		S3: (30 $Y_2W_3O_{12}$ + 10 AlN)$_{p\text{-}\mu m}$	PM	\	13.08	
		S4: (30 $Y_2W_3O_{12}$ + 15 AlN)$_{p\text{-}\mu m}$	PM	\	12.28	
		S5: 30$AlN_{p\text{-}\mu m}$	PM	\	16.17	
		S6: (5 $Y_2W_3O_{12}$ + 30AlN)$_{p\text{-}\mu m}$	PM	\	15.18	
		S7: (10 $Y_2W_3O_{12}$ + 30AlN)$_{p\text{-}\mu m}$	PM	\	14.31	
		S8: (15 $Y_2W_3O_{12}$ + 30AlN)$_{p\text{-}\mu m}$	PM	\	13.63	
	Al	(SiC + Rice husk ash)$_{p\text{-}\mu m}$	Infiltration		9.26	[205]
	Al	1 CNTs + 1 $SiC_{p\text{-}sub\text{-}\mu m}$	PM (SPS)+HR	\	22.56	[112]
		1 CNTs + 3 $SiC_{p\text{-}sub\text{-}\mu m}$	PM (SPS)+HR	\	21.55	
		1 CNTs + 5 $SiC_{p\text{-}sub\text{-}\mu m}$	PM (SPS)+HR	\	19.17	
Mg	AE42	\	Stir casting	\	27.1	[206]
		20 $Saffil_{short\ fibre\text{-}\mu m}$	Stir casting	\	18.2	
		15 $Saffil_{short\ fibre\text{-}\mu m}$ + 5 $SiC_{p\text{-}\mu m}$	Stir casting	\	18.3	
		10 $Saffil_{short\ fibre\text{-}\mu m}$ + 10 $SiC_{p\text{-}\mu m}$	Stir casting	\	17.6	
		10 $Saffil_{short\ fibre\text{-}\mu m}$ + 15 $SiC_{p\text{-}\mu m}$	Stir casting	\	14.0	

metallic matrix and protecting the matrix surface against destructive ploughing during sliding. However, ceramic particles often lead to an increase in coefficient of friction, because these hard particles usually detach from the matrix and can be trapped between the sliding surfaces during sliding process. These trapped particles can act as third body abrasives and accelerate worn surface damage [2]. Adding carbon-based materials into metallic matrix can form self-lubricating film during sliding process which can prevent direct contact of sliding surfaces and reducing ploughing effect of hard asperities, resulting in the decrease in coefficient of friction and improvement in wear resistance [170,171]. However, conventional micron size graphite particles reinforced MMCs can significantly enhance the tribological properties, but their mechanical properties always drop significantly. In contrast, the addition of nano carbon-based materials, such as CNTs and GNPs, can simultaneously improve tribological and mechanical properties, and sometimes the electrical and thermal properties can also be enhanced. Thus, these nano-sized carbonaceous materials reinforced MMCs have great potential in the applications requiring high mechanical and tribological performance [27].

In the following section, the tribological properties of MMCs containing different types of hybrid reinforcements have been discussed systematically. The focus is mainly on light metal, Cu and Fe/steel matrix composites.

5.1. Hybrid reinforced light metal matrix composites

Light metal matrix composites with excellent mechanical and tribological properties have been used in more and more important applications due to the tremendous benefits of improved fuel efficiency so as to reduce green-house gas emissions. The wear resistance of hybrid light metal matrix composites have seen significant improvement during recent years. Khatkar et al. [172] have reviewed the progress in tribological properties of hybrid ceramic and graphite particles reinforced Al and Mg matrix composites. From this report, it was concluded that the graphite particles can significantly enhance the wear resistance of hybrid Al and Mg matrix composites at the expense of the strength, while the reduced strength can be compensated by the strengthening effects of hard ceramic particulates. Thus, high strength and superior wear resistance can be simultaneously achieved by adding hybrid ceramic and graphite particles. In addition, they also stated that applied load, sliding speed and composition of hybrid reinforcements are important parameters which can significantly influence tribological properties, such as wear rate and coefficient of friction of these self-lubricating hybrid composites. However, this review has not discussed the effects of nano carbon-based materials, like CNTs and GNPs, on the tribological properties of hybrid light metal matrix composites, and this section will focus on this part. The tribological properties of hybrid light metal matrix composites are summarized in Table 8.

Zhang et al. [174] compared the effects of SiC nanoparticles, hybrid SiC nanoparticles and graphite micron particles, and hybrid SiC nanoparticles and graphene, respectively, on the tribological properties of Al matrix composites, and the results are shown in Fig. 32. It was found that the hybrid SiC and GNs reinforced Al matrix composite had much lower wear rate, friction of coefficient, and wear scars than that of the other two composites, indicating that the nano GNs can improve the wear resistance much more efficiently than micron graphite particles due to the core-shell

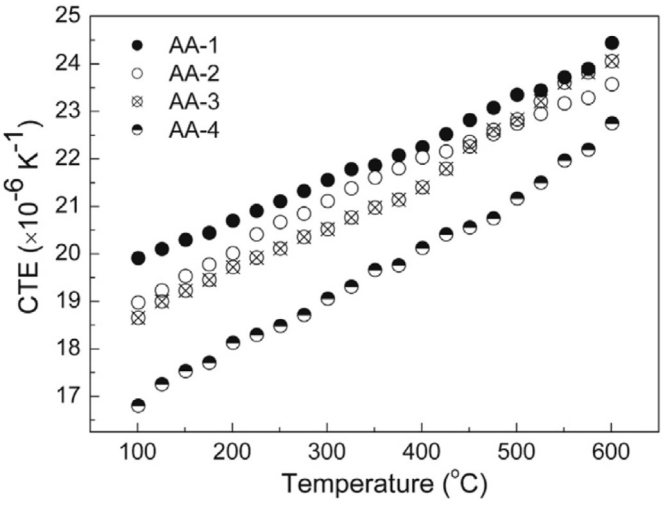

Fig. 37. Comparison of the CTE of different composites [207] (AA-1: (5 Al_2O_{3nm} + 5 $Al_2O_{3\mu m}$)/Al, AA-2: (5 Al_2O_{3nm} + 10 $Al_2O_{3\mu m}$)/Al, AA-3: (10 Al_2O_{3nm} + 5 $Al_2O_{3\mu m}$)/Al, (d) AA-4: (10 Al_2O_{3nm} + 10 $Al_2O_{3\mu m}$)/Al).

structure formed by GNs and SiC nanoparticles. The authors attributed the striking tribological properties to the uniform distribution of GNs in the matrix which can smear on the wear scars and form GNs-rich micro self-lubricating films during sliding wear.

Soleymani et al. [186] investigated the effects of friction stir processing and reinforcement types (ceramic particles (SiC), self-lubricating particles (MoS_2), and hybrid (SiC + MoS_2)) on the tribological properties on the Al5083 matrix composites (see Fig. 33). They reported that friction stir processed sample exhibited higher wear resistance than that of the samples without friction stir process. Compared to the composites containing individual SiC particles or MoS_2 particles, hybrid SiC and MoS_2 particles reinforced composite had the highest wear resistance (lowest weight loss), second highest hardness and second lowest friction of coefficient, which suggested that the hybrid composite has better combination of mechanical and tribological properties.

As for Mg matrix composites, a large number of investigations have also been conducted (Table 8), and similar conclusions can also be drawn that hybrid ceramic particles and self-lubricating reinforced Mg matrix composites have better overall combination of tribological and mechanical performance. In addition, nano carbon-based materials, such as CNTs and GNPs, have superior ability to enhance both tribological properties and mechanical properties when used as a part of hybrid reinforcements when compared to graphite particles.

There are just few works related to the tribological properties of hybrid Ti matrix composites, and these works mainly focused on hybrid TiB whiskers and TiC particles containing Ti matrix composites. The hybrid reinforcements can also both increase the strength and wear resistance of the composites [185]. In addition, with the expansion of the application fields of Ti matrix composites, the investigation on wear performance of these materials is likely to attract more and more attention in near future.

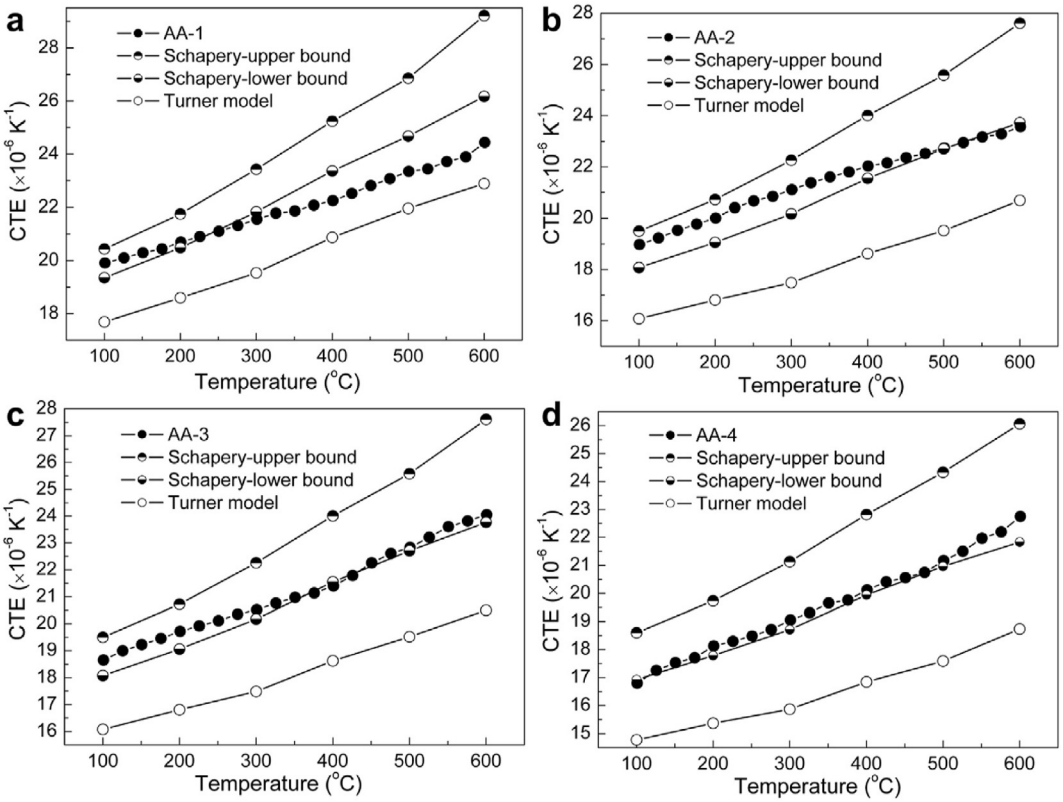

Fig. 38. Instantaneous coefficient of thermal expansion as a function of temperature compared with Schapery and Turner models for: (a) (5 Al_2O_{3nm} + 5 $Al_2O_{3\mu m}$)/Al (AA-1), (b) (5 Al_2O_{3nm} + 10 $Al_2O_{3\mu m}$)/Al (AA-2), (c) (10 Al_2O_{3nm} + 5 $Al_2O_{3\mu m}$)/Al (AA-3), (d) (10 Al_2O_{3nm} + 10 $Al_2O_{3\mu m}$)/Al (AA-4) [207].

Table 12
Electrical properties of hybrid reinforced MMCs.

Matrix	Reinforcements	Processing techniques	Electrical conductivity (% IACS)	Ref.
Cu	\	PM	98.24	[155]
	0.6 RGO (wt%)	PM	71.25	
	0.6 (RGO + $Ag_{p\text{-}nm\text{-}in\text{-}situ}$)	PM (in-situ)	92.69	
Cu	0.5 $C_{f\text{-}short\text{-}\mu m}$ (wt%)	PM	92.3	[153]
	0.5 $C_{f\text{-}short\text{-}\mu m}$ +0.1 GO (wt%)	PM	90.7	
	0.5 $C_{f\text{-}short\text{-}\mu m}$ +0.4 GO (wt%)	PM	80.6	
Cu	\	PM (HP-60 MPa)	82.6	[203]
	0.15 (RGO + $Ag_{p\text{-}nm}$) (wt%)	PM (HP-30 MPa)	95.9	
	0.15 (RGO + $Ag_{p\text{-}nm}$) (wt%)	PM (HP-40 MPa)	96.7	
	0.15 (RGO + $Ag_{p\text{-}nm}$) (wt%)	PM (HP-50 MPa)	97.9	
	0.15 (RGO + $Ag_{p\text{-}nm}$) (wt%)	PM (HP-60 MPa)	92.1	
Cu	\	Casting (in-situ)+HR	93.1	[67]
	(0.7 TiB_{2p} + 0.6 $TiB_{whisker})_{sub\text{-}\mu m}$ (wt%)	Casting (in-situ)+HR	87.9	
	(1.0 TiB_{2p} + 0.9 $TiB_{whisker})_{sub\text{-}\mu m}$ (wt%)	Casting (in-situ)+HR	80.2	
	(1.4 TiB_{2p} + 1.2 $TiB_{whisker})_{sub\text{-}\mu m}$ (wt%)	Casting (in-situ)+HR	62.2	
	2.6 $TiB_{2p\text{-}\mu m}$ (wt%)	Casting (in-situ)+HR	70.7	
	\	Casting (in-situ)+HR + HT	98.9	
	(0.7 TiB_{2p} + 0.6 $TiB_{whisker})_{sub\text{-}\mu m}$ (wt%)	Casting (in-situ)+HR + HT	91.2	
	(1.0 TiB_{2p} + 0.9 $TiB_{whisker})_{sub\text{-}\mu m}$ (wt%)	Casting (in-situ)+HR + HT	85.5	
	(1.4 TiB_{2p} + 1.2 $TiB_{whisker})_{sub\text{-}\mu m}$ (wt%)	Casting (in-situ)+HR + HT	75.2	
	2.6 $TiB_{2p\text{-}\mu m}$ (wt%)	Casting (in-situ)+HR + HT	81.4	

5.2. Hybrid Cu matrix composites

Cu matrix composites containing graphite particles are important self-lubricating materials, which have been widely used for brushes in industrial motors and generators as electrical sliding contacts due to good electrical and thermal conductivities deriving from copper matrix [187]. However, adding micron size graphite particles always reduces the strength of the Cu composites because of the low strength of the graphite. Hence, Cu-graphite composites normally fall short of meeting the desired combination of mechanical and tribological properties. To circumvent this problem, some novel hybrid Cu matrix composites with overall superior combination of properties have been developed. Table 9 summarizes the tribological properties of hybrid Cu matrix composites reported in literature.

Zhan et al. [194] investigated dry sliding wear properties of SiC/Cu and hybrid SiC + graphite/Cu composites in the temperature range of 373–723 K (Fig. 34). They demonstrated that hybrid composite exhibited higher wear resistance, especially at high temperatures up to 723 K and a more stable and lower friction of coefficient indicating that the hybrid SiC + graphite/Cu composite might be suitable for applications in high-temperature sliding wear condition.

Nautiyal et al. [191] fabricated hybrid self-lubricating materials (RGO + MoS_2) reinforced Cu matrix composites by using powder metallurgy method. From Fig. 35, it can be found that the reinforcement composition and fabrication parameters have significant influence on the wear rate and friction of coefficient of the hybrid Cu matrix composites. Thus, it is essential to optimize the reinforcement compositions and processing parameters to obtain superior tribological properties.

The tribological and mechanical properties of hybrid ceramic particles, such as TiC and SiC, and nano carbon-based materials, such as CNTs and GNPs, reinforced Cu matrix composites have also been extensively studied (as shown in Table 9), and the effects of these hybrid reinforcements on overall properties of the hybrid Cu matrix composites are similar with that of hybrid light metal matrix composites.

5.3. Hybrid iron/steel matrix composites

Cast iron and steel have superior mechanical and tribological properties than that of light metals and copper, and hence are widely used in the fields of mining, metallurgy, transportation and so on [195]. However, tribological and wear damage is still inevitable during their service life, usually resulting in huge economic losses. Thus, optimizing their wear resistance is essential to improve economic efficiency. In general, adding micron ceramic particles, like SiC [196] and TiC [197], into iron/steel matrix can help to realize enhanced tribological and wear performance.

In recent years, researchers also paid some attention to the effects of hybrid reinforcements on wear properties of the iron/steel matrix composites. Tan et al. [198] fabricated hybrid in-situ Al_2O_3-$(Cr, Fe)_7C_3$ particles reinforced iron matrix composite coatings on a steel substrate by using laser cladding method through Fe-based alloy powders and Al/Fe_2O_3 thermite reactants, and the results are shown in Fig. 36. From the results of wear losses and worn surface morphologies of the substrate and the composite coatings, it is clear that the hybrid composite coatings possessed much higher wear resistance, and the wear performance improved further as the addition of thermite reactants increased. The authors ascribed the enhanced wear resistance to two main reasons: (i) in-situ hybrid Al_2O_3-$(Cr, Fe)_7C_3$ particles played an effective resisting role to the microplowing of the ring, and (ii) the γ-Fe matrix could provide the hybrid composite coatings with good combination of strength and toughness, which in turn increased the wear resistance.

In addition, wear behavior of several hybrid ceramic particles (such as in-situ TiC + TiB_2) and hybrid ceramic particles and graphite particles (such as SiC + graphite) reinforced iron/steel matrix composites have also been investigated (Table 10), and their effects on wear performance of the hybrid iron/steel matrix composites are similar to that of the hybrid MMCs discussed above.

6. Other properties

6.1. Thermal properties

With the continuous improvement of electronic devices' performance, its power level has also increased leading to premature failure and damage of devices primarily due to overheating [2]. Accordingly, thermal management is essential to ensure the normal operation of these electronic devices, which greatly depends on the heat dissipation efficiency from microchips through the heat

spreader and heat sink. Moreover, electronic devices sometimes experience large temperature change, thus leading to thermally induced mechanical stress due to the difference in coefficient of thermal expansion (CTE) between electronic packaging materials and chips, which can cause damage of the devices. Therefore, the electronic devices with high performance require the heat dissipation materials with low CTE, high thermal conductivity and high mechanical properties. In addition, the light-weighting has also become an inevitable trend in electronic industries in recent years, so low weight of these materials used in this field should also be considered.

Cu and Al matrix composites, such as SiC/Al and diamond/Cu composites, are usually used as packaging materials due to the combination of the high thermal conductivities of the metallic matrices and low CTE of the reinforcements [201]. Tong [202] have introduced the advantages and disadvantages of conventional MMCs containing different reinforcements in his previous book. Moreover, Tjong [2] and Hidalgo-Manrique et al. [25] reviewed thermal properties of CNTs or GNPs reinforced Al and Cu matrix composites. However, the thermal performance of the hybrid reinforced MMCs, which are more likely to have high mechanical and thermal properties, have not been reviewed. Thus, thermal properties of hybrid Cu, Al and Mg matrix composites are summarized in this section and the results are shown in Table 11.

Chu et al. [154] demonstrated that Mo_2C nanoparticles firmly attached on RGO can lead to an enhanced reduction in CTE, much higher mechanical performance but a decreased thermal conductivity for hybrid Mo_2C + RGO/Cu composites compared to RGO/Cu composites and pure Cu. Luo et al. [203] fabricated Ag nanoparticles decorated RGO reinforced Cu matrix composites via powder metallurgy method, and found that the hot pressing parameters could significantly influence the thermal conductivity of the composites.

Guo et al. [107] investigated the effects of post heat treatment on mechanical and thermal properties of hybrid SiC and CNTs reinforced Al matrix composites, and the results revealed that Al_4C_3 can be formed between CNTs and Al matrix during heat treatment, leading to a decrease in the CTE and an improvement in mechanical performance, indicating that heat treatment might be a potential approach for tailoring overall mechanical and thermal properties of Al matrix composites containing CNTs. Lei et al. [207] studied the thermal expansion behavior between 100 °C and 600 °C of Al matrix composites containing hybrid micro-/nano-sized Al_2O_3 particles, and the experimental results and theoretical predictions of different models were also compared (see Figs. 37 and 38). Moreover, the results also revealed that the concentration of nanoparticles has significant effect on CTE of the composites. When the composites contain low nanoparticle concentration, the CTE is controlled by the relaxation of residual stresses, while the CTE of composites containing high nanoparticle content is controlled by a percolation effect.

Kumar et al. [206] examined the thermal cycling behavior of hybrid saffil short fibers and SiC particulates reinforced AE42 alloy matrix composites, and they found that the decrease in CTE with addition of hybrid reinforcements was much greater than that predicted by the simple rule of mixture, which suggested a more complex interaction mechanism of the hybrid reinforcements. It is worth noting that the studies on thermal properties of Mg matrix composites are significantly fewer than that of Cu and Al matrix composites due to the lower thermal conductivity and higher CTE of Mg matrix. However, Mg matrix composites might be more widely used in electronic industries due to the increasing demands for lightweight. Therefore, the investigation of the thermal behavior of Mg matrix composites should be paid more attention.

6.2. Electrical properties

Metals, especially Cu and its alloys, have good electrical conductivity, which have been widely used as electrical conductors in powder transmission for a long time. Graphene displays excellent electron mobility (about 200000 $cm^2V^{-1}s^{-1}$ [208]) and hence is employed as reinforcement for the improvement of electrical properties of Cu. Hidalgo-Manrique et al. [25] reviewed the electrical properties of graphene reinforced Cu matrix composites, and they summarized that the exact enhancements of electrical conductivity depend on the graphene content, the fabrication methods and parameters, and the graphene derivative. Hybrid Cu matrix can provide good comprehensive performance, including high mechanical properties and good electrical conductivity. Therefore, we will mainly discuss the effects of hybrid reinforcements on the electrical properties of Cu matrix composites in this section, and the results are listed in Table 12.

Luo et al. [155] prepared hybrid RGO and Ag nanoparticles reinforced Cu matrix composites by forming Ag nanoparticles on the surface of RGO via in-situ method. Compared to pure Cu and RGO/Cu matrix composite, the hybrid composite displayed superior overall mechanical and electrical performance. They attributed the higher electrical conductivity of hybrid composite than that of RGO/Cu composite to the following two reasons: (i) the electrical conductivity of Ag itself is better than Cu, which is known as “inheritance” [209]; (ii) the Ag nanoparticles distributed on the surface of RGO can strongly bond with carbon atoms and effectively enhance the scattering of electron transport in graphene [210]. Moreover, the authors also found that the hot-pressing parameters can also significantly influence the electrical conductivity of the composites [203].

Liang et al. [67] fabricated hybrid TiB whiskers and TiB_2 particles reinforced Cu matrix composites by using in-situ mixing casting followed by hot rolling. They also found that the annealing heat treatment can significantly enhance both the mechanical and electrical properties. Moreover, compared to the as-annealed 2.6 wt % TiB_{2p}/Cu composite, the as-annealed (1.0 wt% TiB_{2p} + 0.9 wt% TiB_w)/Cu hybrid composites showed both higher strength and better electrical conductivity, indicating that a better strengthening effect can be achieved by adding less hybrid reinforcements due to the synergistic strengthening effect, which can help maintain the electrical performance at a relatively high level.

7. Summary and outlooks

Hybrid MMCs exhibit good overall mechanical, tribological and physical properties. The remarkable combinations of these properties have attracted more and more attentions in this field. Many types of the hybrid reinforcements have been proposed, and different fabrication methods (ex-situ and in-situ) have been developed in recent past. The effects of different hybrid reinforcements on the mechanical, tribological, thermal and electrical properties have been critically investigated. Some relatively accurate prediction models for mechanical properties have also been proposed. For further development of this field, it is essential to further optimize the current fabrication techniques and develop new processing methods and new hybrid composite formulations. In addition, systematic investigations on the properties of the existing hybrid composite systems should be paid more attention.

Application is one of the best ways to promote sustainable development in this field. Conventional MMCs have found wide applications as structural materials components for aerospace, automotive and transportation industries, and as heat dissipation materials for electronic devices as well as electrical conductors in some particular areas [2,3,211,212]. Hybrid reinforced MMCs with

excellent overall properties can be employed to replace these conventional MMCs. The successful commercialization of the hybrid MMCs can also create new markets for innovations and promote the development in some areas closely related to the society.

Although a number of types of hybrid reinforcements have been used, some new types should also be designed and proposed for specific performance. Novel fabrication routes, such as new additive manufacturing methods, should be taken into account to fabricate hybrid MMCs with ideal distribution of hybrid reinforcements. Moreover, designing and constructing hierarchical and multi-scale architecture may assist to overcome the strength-ductility trade-off of the hybrid MMCs. The numerical methods for hybrid reinforcements containing different shapes and scales should be used for fundamental research, which can effectively save researching time and costs. Additionally, the mechanisms of synergistic effects caused by the interaction of hybrid reinforcements have not been fully elucidated and should be addressed. Finally, the prediction models for physical properties, including thermal and electrical properties of hybrid MMCs should also be developed.

Declaration of competing interest

The authors declare that they have no known competing financial interests or personal relationships that could have appeared to influence the work reported in this paper.

Acknowledgements

This work was supported by the China Scholarship Council (201807000021), Key Development Project of Sichuan Province (grant number 2017GZ0399), the 2017 Doctoral Innovation Fund Program of Southwest Jiaotong University (grant number D-CX201733), and the Innovative & Practice Project of Graduate School of Southwest Jiaotong University (grant number 2018KXK05).

References

[1] I.A. Ibrahim, F.A. Mohamed, E.J. Lavernia, Particulate reinforced metal matrix composites- a review, J. Mater. Sci. 26 (5) (1991) 1137–1156.
[2] S.C. Tjong, Recent progress in the development and properties of novel metal matrix nanocomposites reinforced with carbon nanotubes and graphene nanosheets, Mater. Sci. Eng. R 74 (10) (2013) 281–350.
[3] D.B. Miracle, Metal matrix composites - from science to technological significance, Compos. Sci. Technol. 65 (15–16) (2005) 2526–2540.
[4] X. Zhang, N.Q. Zhao, C.N. He, The superior mechanical and physical properties of nanocarbon reinforced bulk composites achieved by architecture design–a review, Prog. Mater. Sci. (2020), 100672. In press.
[5] A. Mortensen, J. Llorca, Metal matrix composites, Annu. Rev. Mater. Res. 9 (6) (2010) 1–16.
[6] M. Malaki, W.W. Xu, A.K. Kasar, P.L. Menezes, H. Dieringa, R.S. Varma, M. Gupta, Advanced metal matrix nanocomposites, Metals 9 (3) (2019), 330.
[7] M. Gupta, W.L.E. Wong, Magnesium-based nanocomposites: lightweight materials of the future, Mater. Char. 105 (2015) 30–46.
[8] L.Y. Chen, J.Q. Xu, H. Choi, M. Pozuelo, X.L. Ma, S. Bhowmick, J.M. Yang, S. Mathaudhu, X.C. Li, Processing and properties of magnesium containing a dense uniform dispersion of nanoparticles, Nature 528 (2015) 539–543.
[9] Z. Li, Q. Guo, Z.Q. Li, G.L. Fan, D.B. Xiong, Y.S. Su, J. Zhang, D. Zhang, Enhanced mechanical properties of graphene (reduced graphene oxide)/aluminium composites with a bioinspired nanolaminated structure, Nano Lett. 15 (12) (2015) 8077–8083.
[10] M.A. Meyers, P.Y. Chen, A.Y.M. Lin, Y. Seki, Biological materials: structure and mechanical properties, Prog. Mater. Sci. 53 (1) (2008) 1–206.
[11] J.W.C. Dunlop, P. Fratzl, Biological composites, Annu. Rev. Mater. Res. 40 (1) (2010) 1–24.
[12] U.G.K. Wegst, H. Bai, E. Saiz, A.P. Tomsia, R.O. Ritchie, Bioinspired structural materials, Nat. Mater. 14 (1) (2015) 23–36.
[13] T.J. Kang, J.W. Yoon, D.I. Kim, S.S. Kum, Sandwich-type laminated nanocomposites developed by selective dip-coating of carbon nanotubes, Adv. Mater. 19 (3) (2007) 427–432.
[14] Y.Y. Xiang, X.J. Wang, X.S. Hu, L.L. Meng, Z.X. Song, X.J. Li, Z.M. Sun, Q. Zhang, K. Wu, Achieving ultra-high strengthening and toughening efficiency in carbon nanotubes/magnesium composites via constructing micro-nano layered structure, Compos. Part A 119 (2019) 225–234.
[15] Z. Li, G. Fan, Z. Tan, Q. Guo, D. Xiong, Y. Su, Z. Li, D. Zhang, Uniform dispersion of graphene oxide in aluminium powder by direct electrostatic adsorption for fabrication of graphene/aluminium composites, Nanotechnology 25 (32) (2014), 325601.
[16] L. Zhao, Q. Guo, Z. Li, Z. Li, G. Fan, D.B. Xiong, T. Su, J. Zhang, Z. Tan, D. Zhang, Strain-rate dependent deformation mechanism of graphene-Al nanolaminated composites studied using micro-pillar compression, Int. J. Plast. 105 (2018) 128–140.
[17] Z. Li, G.L. Fan, Q. Guo, Z.Q. Li, Y.S. Su, D. Zhang, Synergistic strengthening effect of graphene-carbon nanotube hybrid structure in aluminium matrix composites, Carbon 95 (2015) 419–427.
[18] M.J. Shen, X.J. Wang, M.F. Zhang, M.Y. Zheng, K. Wu, Significantly improved strength and ductility in bimodal-size grained microstructural magnesium matrix composites reinforced by bimodal sized SiCp over traditional magnesium matrix composites, Compos. Sci. Technol. 118 (2015) 85–93.
[19] K. Umanath, K. Palanikumar, S.T. Selvamani, Analysis of dry sliding wear behaviour of Al6061/SiC/Al_2O_3 hybrid metal matrix composites, Compos. Part B 53 (2013) 159–168.
[20] S.L. Wei, L.J. Huang, X.T. Li, Q. An, L. Geng, Interactive effects of cyclic oxidation and structural evolution for Ti-6Al-4V/(TiC+TiB) alloy composites at elevated temperatures, J. Alloys Compd. 752 (5) (2018) 164–178.
[21] M. Rashad, F.S. Pan, A. Tang, M. Asif, M. Aamir, Synergetic effect of graphene nanoplatelets (GNPs) and multi-walled carbon nanotube (MW-CNTs) on mechanical properties of pure magnesium, J. Alloys Compd. 603 (5) (2014) 111–118.
[22] S.K. Thakur, G.T. Kwee, M. Gupta, Development and characterization of magnesium composites containing nano-sized silicon carbide and carbon nanotubes as hybrid reinforcements, J. Mater. Sci. 42 (24) (2007) 10040–10046.
[23] V.K.S. Jain, K.U. Yazar, S. Muthukumaran, Development and characterization of Al5083-CNTs/SiC composites via friction stir processing, J. Alloys Compd. 798 (25) (2019) 82–92.
[24] M.J. Shen, X.J. Wang, M.F. Zhang, X.S. Hu, M.Y. Zhang, K. Wu, Fabrication of bimodal size SiCp reinforced AZ31B magnesium matrix composites, Mater. Sci. Eng. A 601 (17) (2014) 58–64.
[25] P. Hidalgo-Manrique, X. Lei, R. Xu, M.Y. Zhou, I.A. Kinloch, R.J. Young, Copper/graphene composites: a review, J. Mater. Sci. 54 (19) (2019) 12236–12289.
[26] L. Xiao, W.J. Lu, J.L. Qin, Y.F. Chen, D. Zhang, M.M. Wang, F. Zhu, B. Ji, Effects of reinforcements on creep resistance of hybrid-reinforced titanium matrix composites, Metall. Mater. Trans. A 41 (7) (2010) 1855–1863.
[27] A.D. Moghadam, E. Omrani, P.L. Menezes, P.K. Rohatgi, Mechanical and tribological properties of self-lubricating metal matrix nanocomposites reinforced by carbon nanotubes (CNTs) and graphene - a review, Compos. Part B 77 (2015) 402–420.
[28] S.R. Bakshi, D. Lahiri, A. Agarwal, Carbon nanotube reinforced metal matrix composites-a review, Int. Mater. Rev. 55 (1) (2010) 41–64.
[29] M. Yang, Y. Liu, T.X. Fan, D. Zhang, Metal-graphene interfaces in epitaxial and bulk systems: a review, Prog. Mater. Sci. 110 (2020), 100652.
[30] M.L. Chen, G.L. Fan, Z.Q. Tan, D.D. Xiong, Q. Guo, Y.S. Su, J. Zhang, Z.Q. Li, M. Naito, D. Zhang, Design of an efficient flake powder metallurgy route to fabricate CNT/6061Al composites, Mater. Des. 142 (15) (2018) 288–296.
[31] K. Morsi, A. Esawi, Effect of mechanical alloying time and carbon nanotube (CNT) content on the evolution of aluminium (Al)–CNT composite powders, J. Mater. Sci. 42 (2007) 4954–4959.
[32] X.F. Chen, J.M. Tao, Y.C. Liu, R. Bao, F.X. Li, C.J. Li, J.H. Yi, Interface interaction and synergistic strengthening behaviour in pure copper matrix composites reinforced with functionalized carbon nanotube-graphene hybrids, Carbon 146 (2019) 736–755.
[33] M.Y. Zhou, L.B. Ren, L.L. Fan, K.S. Tun, M. Gupta, Y.W.X. Zhang, T.H. Lu, G.F. Quan, Achieving ultra-high strength and good ductility in AZ61 alloy composites containing hybrid micron SiC and carbon nanotubes reinforcements, Mater. Sci. Eng. A 768 (19) (2019), 138447.
[34] A. Azarniya, A. Azarniya, S. Sovizi, H.R.M. Hosseini, T. Varol, A. Kawasaki, S. Ramakrishna, Physicomechanical properties of spark plasma sintered carbon nanotube-reinforced metal matrix nanocomposites, Prog. Mater. Sci. 90 (2017) 276–324.
[35] X. Zhang, S.F. Li, D. Pan, B. Pan, K. Kondoh, Microstructure and synergistic-strengthening efficiency of CNTs-SiC_p dual-nano reinforcements in aluminium matrix composites, Compos. Part A 105 (2018) 87–96.
[36] X.J. Zhang, P.Y. Dong, B.G. Zhang, S.Y. Tang, Z. Yang, Y. Chen, W.C. Yang, Preparation and characterization of reduced graphene oxide/copper composites incorporated with nano-SiO_2 particles, J. Alloys Compd. 671 (25) (2016) 465–472.
[37] N. Saheb, Z. Iqbal, A. Khalil, A.S. Hakeem, N.A. Aqeeli, T. Laoui, A. Al-qutub, R. Kirchner, Spark plasma sintering of metals and metal matrix nanocomposites: a review, J. Nanomater. 2012 (2012) 1–13.
[38] W. Wai, L. Eugene, M. Gupta, Characteristics of aluminium and magnesium based nanocomposites processed using hybrid microwave sintering, J. Microw. Power 44 (1) (2010) 14–27.
[39] D.P. Jiang, J.K. Yu, Fabrication of Al_2O_3/SiC/Al hybrid nanocomposites through solidification process for improved mechanical properties, Metals 8 (8)

(2018) 572–587.
[40] X.F. Niu, G. Li, Z.Y. Zhang, P.W. Zhou, H.X. Wang, S.X. Zhang, W.L. Cheng, Simultaneously improving the strength and ductility of extruded bimodal size SiC_p/AZ61 composites: synergistic effect of micron/nano SiCp and submicron $Mg_{17}Al_{12}$ precipitates, Mater. Sci. Eng. A 743 (16) (2019) 207–216.
[41] G. Nageswaran, S. Natarajan, K.R. Ramkumar, Synthesis, structural characterization, mechanical and wear behaviour of Cu-TiO_2-Gr hybrid composite through stir casting technique, J. Alloys Compd. 768 (5) (2018) 733–741.
[42] M.R. Ghomashchi, A. Vikhrov, Squeeze casting: an overview, J. Mater. Process. Technol. 101 (1) (2000) 1–9.
[43] I.G. Crouch, Aluminium squeeze casting technology - a European researches viewpoint, in: Australian Conference on Materials for Industrial Development, Christchurch, New Zealand, 24-26 August 1987, 1987.
[44] X.N. Zhang, L. Geng, G.S. Wang, Fabrication of Al-based hybrid composites reinforced with SiC whiskers and SiC nanoparticles by squeeze casting, J. Mater. Process. Technol. 176 (1) (2006) 146–151.
[45] A. Agarwal, S.R. Bakshi, D. Lahiri, Carbon Nanotube Reinforced Metal Matrix Composites, CRC Press, 2011.
[46] H.W. Zhang, J. Loukus, A. Loukus, Improvement of the bonding interface in hybrid fiber/particle preform reinforced Al matrix composite, Mater. Lett. 63 (2) (2009) 310–312.
[47] J. Babu, A. Srinivasan, C.G. Kang, Nano and macromechanical properties of aluminium (A356) based hybrid composites reinforced with multiwall carbon nanotubes/alumina fiber, J. Compos. Mater. 51 (11) (2016) 1631–1642.
[48] J.S.S. Babu, C.G. Kang, Nanomechanical properties of magnesium-based hybrid composites with graphite nanofiber and alumina short fiber, J. Compos. Mater. 45 (25) (2011) 2685–2695.
[49] S. Sankaranarayanan, S. Jayalakshmi, M. Gupta, Effect of ball milling the hybrid reinforcements on the microstructure and mechanical properties of Mg-(Ti+n-Al_2O_3) composites, J. Alloys Compd. 509 (26) (2011) 7229–7237.
[50] M. Khan, A. Rehman, T. Aziz, K. Naveed, I. Ahmad, T. Subhani, Cold formability of friction stir processed aluminium composites containing carbon nanotubes and boron carbide particles, Mater. Sci. Eng. A 701 (31) (2017) 382–388.
[51] H. Eskandari, R. Taheri, F. Khodabakhshi, Friction-stir processing of an AA8026-TiB_2-Al_2O_3 hybrid nanocomposite: microstructural developments and mechanical properties, Mater. Sci. Eng. A 660 (13) (2016) 84–96.
[52] M. Sharifitabar, M. Kashefi, S. Khorshahian, Effect of friction stir processing pass sequence on properties of Mg-$ZrSiO_4$-Al_2O_3 surface hybrid micro/nanocomposites, Mater. Des. 108 (15) (2016) 1–7.
[53] Z.Y. Liu, B.L. Xiao, W.G. Wang, Z.Y. Ma, Developing high-performance aluminium matrix composites with directionally aligned carbon nanotubes by combining friction stir processing and subsequent rolling, Carbon 62 (2013) 35–42.
[54] S.M. Ghalehbandi, M. Malaki, M. Gupta, Accumulative roll bonding - a review, Appl. Sci. 9 (17) (2019) 3627–3659.
[55] S.J. Yoo, S.H. Han, W.J. Kim, Magnesium matrix composites fabricated by using accumulative roll bonding of magnesium sheets coated with carbon-nanotube-containing aluminium powders, Scripta Mater. 67 (2) (2012) 129–132.
[56] L.L. Meng, X.J. Wang, J.L. Ning, X.S. Hu, G.H. Fan, K. Wu, Beyond the dimensional limitation in bio-inspired composite: insertion of carbon nanotubes induced laminated Cu composite and the simultaneously enhanced strength and toughness, Carbon 130 (2018) 222–232.
[57] S. Baazamat, M. Tajally, E. Borhani, Fabrication and characteristic of Al-based hybrid nanocomposite reinforced with WO_3 and SiC by accumulative roll bonding process, J. Alloys Compd. 653 (25) (2015) 39–46.
[58] S.C. Tjong, Z.Y. Ma, Microstructural and mechanical characteristics of in situ metal matrix composites, Mater. Sci. Eng. R 29 (3) (2000) 49–113.
[59] J. David Raja Selvam, I. Dinaharan, S. Vibin Philip, P.M. Mashinini, Microstructure and mechanical characterization of in situ synthesized AA6061/(TiB_2+Al_2O_3) hybrid aluminium matrix composites, J. Alloys Compd. 740 (2018) 529–535.
[60] C.F. Feng, L. Froyen, On the reaction mechanism of an Al–TiO_2–B system for producing in-situ (Al_2O_3+ TiB_2)/Al composites, Scripta Mater. 39 (1) (1998) 109–118.
[61] C. Liu, L.J. Huang, L. Geng, Y. Jiao, A. Tang, In situ synthesis of (TiC + Ti_3SiC_2 + Ti_5Si_3)/Ti_6Al_4V composites with tailored two-scale architecture, Adv. Eng. Mater. 17 (7) (2015) 933–941.
[62] Y.Y. Chen, D.D.L. Chung, In situ Al-TiB composite obtained by stir casting, J. Mater. Sci. 31 (2) (1996) 311–315.
[63] Z.Y. Ma, J.H. Li, S.X. Li, X.G. Ning, Y.X. Lu, J. Bi, Property-microstructure correlation in in situ formed Al_2O_3, TiB_2 and Al_3Ti mixture-reinforced aluminium composites, J. Mater. Sci. 31 (3) (1996) 741–747.
[64] P. Xiao, Y.M. Gao, C.C. Yang, Z.W. Liu, T.F. Li, F.X. Xu, Microstructure, mechanical properties and strengthening mechanisms of Mg matrix composites reinforced with in situ nanosized TiB_2 particles, Mater. Sci. Eng. A 710 (2018) 251–259.
[65] H. Nakata, T. Choh, N. Kanetake, Fabrication and mechanical properties of in situ formed carbide particulate reinforced aluminium composite, J. Mater. Sci. 30 (7) (1995) 1719–1727.
[66] S.L. Zhang, Y.T. Zhao, G. Chen, X.N. Cheng, X.Y. Huo, Fabrication and dry sliding wear behaviour of in situ Al-K_2ZrF_6-KBF_4 composites reinforced by Al_3Zr and ZrB_2 particles, J. Alloys Compd. 450 (1–2) (2008) 185–192.
[67] S.H. Liang, W.Z. Li, Y.H. Jiang, F. Cao, G.Z. Dong, P. Xiao, Microstructures and properties of hybrid copper matrix composites reinforced by TiB whiskers and TiB_2 particles, J. Alloys Compd. 797 (2019) 589–594.
[68] B.N. Sahoo, S.K. Panigrahi, Synthesis, characterization and mechanical properties of in-situ (TiC-TiB_2) reinforced magnesium matrix composite, Mater. Des. 109 (2016) 300–313.
[69] M. Shamanian, M. Mohammadnezhad, H. Asgari, J. Szpunar, Fabrication and characterization of Al–Al_2O_3–ZrC composite produced by accumulative roll bonding (ARB) process, J. Alloys Compd. 618 (2015) 19–26.
[70] M.R. Nasresfahani, M. Shamanian, Development and characterization of Al/MWCNT–Al_2O_3 hybrid composite by accumulative roll bonding, J. Mater. Sci. 53 (15) (2018) 10812–10821.
[71] H. Farajzadeh Dehkordi, M.R. Toroghinejad, K. Raeissi, Fabrication of Al/Al_2O_3/TiC hybrid composite by anodizing and accumulative roll bonding processes and investigation of its microstructure and mechanical properties, Mater. Sci. Eng. A 585 (2013) 460–467.
[72] A. Ahmadi, M.R. Toroghinejad, A. Najafizadeh, Evaluation of microstructure and mechanical properties of Al/Al_2O_3/SiC hybrid composite fabricated by accumulative roll bonding process, Mater. Des. 53 (1) (2013) 13–19.
[73] X.D. Yang, C.S. Shi, C.N. He, E.Z. Liu, J.J. Li, N.Q. Zhao, Synthesis of uniformly dispersed carbon nanotube reinforcement in Al powder for preparing reinforced Al composites, Compos. Part A 42 (11) (2011) 1833–1839.
[74] H.P. Li, J.W. Fan, X.X. Geng, B.E. Li, C.Y. Liang, H.S. Wang, Y.X. Li, Z.J. Qiao, J.L. Kang, Alumina powder assisted carbon nanotubes reinforced Mg matrix composites, Mater. Des. 60 (2014) 637–642.
[75] C.N. He, N.Q. Zhao, C.S. Shi, X. Du, J. Li, H. Li, Q. Cui, An approach to obtaining homogeneously dispersed carbon nanotubes in Al powders for preparing reinforced Al-matrix composites, Adv. Mater. 19 (8) (2007) 1128–1132.
[76] F.J. Sun, C.S. Shi, K.Y. Rhee, N.Q. Zhao, In situ synthesis of CNTs in Mg powder at low temperature for fabricating reinforced Mg composites, J. Alloys Compd. 551 (2013) 496–501.
[77] X.D. Yang, E.Z. Liu, C.S. Shi, C.N. He, J.J. Li, N.Q. Zhao, K. Kondoh, Fabrication of carbon nanotube reinforced Al composites with well-balanced strength and ductility, J. Alloys Compd. 563 (2013) 216–220.
[78] S.S. Li, Y.S. Su, Q. Ouyang, D. Zhang, In-situ carbon nanotube-covered silicon carbide particle reinforced aluminium matrix composites fabricated by powder metallurgy, Mater. Lett. 167 (2016) 118–121.
[79] S.S. Li, Y.S. Su, X.H. Zhu, H.L. Jin, Q. Ouyang, D. Zhang, Enhanced mechanical behaviour and fabrication of silicon carbide particles covered by in-situ carbon nanotube reinforced 6061 aluminium matrix composites, Mater. Des. 107 (2016) 130–138.
[80] X. Zhang, C.S. Shi, E.Z. Liu, F. He, L.Y. Ma, Q.Y. Li, J.J. Li, N.Q. Zhao, C.N. He, In-situ space-confined synthesis of well-dispersed three-dimensional graphene/carbon nanotube hybrid reinforced copper nanocomposites with balanced strength and ductility, Compos. Part A 103 (2017) 178–187.
[81] T. Debroy, H.L. Wei, J.S. Zuback, T. Mukherjee, J.W. Elmer, J.O. Milewski, A.M. Beese, A. Wilson-Heid, A. De, W. Zhang, Additive manufacturing of metallic components- Process, structure and properties, Prog. Mater. Sci. 92 (2018) 112–224.
[82] W.J. Sames, F.A. List, S. Pannala, R.R. Dehoff, S.S. Babu, The metallurgy and processing science of metal additive manufacturing, Int. Mater. Rev. 61 (5) (2016) 315–360.
[83] B. Almangour, Additive Manufacturing of Emerging Materials, Springer, 2019.
[84] W.H. Yu, S.L. Sing, C.K. Chua, C.N. Kuo, X.L. Tian, Particle-reinforced metal matrix nanocomposites fabricated by selective laser melting: a state of the art review, Prog. Mater. Sci. 104 (2019) 330–379.
[85] S. Dadbakhsh, R. Mertens, L. Hao, J.V. Humbeeck, J.P. Kruth, Selective laser melting to manufacture “in situ” metal matrix composites: a review, Adv. Eng. Mater. 21 (3) (2019), 1801244.
[86] D. Herzog, V. Seyda, E. Wycisk, C. Emmelmann, Additive manufacturing of metals, Acta Mater. 117 (2016) 371–392.
[87] S. Dadbakhsh, L. Hao, In situ formation of particle reinforced Al matrix composite by selective laser melting of Al/Fe_2O_3 powder mixture, Adv. Eng. Mater. 14 (1–2) (2012) 45–48.
[88] S. Dadbakhsh, L. Hao, P.G.E. Jerrard, D.Z. Zhang, Experimental investigation on selective laser melting behaviour and processing windows of in situ reacted Al/Fe_2O_3 powder mixture, Powder Technol. 231 (2012) 112–121.
[89] S. Dadbakhsh, L. Hao, Effect of Al alloys on selective laser melting behaviour and microstructure of in situ formed particle reinforced composites, J. Alloys Compd. 541 (2012) 328–334.
[90] F. Chang, D.D. Gu, D.H. Dai, P.P. Yuan, Selective laser melting of in-situ Al_4SiC_4 + SiC hybrid reinforced Al matrix composites: influence of starting SiC particle size, Surf. Coating. Technol. 272 (2015) 15–24.
[91] Y. Zhang, J. Sun, R. Vilar, Haracterization of (TiB+TiC)/TC4 in situ titanium matrix composites prepared by laser direct deposition, J. Mater. Process. Technol. 211 (4) (2011) 597–601.
[92] M. Das, V.K. Balla, D. Basu, I. Manna, T.S.S. Kumar, A. Bandyopadhyay, Laser processing of in situ synthesized TiB–TiN-reinforced Ti6Al4V alloy coatings, Scripta Mater. 66 (8) (2012) 578–581.
[93] B. Song, S.J. Dong, P. Coddet, G.S. Zhou, S. Ouyang, H.L. Liao, C. Coddet, Microstructure and tensile behavior of hybrid nano-micro SiC reinforced iron matrix composites produced by selective laser melting, J. Alloys Compd. 579 (2013) 415–421.
[94] N.K. Bhoi, H. Singh, S. Pratap, Developments in the aluminium metal matrix composites reinforced by micro/nano particles - a review, J. Compos. Mater.

(2019) 1–21, 0 (0).
[95] C. Kim, K. Cho, M.H. Manjili, M. Nezafati, Mechanical performance of particulate-reinforced Al metal-matrix composites (MMCs) and Al metal-matrix nano-composites (MMNCs), J. Mater. Sci. 52 (23) (2017) 13319–13349.
[96] J. Hu, G.H. Wu, Q. Zhang, H.S. Gou, Mechanical properties and damping capacity of SiCp/TiNi$_f$/Al composite with different volume fraction of SiC particle, Compos. Part B 66 (2014) 400–406.
[97] K.H. Oh, K.S. Han, Short-fiber/particle hybrid reinforcement: effects on fracture toughness and fatigue crack growth of metal matrix composites, Compos. Sci. Technol. 67 (7–8) (2007) 1719–1726.
[98] T.W. Lu, W.P. Chen, P. Wang, M.D. Mao, Y.X. Liu, Z.Q. Fu, Enhanced mechanical properties and thermo-physical properties of 7075Al hybrid composites reinforced by the mixture of Cr particles and SiCp, J. Alloys Compd. 735 (2018) 1137–1144.
[99] K. Ravi Kumar, T. Pridhar, V.S. Sree Balaji, Mechanical properties and characterization of zirconium oxide (ZrO_2) and coconut shell ash (CSA) reinforced aluminium (Al 6082) matrix hybrid composite, J. Alloys Compd. 765 (2018) 171–179.
[100] Y.X. Liu, C. Yang, W.P. Chen, D.Z. Zhu, Y.Y. Li, Effects of particle size and properties on the microstructures, mechanical properties, and fracture mechanisms of 7075Al hybrid composites prepared by squeeze casting, J. Mater. Sci. 49 (22) (2014) 7855–7863.
[101] E.A.M. Shalaby, A.Y. Churyumov, A.N. Solonin, A. Lotfy, Preparation and characterization of hybrid A359/($SiC+Si_3N_4$) composites synthesized by stir/squeeze casting techniques, Mater. Sci. Eng. A 674 (2016) 18–24.
[102] T.W. Lu, S. Scudino, W.P. Chen, P. Wang, D.Y. Li, M.D. Mao, L.M. Kang, Y.X. Liu, Z.Q. Fu, The influence of nanocrystalline $CoNiFeAl_{0.4}Ti_{0.6}Cr_{0.5}$ high-entropy alloy particles addition on microstructure and mechanical properties of SiCp/7075Al composites, Mater. Sci. Eng. A 726 (2018) 126–136.
[103] S.L. Zhang, Y.T. Zhao, G. Chen, X.N. Cheng, ($Al_2O_3+Al_3Zr$)/A356 nanocomposites fabricated by magnetochemistry in situ reaction, J. Alloys Compd. 475 (1–2) (2009) 261–267.
[104] J. Wang, X. Zhang, N.Q. Zhao, C.N. He, In situ synthesis of copper-modified graphene-reinforced aluminium nanocomposites with balanced strength and ductility, J. Mater. Sci. 54 (7) (2019) 5498–5512.
[105] H. Kwon, G.G. Lee, S.G. Kim, B.W. Lee, W.C. Seo, M. Leparoux, Mechanical properties of nanodiamond and multi-walled carbon nanotubes dual-reinforced aluminium matrix composite materials, Mater. Sci. Eng. A 632 (24) (2015) 72–77.
[106] W.J. Kim, Y.J. Yu, The effect of the addition of multiwalled carbon nanotubes on the uniform distribution of TiC nanoparticles in aluminium nanocomposites, Scripta Mater. 72–73 (2014) 25–28.
[107] B.S. Guo, B. Chen, X.M. Zhang, X. Cen, X.H. Wang, M. Song, S. Ni, J.H. Yi, T. Shen, Y. Du, Exploring the size effects of Al_4C_3 on the mechanical properties and thermal behaviours of Al-based composites reinforced by SiC and carbon nanotubes, Carbon 135 (2018) 224–235.
[108] X.Q. Liu, C.J. Li, J.H. Yi, K.G. Prashanth, N. Chawake, J.M. Tao, X. You, Y.C. Liu, J. Eckert, Enhancing the interface bonding in carbon nanotubes reinforced Al matrix composites by the in situ formation of $TiAl_3$ and TiC, J. Alloys Compd. 765 (15) (2018) 98–105.
[109] S. Polat, Y. Sun, E. Çevik, H. Colijn, Microstructure and synergistic reinforcing activity of GNPs-B_4C dual-micro and nano supplements in Al-Si matrix composites, J. Alloys Compd. 806 (25) (2019) 1230–1241.
[110] B. Kaveendran, G.S. Wang, L.J. Huang, L. Geng, H.X. Peng, In situ (Al_3Zr +Al_2O_{3np})/2024Al metal matrix composite with novel reinforcement distributions fabricated by reaction hot pressing, J. Alloys Compd. 581 (25) (2013) 16–22.
[111] B.C. Ko, Y.C. Yoo, The effect of aging treatment on the microstructure and mechanical properties of AA2124 hybrid composites reinforced with both SiC whiskers and SiC particles, Compos. Sci. Technol. 59 (5) (1999) 775–779.
[112] B.S. Guo, X.M. Zhang, X. Cen, X.H. Wang, M. Song, S. Ni, J.H. Yi, T. Shen, Y. Du, Ameliorated mechanical and thermal properties of SiC reinforced Al matrix composites through hybridizing carbon nanotubes, Mater. Char. 136 (2018) 272–280.
[113] G.P. Zhang, Q.S. Mei, F. Chen, Y. Ma, X.M. Mei, J.Y. Li, X.F. Ruan, L. Wan, Production of a high strength Al/($TiAl_3+Al_2O_3$) composite from an Al-TiO_2 system by accumulative roll-bonding and spark plasma sintering, Mater. Sci. Eng. A 752 (3) (2019) 192–198.
[114] S. Tahamtan, A. Halvaee, M. Emamy, Z.Y. Jiang, A.F. Boostani, Exploiting superior tensile properties of a novel network-structure AlA206 matrix composite by hybridizing micron-sized Al_3Ti with Al_2O_3 nano particulates, Mater. Sci. Eng. A 619 (1) (2014) 190–198.
[115] A.A. Mostafapour, S.T. Khandani, Role of hybrid ratio in microstructural, mechanical and sliding wear properties of the Al5083/Graphite$_p$/Al_2O_{3p} a surface hybrid nanocomposite fabricated via friction stir processing method, Mater. Sci. Eng. A 559 (1) (2013) 549–557.
[116] M.S. Romano, N. Li, D. Antiohos, J.M. Razal, A. Nattestad, S. Beirne, S.L. Fang, Y.S. Chen, R. Jalili, G.G. Wallace, R. Baughman, J. Chen, Carbon nanotube - reduced graphene oxide composites for thermal energy harvesting applications, Adv. Mater. 25 (45) (2013) 6602–6606.
[117] H.Z. Ye, X.Y. Liu, Review of recent studies in magnesium matrix composites, J. Mater. Sci. 39 (20) (2004) 6153–6171.
[118] T. Zhang, L.H. Qi, J.W. Fu, J.M. Zhou, X.J. Chao, Effect of SiC nanowires addition on the interfacial microstructure and mechanical properties of the C$_f$-SiCNWs/AZ91D composite, J. Alloys Compd. 776 (5) (2019) 746–756.
[119] J.M. Zhou, M.Q. Yuan, Z. Li, H.M. Meng, T. Zhang, L.H. Qi, A great improvement of tensile properties of C$_f$/AZ91D composite through grafting CNTs onto the surface of the carbon fibers, Mater. Sci. Eng. A 762 (5) (2019), 138061.
[120] J.X. Zhou, L.Y. Ren, X.Y. Geng, L. Fang, H. Hu, As-cast magnesium AM60-based hybrid nanocomposite containing alumina fibres and nanoparticles: microstructure and tensile behaviour, Mater. Sci. Eng. A 740–741 (7) (2019) 305–314.
[121] B.N. Sahoo, M.D. Fhan, S. Babu, S.K. Panigrahi, G.D. Janaki Ram, Microstructural modification and its effect on strengthening mechanism and yield asymmetry of in-situ TiC-TiB_2/AZ91 magnesium matrix composite, Mater. Sci. Eng. A 724 (2) (2018) 269–282.
[122] B.N. Sahoo, S.K. Panigrahi, Effect of in-situ (TiC-TiB_2) reinforcement on aging and mechanical behaviour of AZ91 magnesium matrix composite, Mater. Char. 139 (2018) 221–232.
[123] B.N. Sahoo, S.K. Panigrahi, A study on the combined effect of in-situ (TiC-TiB_2) reinforcement and aging treatment on the yield asymmetry of magnesium matrix composite, J. Alloys Compd. 737 (15) (2018) 575–589.
[124] X.N. Zhang, D. Zhang, R.J. Wu, Z.G. Zhu, C. Wang, Mechanical properties and damping capacity of (SiC_w + B_4C_p)/ZK60A Mg alloy matrix composite, Scripta Mater. 37 (11) (1997) 1631–1635.
[125] Y.C. Guo, K.B. Nie, X.K. Kang, K.K. Deng, J.G. Han, Z.H. Zhu, Achieving high-strength magnesium matrix nanocomposite through synergistical effect of external hybrid (SiC+TiC) nanoparticles and dynamic precipitated phase, J. Alloys Compd. 771 (15) (2019) 847–856.
[126] Q.B. Nguyen, K.S. Tun, C.Y.H. Lim, M. Gupta, Influence of nano-alumina and sub-micron copper on mechanical properties of magnesium alloy AZ31, Compos. Part B 55 (2013) 486–491.
[127] S. Sankaranarayanan, R.K. Sabat, S. Jayalakshmi, S. Suwas, M. Gupta, Effect of hybridizing micron-sized Ti with nano-sized SiC on the microstructural evolution and mechanical response of Mg-5.6Ti composite, J. Alloys Compd. 575 (25) (2013) 207–217.
[128] H.P. Li, L. Cheng, X.W. Sun, Y.J. Li, B.E. Li, C.Y. Liang, H.S. Wang, J.W. Fan, Fabrication and properties of magnesium matrix composite reinforced by urchin-like carbon nanotube-alumina in situ composite structure, J. Alloys Compd. 746 (25) (2018) 320–327.
[129] M. Rashad, F.S. Pan, W. Guo, H. Lin, M. Asif, M. Irfan, Effect of alumina and silicon carbide hybrid reinforcements on tensile, compressive and microhardness behaviour of Mg–3Al–1Zn alloy, Mater. Char. 106 (2015) 382–389.
[130] M.D. Hayat, H. Singh, Z. He, P. Cao, Titanium metal matrix composites: an overview, Compos. Part A 121 (2019) 418–438.
[131] Y. Jiao, L.J. Huang, L. Geng, Progress on discontinuously reinforced titanium matrix composites, J. Alloys Compd. 767 (30) (2018) 1196–1215.
[132] L.J. Huang, L. Geng, Discontinuously Reinforced Titanium Matrix Composites, Springer, 2017.
[133] C. Liu, L.J. Huang, L. Geng, Y. Jiao, A. Tang, In situ synthesis of (TiC + Ti_3SiC_2+Ti_5Si_3)/Ti6Al4V composites with tailored two-scale architecture, Adv. Eng. Mater. 17 (7) (2015) 933–941.
[134] L.J. Huang, S. Wang, L. Geng, B. Kaveendran, H.X. Peng, Low volume fraction in situ (Ti_5Si_3+Ti_2C)/Ti hybrid composites with network microstructure fabricated by reaction hot pressing of Ti–SiC system, Compos. Sci. Technol. 82 (2013) 23–28.
[135] S.Y. Sun, M.M. Wang, L.Q. Wang, J.N. Qin, W.J. Lu, D. Zhang, The influences of trace TiB and TiC on microstructure refinement and mechanical properties of in situ synthesized Ti matrix composite, Compos. Part B 43 (8) (2012) 3334–3337.
[136] X.Y. Huang, Y.M. Gao, Z.P. Wang, Y.L. Yi, Y.R. Wang, Microstructure, mechanical properties and strengthening mechanisms of in-situ prepared (Ti_5Si_3 + $TiC_{0.67}$)/TC4 composites, J. Alloys Compd. 792 (5) (2019) 907–917.
[137] Z.Y. Hu, X.W. Cheng, S.L. Li, H.M. Zhang, H. Wang, Z.H. Zhang, F.C. Wang, Investigation on the microstructure, room and high temperature mechanical behaviours and strengthening mechanisms of the (TiB+TiC)/TC_4 composites, J. Alloys Compd. 726 (5) (2017) 240–253.
[138] Z.F. Yang, W.J. Lu, L. Zhao, J.N. Qin, D. Zhang, Microstructure and mechanical property of in situ synthesized multiple-reinforced (TiB+TiC+La_2O_3)/Ti composites, J. Alloys Compd. 455 (1–2) (2008) 210–214.
[139] H.K.S. Rahoma, Y.Y. Chen, X.P. Wang, S.L. Xiao, Influence of (TiC+TiB) on the microstructure and tensile properties of Ti-B20 matrix alloy, J. Alloys Compd. 627 (5) (2015) 415–422.
[140] L.J. Huang, L. Geng, H.X. Peng, In situ (TiB_w+TiC_p)/Ti6Al4V composites with a network reinforcement distribution, Mater. Sci. Eng. A 527 (24–25) (2010) 6723–6727.
[141] G.F. Huang, Y.F. Han, X.L. Guo, D. Qiu, L.Q. Wang, W.J. Lu, D. Zhang, Effects of extrusion ratio on microstructural evolution and mechanical behaviour of in situ synthesized Ti-6Al-4V composites, Mater. Sci. Eng. A 688 (14) (2017) 155–163.
[142] Y. Jiao, L.J. Huang, Q. An, S. Jiang, Y.N. Gao, X.P. Cui, L. Geng, Effects of Ti_5Si_3 characteristics adjustment on microstructure and tensile properties of in-situ (Ti_5Si_3+TiBw)/Ti6Al4V composites with two-scale network architecture, Mater. Sci. Eng. A 673 (15) (2016) 595–605.
[143] J.P. Qu, C.J. Zhang, S.Z. Zhang, J.C. Han, L.H. Chai, Z.Y. Chen, Y.Y. Chen, Relationships among reinforcement volume fraction, microstructure and tensile properties of (TiB_w + TiC_p)/Ti composites after ($\alpha + \beta$) forging, Mater. Sci. Eng. A 701 (31) (2017) 16–23.

[144] C.J. Zhang, F.T. Kong, S.L. Xiao, E.T. Zhao, L.J. Xu, Y.Y. Chen, Evolution of microstructure and tensile properties of in situ titanium matrix composites with volume fraction of (TiB+TiC) reinforcements, Mater. Sci. Eng. A 548 (30) (2012) 152–160.

[145] X.L. Guo, L.Q. Wang, M.M. Wang, J.N. Qin, D. Zhang, W.J. Lu, Effects of degree of deformation on the microstructure, mechanical properties and texture of hybrid-reinforced titanium matrix composites, Acta Mater. 60 (6–7) (2012) 2656–2667.

[146] P.K. Qiu, H. Li, X.L. Sun, Y.F. Han, G.F. Huang, W.J. Lu, D. Zhang, Reinforcements stimulated dynamic recrystallization behaviour and tensile properties of extruded (TiB +TiC + La_2O_3)/Ti6Al4V composites, J. Alloys Compd. 699 (30) (2017) 874–881.

[147] S. Li, K. Kondoh, H. Imai, B. Chen, L. Jia, J. Umeda, Y.B. Fu, Strengthening behaviour of in situ-synthesized (TiC-TiB)/Ti composites by powder metallurgy and hot extrusion, Mater. Des. 95 (2016) 127–132.

[148] L. Jia, X. Li, K. Kondoh, B. Chen, S.F. Li, J.K. Umeda, Z.L. Lu, Hybrid effect of TiC_p and TiB_w co-strengthening Ti matrix composites prepared by spark plasma sintering and hot extrusion, Mater. Charact. 151 (2019) 6–14.

[149] S.F. Li, K. Kondoh, H. Imai, B. Chen, L. Jia, J. Umeda, Microstructure and mechanical properties of P/M titanium matrix composites reinforced by in-situ synthesized TiC-TiB, Mater. Sci. Eng. A 628 (25) (2015) 75–83.

[150] G.F. Huang, X.L. Guo, Y.F. Han, L.Q. Wang, W.J. Lu, D. Zhang, Effect of extrusion dies angle on the microstructure and properties of (TiB+TiC)/Ti6Al4V in situ titanium matrix composite, Mater. Sci. Eng. A 667 (2016) 317–325.

[151] Y. Jiao, L.J. Huang, T.B. Duan, S.L. Wei, B. Kaveendran, L. Geng, Controllable two-scale network architecture and enhanced mechanical properties of (Ti_5Si_3+TiB_w)/Ti6Al4V composites, Sci. Rep. 6 (1) (2016), 32991.

[152] T. Thankachan, K.S. Prakash, V. Kavimani, Investigating the effects of hybrid reinforcement particles on the microstructural, mechanical and tribological properties of friction stir processed copper surface composites, Compos. Part B 174 (2019), 107057.

[153] X.J. Zhang, W.C. Yang, J.Y. Zhang, X.Y. Ge, X.R. Liu, Y.Z. Zhan, Multiscale graphene/carbon fiber reinforced copper matrix hybrid composites: microstructure and properties, Mater. Sci. Eng. A 743 (2019) 512–519.

[154] K. Chu, F. Wang, Y.B. Li, X.H. Wang, D.J. Huang, Z.R. Geng, Interface and mechanical/thermal properties of graphene/copper composite with Mo_2C nanoparticles grown on graphene, Compos. Part B 109 (2018) 267–279.

[155] H.B. Luo, Y.W. Sui, J.Q. Qi, Q.K. Meng, F.X. Wei, Y.Z. He, Mechanical enhancement of copper matrix composites with homogeneously dispersed graphene modified by silver nanoparticles, J. Alloys Compd. 729 (2017) 293–302.

[156] Y.X. Tang, X.M. Yang, R.R. Wang, M.X. Li, Enhancement of the mechanical properties of graphene-copper composites with graphene-nickel hybrids, Mater. Sci. Eng. A 599 (2014) 247–254.

[157] M.R. Akbarpour, E. Salahi, H.F. Alikhani, A. Simchi, H.S. Kim, Fabrication, characterization and mechanical properties of hybrid composites of copper using the nanoparticulates of SiC and carbon nanotubes, Mater. Sci. Eng. A 572 (2013) 83–90.

[158] F. Akhtar, Microstructure evolution and wear properties of in situ synthesized TiB_2 and TiC reinforced steel matrix composites, J. Alloys Compd. 459 (1–2) (2008) 491–497.

[159] Q.C. Jiang, B.X. Ma, H.Y. Wang, Y. Wang, Y.P. Dong, Fabrication of steel matrix composites locally reinforced with in situ TiB_2-TiC particulates using self-propagating high-temperature synthesis reaction of Al-Ti-B_4C system during casting, Compos. Part A 37 (1) (2006) 133–138.

[160] T. Wen, K. Fan, F. Zhang, High strength and high ductility in nickel matrix nanocomposites reinforced by carbon nanotubes and onion-like-carbon hybrid reinforcements, J. Alloys Compd. 814 (2020), 152303.

[161] Z. Fattahi, S.A. Sajjadi, A. Babakhani, F. Saba, Ni–Cr matrix composites reinforced with nano- and micron-sized surface-modified zirconia: synthesis, microstructure and mechanical properties, J. Alloys Compd. 817 (2020), 152755.

[162] C. Kim, I. Sohn, M. Nezafati, J.B. Ferguson, B.F. Schultz, G.Z. Bajestani, P.K. Rohatgi, K. Cho, Prediction models for the yield strength of particle-reinforced unimodal pure magnesium (Mg) metal matrix nanocomposites (MMNCs), J. Mater. Sci. 48 (12) (2013) 4191–4204.

[163] X. Zhang, S.F. Li, B. Pan, D. Pan, S.Y. Zhou, S.H. Yang, L. Jia, K. Kondoh, A novel strengthening effect of in-situ nano Al_2O_{3w} on CNTs reinforced aluminium matrix nanocomposites and the matched strengthening mechanisms, J. Alloys Compd. 764 (2018) 279–288.

[164] C. Goh, J. Wei, L.C. Lee, M. Gupta, Properties and deformation behaviour of Mg-Y_2O_3 nanocomposites, Acta Mater. 55 (15) (2007) 5115–5121.

[165] Z. Zhang, D.L. Chen, Consideration of Orowan strengthening effect in particulate-reinforced metal matrix nanocomposites: a model for predicting their yield strength, Scripta Mater. 54 (7) (2006) 1321–1326.

[166] N. Hansen, Hall-Petch relation and boundary strengthening, Scripta Mater. 51 (8) (2004) 801–806.

[167] K.K. Deng, J.Y. Shi, C.J. Wang, X.J. Wang, Y.W. Wu, K.B. Nie, K. Wu, Microstructure and strengthening mechanism of bimodal size particle reinforced magnesium matrix composite, Compos. Part A 43 (8) (2012) 1280–1284.

[168] B. Chen, J. Shen, X. Ye, L. Jia, S. Li, J. Umeda, M. Takahashi, K. Kondoh, Length effect of carbon nanotubes on the strengthening mechanisms in metal matrix composites, Acta Mater. 140 (2017) 317–325.

[169] V.C. Nardone, K.M. Prewo, On the strength of discontinuous silicon carbide reinforced aluminium composites, Scripta Metall. 20 (1) (1986) 43–48.

[170] M.Y. Zhou, X.N. Qu, L.B. Ren, L.L. Fan, Y.W.X. Zhang, Y.Y. Guo, G.F. Quan, Q. Tang, B. Liu, H. Sun, The effects of carbon nanotubes on the mechanical and wear properties of AZ31 alloy, Materials 10 (12) (2017), 1385.

[171] F. Akhlaghi, A. Zare-Bidaki, Influence of graphite content on the dry sliding and oil impregnated sliding wear behaviour of Al 2024-graphite composites produced by in situ powder metallurgy method, Wear 266 (1–2) (2009) 37–45.

[172] S.K. Khatkar, N.M. Suri, S. Kant, Pankaj, A review on mechanical and tribological properties of graphite reinforced self-lubricating hybrid metal matrix composites, Rev. Adv. Mater. Sci. 56 (1) (2018) 1–20.

[173] B. Hekner, J. Myalski, N. Valle, P.A. Botor, L.M. Sopicka, J. Wieczorek, Friction and wear behaviour of Al-SiC(n) hybrid composites with carbon addition, Compos. Part B 108 (2017) 291–300.

[174] J.S. Zhang, S.F. Yang, Z.X. Chen, H. Wu, J.W. Zhao, Z.Y. Jiang, Graphene encapsulated SiC nanoparticles as tribology-favoured nanofillers in aluminium composite, Compos. Part B 162 (2019) 445–453.

[175] S. Polat, Y. Sun, E. Çevik, H. Colijn, M.E. Turan, Investigation of wear and corrosion behaviour of graphene nanoplatelet-coated B_4C reinforced Al-Si matrix semi-ceramic hybrid composites, J. Compos. Mater. 53 (25) (2019) 3549–3565.

[176] G. Elango, B.K. Raghunath, K. Palanikumar, K. Thamizhmaran, Sliding wear of LM25 aluminium alloy with 7.5% SiC+2.5% TiO_2 and 2.5% SiC+7.5% TiO_2 hybrid composites, J. Compos. Mater. 48 (18) (2013) 2227–2236.

[177] S.A. Alidokht, A. Abdollah-zadeh, H. Assadi, Effect of applied load on the dry sliding wear behaviour and the subsurface deformation on hybrid metal matrix composite, Wear 305 (1–2) (2013) 291–298.

[178] E.M. Sharifi, F. Karimzadeh, Wear behaviour of aluminium matrix hybrid nanocomposites fabricated by powder metallurgy, Wear 271 (7–8) (2011) 1072–1079.

[179] P. Ravindran, K. Manisekar, P. Narayanasamy, N. Selvakumar, R. Narayanasamy, Application of factorial techniques to study the wear of Al hybrid composites with graphite addition, Mater, DES 39 (2012) 42–54.

[180] A.K. Mondal, S. Kumar, Dry sliding wear behaviour of magnesium alloy based hybrid composites in the longitudinal direction, Wear 267 (1–4) (2009) 458–466.

[181] V. Kavimani, K.S. Prakash, T. Thankachan, Experimental investigations on wear and friction behaviour of SiC@r-GO reinforced Mg matrix composites produced through solvent-based powder metallurgy, Compos. Part B 162 (2019) 508–521.

[182] B.X. Ma, H.Y. Wang, Y.H. Wang, Q.C. Jiang, Fabrication of (TiB_2-TiC)$_p$/AZ91 magnesium matrix hybrid composite, J. Mater. Sci. 40 (17) (2005) 4501–4504.

[183] J. Umeda, K. Kondoh, H. Imai, Friction and wear behaviour of sintered magnesium composite reinforced with CNT-Mg_2Si/MgO, Mater. Sci. Eng. A 504 (1–2) (2009) 157–162.

[184] B.M. Girish, B.M. Satish, S. Sarapure, Basawaraj, Optimization of wear behaviour of magnesium alloy AZ91 hybrid composites using taguchi experimental design, Metall. Mater. Trans. A 47 (6) (2016) 3193–3200.

[185] Y.L. Qin, L. Geng, D.R. Ni, Dry sliding wear behaviour of titanium matrix composites hybrid-reinforced by in situ TiBw and TiCp, J. Compos. Mater. 46 (21) (2012) 2637–2645.

[186] S. Soleymani, A. Abdollah-zadeh, S.A. Alidokht, Microstructural and tribological properties of Al5083 based surface hybrid composite produced by friction stir processing, Wear 278–279 (2012) 41–47.

[187] J. Slavič, M. Boltežar, Measuring the dynamic forces to identify the friction of a graphite-copper contact for variable temperature and current, Wear 260 (9) (2006) 1136–1144.

[188] N. Sadeghi, H. Aghajani, M.R. Akbarpour, Microstructure and tribological properties of in-situ TiC-C/Cu nanocomposites synthesized using different carbon sources (graphite, carbon nanotube and graphene) in the Cu-Ti-C system, Ceram. Int. 44 (18) (2018) 22059–22067.

[189] M.R. Akbarpour, S. Alipour, A. Safarzadeh, H.S. Kim, Wear and friction behaviour of self-lubricating hybrid Cu-(SiC+xCNT) composites, Compos. Part B 158 (2019) 92–101.

[190] H.M. Mallikarjuna, C.S. Ramesh, P.G. Koppad, R. Keshavamurthy, K.T. Kashyap, Effect of carbon nanotube and silicon carbide on microstructure and dry sliding wear behaviour of copper hybrid nanocomposites, Trans. Nonferrous Metals Soc. China 26 (12) (2016) 3170–3182.

[191] H. Nautiyal, S. Kumari, O.P. Khatri, R. Tyagi, Copper matrix composites reinforced by rGO-MoS_2 hybrid: strengthening effect to enhancement of tribological properties, Compos. Part B 173 (2019), 106931.

[192] Y.Z. Zhan, G.D. Zhang, Friction and wear behaviour of copper matrix composites reinforced with SiC and graphite particles, Tribol. Lett. 17 (1) (2004) 91–98.

[193] K. Rajkumar, S. Aravindan, Tribological performance of microwave sintered copper-TiC-graphite hybrid composites, Tribol. Int. 44 (4) (2011) 347–358.

[194] Y.Z. Zhan, G.D. Zhang, The role of graphite particles in the high-temperature wear of copper hybrid composites against steel, Mater. Des. 27 (1) (2006) 79–84.

[195] Y.X. Jian, J.D. Xing, Z.F. Huang, T.H. Wu, Quantitative characterization of the wear interactions between the boride and metallic matrix in Fe-3.0 wt % B duplex alloy, Wear 436–437 (2019), 203021.

[196] C.S. Ramesh, C.K. Srinivas, B.H. Channabasappa, Abrasive wear behaviour of laser sintered iron–SiC composites, Wear 267 (2009) 1777–1783.

[197] Ö.N. Doğan, J.A. Hawk, J.H. Tylczak, Wear of cast chromium steels with TiC reinforcement, Wear 250 (2001) 462–469.
[198] H. Tan, Z. Luo, Y. Li, F. Yan, R. Duan, Y. Huang, Effect of strengthening particles on the dry sliding wear behavior of Al_2O_3–M_7C_3/Fe metal matrix composite coatings produced by laser cladding, Wear 324–325 (2015) 36–44.
[199] G. Hammes, K.J. Mucelin, P.C. Goncalves, C. Binder, R. Binder, R. Janssen, A.N. Klein, J.D.B. Mello, Effect of hexagonal boron nitride and graphite on mechanical and scuffing resistance of self lubricating iron based composite, Wear 376–377 (2017) 1084–1090.
[200] T.R. Prabhu, V.K. Varma, S. Vedantam, Effect of SiC volume fraction and size on dry sliding wear of Fe/SiC/graphite hybrid composites for high sliding speed applications, Wear 309 (2014) 1–10.
[201] X.H. Qu, L. Zhang, M. Wu, S.B. Ren, Review of metal matrix composites with high thermal conductivity for thermal management applications, Prog. Nat. Sci. Mater. Int. 21 (3) (2011) 189–197.
[202] X.C. Tong, Advanced Materials for Thermal Management of Electronic Packaging, Springer, 2011.
[203] H.B. Luo, Y.W. Sui, J.Q. Qi, Q.K. Meng, F.X. Wei, Y.Z. He, Copper matrix composites enhanced by silver/reduced graphene oxide hybrids, Mater. Lett. 196 (2017) 354–357.
[204] J. Sethi, S. Das, K. Das, Study on thermal and mechanical properties of yttrium tungstate-aluminium nitride reinforced aluminium matrix hybrid composites, J. Alloys Compd. 774 (2019) 848–855.
[205] A. Bahrami, N. Soltani, S. Soltani, M.I. Pech-Canul, L.A. Gonzalez, C.A. Gutierrez, A. Moller, J. Tapp, A. Gurlo, Mechanical, thermal and electrical properties of monolayer and bilayer graded Al/SiC/rice husk ash (RHA) composite, J. Alloys Compd. 699 (2017) 308–322.
[206] S. Kumar, H. Dieringa, K. Kainer, Thermal cycling behaviour of the magnesium alloy based hybrid composites in the transverse direction, Mater. Sci. Eng. A 454–455 (2007) 367–370.
[207] Z.B. Lei, K. Zhao, Y.G. Wang, L.N. An, Thermal expansion of Al matrix composites reinforced with hybrid micro-/nano-sized Al_2O_3 particles, J. Mater. Sci. Technol. 30 (1) (2014) 61–64.
[208] A. Barker, X. Du, I. Skachko, E.Y. Andrei, Approaching ballistic transport in suspended graphene, Nat. Nanotechnol. 3 (8) (2008) 491–495.
[209] X. Gao, H.Y. Yue, E. Guo, H. Zhang, X.Y. Lin, L.H. Yao, B. Wang, Mechanical properties and thermal conductivity of graphene reinforced copper matrix composites, Powder Technol. 301 (2016) 601–607.
[210] Y.K. Chen, X. Zhang, E.Z. Liu, C.N. He, C.S. Shi, J.J. Li, P. Nash, N.Q. Zhao, Fabrication of in-situ grown graphene reinforced Cu matrix composites, Sci. Rep. 6 (2016), 19363.
[211] A. Miranda, N. Barekar, B.J. McKay, MWCNTs and their use in Al-MMCs for ultra-high thermal conductivity applications: a review, J. Alloys Compd. 774 (2019) 820–840.
[212] T.S. Srivatsan, T.S. Sudarshan, E.J. Lavernia, Processing of discontinuously-reinforced metal matrix composites by rapid solidification, Prog. Mater. Sci. 39 (4–5) (1995) 317–409.